5-2018

Functional Organization of the Brain at Rest and During Complex Tasks Using fMRI

Lauren Kelly Lynch
Purdue University

FUNCTIONAL ORGANIZATION OF THE BRAIN AT REST AND DURING COMPLEX TASKS USING FMRI

by

Lauren Kelly Lynch

A Dissertation

Submitted to the Faculty of Purdue University

In Partial Fulfillment of the Requirements for the degree of

Doctor of Philosophy

Weldon School of Biomedical Engineering

West Lafayette, Indiana

May 2018

THE PURDUE UNIVERSITY GRADUATE SCHOOL
STATEMENT OF COMMITTEE APPROVAL

Dr. Zhongming Liu, Ph.D., Chair

Weldon School of Biomedical Engineering

School of Electrical and Computer Engineering

Dr. Edward Bartlett, Ph.D.

Department of Biological Sciences

Weldon School of Biomedical Engineering

Dr. Riyi Shi, M.D., Ph.D.

Weldon School of Biomedical Engineering

Department of Basic Medical Sciences

Dr. Andrew Saykin, Psy.D.

Center for Neuroimaging, Indiana Alzheimer Disease Center, Indiana University School of Medicine, Indianapolis, Indiana, USA

Approved by:

Dr. George R. Wodicka

Head of the Graduate Program

For my parents and husband - who gave me guidance and support every step of the way.

ACKNOWLEDGMENTS

The work presented in this dissertation would not have been possible without the contributions of many individuals who have been instrumental at many stages of my education, training, and career. It is not possible for me to individually name all of you here, but please know that your guidance and support has been invaluable to me.

First, I would like to acknowledge the role of my advisor, Dr. Zhongming Liu, in developing my scientific thinking, communication skills, and analytical skills. It has been a pleasure to work with you the last few years and to learn from such a strong scientist and engineer. Your future as a professor is extremely bright. Likewise, I would like to thank Dr. Andrew Saykin and our collaborators at the Indiana Alzheimer Disease, Center for Neuroimaging. It has been a great learning experience for me to get exposure to clinical research and to gain the perspective of another group. It was especially impactful to me to have had this opportunity because of my personal interest in the field. In addition, I would like to thank my other committee members, Dr. Riyi Shi and Dr. Edward Bartlett, for their critical comments and feedback at various stages of the PhD qualification process here at Purdue. I am also extremely appreciative of the Indiana Clinical and Translational Sciences Institute (Dr. Colleen Gabauer, Dr. Jon Story, Dr. Anantha Shekhar) for sponsoring my research over the last two years through a predoctoral fellowship and for the many educational opportunities associated with the program.

Second, without my colleagues in the Laboratory for Integrated Brain Imaging (LIBI), this work would not have been possible. Everyone I have worked with has been intelligent, hard-working, thoughtful, and helpful. Thank you Haiguang, Kun-Han ("Tom"), Yizhen, Jung-Hoon, Jiayue ("Cherry"), Ranajay, Nishant, Kuan, Steven, Jun Young, Shao-Chin, and Junxing for the critical feedback, signal processing and statistics help, and random conversations about celebrities in your home countries. I would also like to express my gratitude toward Dr. Greg Tamer for his assistance with the MRI scanner at Innervision West, where many of these scans were conducted. Thank you for helping me learn the machines and for always being available when problems would arise. At the Center for Neuroimaging at IU, I would like to thank Dr. Shannon Risacher, John West, Dr. Brenna McDonald, Dr. Liana Apostolova, Dr. Frederick Unverzagt, Eileen Tallman, Dr. Brad Glazier, Dr. Debomoy Lahiri, and Dr. Diana Svaldi for your assistance with the clinical

portion of the contents of this dissertation. From working with all of you, I have seen first-hand that science is a “team” effort and gotten some valuable feedback.

In addition, I would like to thank the directors of the Indiana University-Purdue University Medical Scientist Training Program (MSTP), Dr. Raghu Mirmira and Dr. Maureen Harrington, and Janice Receveur, the program administrator. Thank you all for believing in me, for fostering my career development, and for the many conversations. This program has been an incredible opportunity for me, and I am so grateful to have been a part of it. I want to also thank my MSTP colleagues for answering my many, many questions about what to expect in each phase of the training and for quelling my anxieties. There are too many of you to list here, but please know that I really appreciate each and every one of you for helping me.

Finally, I have a few individuals to acknowledge who gave me experiences that were instrumental to me getting to Purdue and the MSTP. Dr. Gaines, thank you so much for your help, career advice, and for your role in administering the FGLSAMP program. Being a part of FGLSAMP was crucial to my success in research and exposure to it. Moreover, Dr. Fabrice Manns, Dr. Jean-Marie Parel, Dr. Bianca Maceo, and Mariela Aguilar – thank you for a fabulous undergraduate research experience at the Ophthalmic Biophysics Center (OBC) at Bascom Palmer. Dr. Ramarathnam Narasimhan (“Dr. Ram”), thank you for telling me about MD/PhD programs at my scholarship interview during my senior year of high school. My experiences in FGLSAMP, the OBC, and in the College of Engineering at the University of Miami, inspired me to pursue MSTP programs and research long-term. Lastly, Mr. Brian Murray, thank you for designing and facilitating the Math, Science, and Engineering (MSE) program at Suncoast Community High School, and for teaching me three years of high school physics in a fun and engaging way. The extensive exposure I had to these concepts at the high school level was vital to my success in an undergraduate engineering curriculum in the first place.

TABLE OF CONTENTS

LIST OF FIGURES

LIST OF TABLES

LIST OF ABBREVIATIONS

Abbreviation	Term
AD	Alzheimer's Disease
AFNI	Analysis of Functional NeuroImages
BOLD	Blood Oxygen Level-Dependent
CN	Cognitively Normal
DMN	Default Mode Network
FC	Functional Connectivity
FDR	False Discovery Rate
fMRI	functional Magnetic Resonance Imaging
FSL	FMRIB (Oxford) Software Library
GM	Gray Matter
IADC	Indiana Alzheimer’s Disease Center
IC	Independent Component
ICA	Independent Component Analysis
IFJ	Inferior Frontal Junction
ILF	Inferior Longitudinal Fasciculus
ISFC	Inter-Subject Functional Correlation
LFP	Local Field Potential
LGN	Lateral Geniculate Nucleus
M1	Primary Motor Cortex
MCI	Mild Cognitive Impairment
MR	Magnetic Resonance
OR	Optic Radiations
PCA	Principal Component Analysis
PPhG	Posterior Parahippocampal Gyrus
RSN	Resting State Network
SCD	Subjective Cognitive Decline
V1	Primary Visual Cortex

V5/MT+	Middle Temporal Visual Area
WM	White Matter

*This table does not include cytoarchitecture or network labels used in parcellation analyses using the 240-region Brainnetome Atlas, the 17-network Yeo et al. (2011) Atlas, or ICA. For these abbreviations, please see http://atlas.brainnetome.org/, http://surfer.nmr.mgh.harvard.edu/fswiki/CorticalParcellation_Yeo2011, or refer to the figure at the end of the chapter in question, respectively.

ABSTRACT

Author: Lynch, Lauren, K. PhD
Institution: Purdue University
Degree Received: May 2018
Title: Functional Organization of the Brain at Rest and During Complex Tasks Using fMRI.
Major Professor: Dr. Zhongming Liu, Ph.D.

How and why functional connectivity (FC), which captures the correlations among brain regions and/or networks, differs in various brain states has been incompletely understood. I review high-level background on this problem and how it relates to 1) the contributions of task-evoked activity, 2) white-matter fMRI, and 3) disease states in Chapter 1. In Chapter 2, based on the notion that brain activity during a task reflects an unknown mixture of spontaneous activity and task-evoked responses, we uncovered that the difference in FC between a task state (a naturalistic movie) and resting state only marginally (3-15%) reflects task-evoked connectivity. Instead, these changes may reflect changes in spontaneously emerging networks. In Chapter 3, we were able to show subtle task-related differences in the white matter using fMRI, which has only rarely been used to study functions in this tissue type. In doing so, we also demonstrated that white matter independent components were also hierarchically organized into axonal fiber bundles, challenging the conventional practice of taking white-matter signals as noise or artifacts. Finally, in Chapter 4, we examined the utility of combining FC with task-activation studies in uncovering changes in brain activity during preclinical Alzheimer's Disease (mild cognitive impairment (MCI) and subjective cognitive decline (SCD) populations), based on data collected at the Indiana University School of Medicine. We found a reduction in neural task-based activations and resting-state FC that appeared to be directly related to diagnostic severity. Taken together, the work presented in this dissertation paves the way for a novel framework for understanding neural dynamics in health and disease.

1. INTRODUCTION

1.1 Defining the Problem

For centuries, what has become known as the "mind-body problem" has endured as a challenge for philosophers, scientists, and religious scholars. This famous conundrum can be simplified as follows: what is the relationship between the mind – that which is responsible for mental processes, such as consciousness, perception, memory, and thinking – and the body (i.e. the brain)? We now know, with the aid of measurement techniques (Hubel and Wiesel, 1959; Martinez et al., 2005), such as neural recordings and functional magnetic resonance imaging (fMRI) (Kwong et al., 1992; Ogawa et al., 1992), as well as from clinical observations (Broca, 1861; Harlow, 1848), that there is significant overlap between physical form and cognitive function. In spite of the numerous advances we have made about the innerworkings of the human brain, there is still much that remains to be explored in what may be considered a "final frontier" of understanding in human physiology.

We know that the brain is an enormously costly organ in terms of energy consumption; it accounts for about 2% of body weight, yet it uses about 20% of the body's energy (Raichle, 2015). Metabolically, ~85% of the brain's activity at rest is associated with glutamate recycling and thus, neural signaling processes (Raichle and Mintun, 2006; Shulman et al., 2004). Action potentials, the mechanism for electrical information propagation from one neuron to the next (i.e. neuronal signaling), are metabolically expensive (Attwell and Laughlin, 2001). Nevertheless, relative to rest, additional energy consumption related to engaging in various tasks is very small (less than 5%) (Raichle, 2010; Roland et al., 1987; Sokoloff et al., 1955).

Therefore, we can divide brain energetics and metabolism into two types of processes: 1) intrinsic, based on spontaneous, baseline brain signaling occurring at rest, and 2) extrinsic, "task-evoked activity, which is associated with the engagement of various cognitive tasks. **Unfortunately, the problem is that there is no clear consensus about the complex interplay between spontaneous, "intrinsic" processes and task-evoked activities.** Findings range from reports of spontaneous and task-evoked activities being linearly additive (Arieli et al., 1996; Azouz and Gray, 1999; Fox et al., 2006b), to tasks suppressing spontaneous activity (Bianciardi et al., 2009a; Borg-Graham et al., 1998; Churchland et al., 2010; He, 2013; Ponce-Alvarez et al., 2013),

to task-related increases in neuronal variability (Nir et al., 2006). Further, the role of the rest-task interaction in the brain's organization in gray matter (Chapter 2), white matter (Chapter 3), and disease (Chapter 4) is unclear.

1.2 fMRI Is a Measurement Technique

Functional magnetic resonance imaging (fMRI) measures changes in blood flow that *indirectly* relate to the activity of a particular region via metabolic and hemodynamic processes. Specifically, the blood oxygen level-dependent (BOLD) contrast is based on paramagnetic differences between oxygenated and deoxygenated hemoglobin, the oxygen-carrying protein in red blood cells (Bandettini et al., 1992; Kwong et al., 1992; Ogawa et al., 1992). Deoxygenated hemoglobin creates magnetic field inhomogeneities within and around vessels in the brain, dephasing the spins of the magnetized ions and reducing the value of the observed signal (Ogawa et al., 1990; Villringer et al., 1988). In response to a stimulus, the local BOLD signal can be described by 1) an initial dip in the signal, corresponding to increased deoxyhemoglobin from enhanced blood flow; 2) a compensatory overshoot as blood volume greatly increases relative to flow (reduced ratio of deoxyhemoglobin) (~4-6 seconds after stimulus onset); 3) a post-stimulus undershoot as blood volume decreases more slowly than flow (~10-20 seconds after stimulus onset) (Buxton et al., 1998). Thus, the BOLD fluctuation reflects the combined effects of cerebral blood flow (CBF), blood volume (CBV), and the metabolic rate of oxygen ($CMRO_2$). Moreover, BOLD is thought to be closely related to neuronal synaptic activity, and to some degree, spiking activity (Lauritzen, 2001; Logothetis et al., 2001; Mukamel et al., 2005), and astrocytes are thought to be the important mediators linking neuronal activity to vasodilation (for review, see Petzold and Murthy (2011)). Various analysis methods, such as a general linear model approach, functional connectivity (which captures correlations between regions), and/or effective connectivity (which establishes directionality of neuronal processes), are then used to establish a relationship between vascular changes and behavioral or disease states after the T_2^*-weighted acquisitions.

Ultimately, the BOLD fMRI contrast allows for non-invasive, non-ionizing, high spatial resolution visualization of activated neuroanatomical regions associated with brain functions. From its inception in the early 1990s, fMRI has since become a preeminent imaging modality in

neuroscience, with over 40,000 research articles published as of 2017[1]. The technique has vastly improved our understanding of how the brain functions, but is still primarily a research tool (Rosen and Savoy, 2012).

1.3 Experimental Paradigms in fMRI

fMRI research is primarily divided into two fields: task activation and resting-state. The early days of fMRI were particularly focused on task-evoked responses. The traditional approach utilizes intermittent periods of task (through block- or event-related designs, Fig. 1.1) to activate and thus, identify brain areas associated with a specific cognitive function (e.g. flickering checkboards for the visual cortex, finger tapping for the motor cortex). Analytically, the general linear model (GLM) has long been used to relate neural activity to these types experimental designs (Friston et al., 1995). In spite of the abundance of information gained from using these types of designs, such approaches are limited in that they 1) neglect the role of intrinsic activity of the brain, which composes the majority of metabolic activity; and 2) tend to be overly simplistic: the cognitive demands of daily life extend far beyond highly controlled task paradigms, such as simple button presses or the viewing of sinusoidal gratings.

Resting-state fMRI is used to describe a task-free paradigm in which subjects are asked to lie still in the scanner with their eyes closed. It is based upon the observation that the fMRI time series from one part of the motor cortex was temporally correlated with other related areas within the motor "system" (e.g. supplementary motor area), in the absence of any motor task (Biswal et al., 1995). Resting-state correlations have also been reproduced among brain regions involved in other sensory or cognitive processes (e.g. auditory, visual, attentional) (Cordes et al., 2000; Fox et al., 2006a; Lowe et al., 1998), and has been expanded to include the analysis of correlations even across unrelated brain regions (i.e. functional connectivity). In addition, resting-state work has been instrumental to identifying the default mode network (DMN), a collection of regions that decrease their activity across a broad spectrum of task conditions when compared to rest (Raichle et al., 2001). The discovery of the DMN was one example of an important fundamental contribution to our understanding of brain function and neuroscience made using fMRI.

[1] This statistic is based on a December 20, 2017 PubMed (https://www.ncbi.nlm.nih.gov/pubmed/) search with "fMRI" as a keyword.

Over the last decade, resting-state studies have indeed come to dominate the field of fMRI. However, there are certain caveats to resting-state studies (see Duncan and Northoff (2013) for review). First, there is little consensus on how to perform these studies – the instructions given to the participant (e.g. whether told to relax and be still, ignore the scanner noise, etc.) has been shown to have an effect on the connectivity of the DMN at rest (Benjamin et al., 2010). Likewise, there is little consensus on whether subjects are instructed to keep their eyes opened or closed, and this does indeed have an impact on the data (Patriat et al., 2013) (Lynch, unpublished data; Fig. 1.2). Second, during resting-state, subjects actually engage in a variety of introspective tasks that are not temporally controlled, raising the question of whether the resting-state is indeed simply a poorly controlled task (Delamillieure et al., 2010). These activities include, but are not limited to, mental imagery, inner language, somatosensory awareness, inner musical experiences, and inner processing of numbers, and they have also been shown to modulate fMRI findings (Doucet et al., 2012). Third, resting-state, like simplistic block-design and event-related paradigms, does not mimic the cognitive demands of daily life in which functional demands (or deficits) may be exposed.

In contrast, naturalistic tasks, in which subjects engage in the free-viewing of film clips or recorded narratives, are gaining popularity (Fig. 1.3). These tasks provide a rich behavioral context reflecting the activities of daily life. In natural vision (i.e. movie-watching), scenes with sharp moving edges that unfold over relatively long time scales simulate the interactions a person has regularly in his or her environment; recorded narratives reflect conversations and stories that develop sequentially. Further, neural responses to naturalistic stimuli, measured through inter-subject or intra-subject correlations, are reliable and widespread (Hasson et al., 2010; Hasson et al., 2004; Jääskeläinen et al., 2008; McMahon et al., 2015; Mukamel et al., 2005), and that the high-level natural content of the movie is needed for reproducible responses (Lu et al., 2016) (Figs. 1.4-1.5). Although also correlation-based, the inter-subject and intra-subject correlations central to this method isolate task-evoked activities, and thus do not reveal anything about the brain's underlying intrinsic architecture (Simony et al., 2016).

Each of these experimental paradigms has strengths and weaknesses. Because I am interested in uncovering the rest-task interaction, none of these methods were used in an isolated fashion. Instead, complementary information was obtained by using naturalistic task paradigms and resting-state studies in parallel, on the same subjects, in studies of that brain's gray matter

(Chapter 2), white matter (Chapter 3), and at the onset of disease (Chapter 4). The next three sections provide a brief introduction to each of these chapters and how they relate to the problem presented in Section 1.1. A more complete rationale for the research conducted is contained within the "Rationale" sections within each chapter (Sections 2.1, 3.1, and 4.1, respectively).

1.4 Functional Connectivity at Rest and During Tasks

As previously mentioned, functional connectivity (FC) captures the correlations of different regions and/or networks[2], and it is used to characterize the brain's functional organization in various behavioral and disease states. FC is mostly conserved across states of consciousness (Horovitz et al., 2008; Vincent et al., 2007) and during the performance of various tasks (Arfanakis et al., 2000; Cole et al., 2014; Fair et al., 2007; Gratton et al., 2016; Harrison et al., 2008; Krienen et al., 2014). Preliminary work early in my doctoral training has also supported this finding (Figs. 1.6-1.7). However, increasing evidence suggests that FC is altered within and between brain states (Buckner et al., 2013; Mennes et al., 2013; Rehme et al., 2013; Sepulcre et al., 2010; Van Dijk et al., 2010). Along these lines, I also found significant differences in FC between a visual task and the resting-state, which included significantly negative FC differences between visual areas and non-visual task related areas and positive FC differences between visual areas and the ventral DMN (task state relative to rest) (Fig. 1.8). Consistent alterations in FC leads to the potential use of this feature as a "network signature" of how the brain engages itself in various behavioral or cognitive tasks.

Indeed, additional studies using dynamic functional connectivity found that differences in task FC over short temporal intervals (≥ 30 seconds) can be used to identify behavioral states with very high accuracy (Gonzalez-Castillo et al., 2015; Shirer et al., 2012). However, Shirer et al. (2012) also demonstrated the ability to classify four different tasks with temporal windows as long as 10 minutes at >80% accuracy, implying that stationary studies of FC differences provide similar utility in classification.

To fully understand FC differences between different tasks and/or resting-state, it is necessary to disentangle the different contributions of spontaneous (intrinsic) and task-evoked (extrinsic) activities. If the FC differences between rest and task are due to the task-evoked activity,

[2] The brain's functional networks are conserved across different states (Fig. 1.9; see also Smith et al. (2009)). This enables us to perform network-based analyses using a common set of networks across different tasks.

this pattern reflects only network interactions directly involved in task execution. If instead this difference in FC is attributed to ongoing activity, the pattern is driven by the brain's intrinsic functional re-organization to facilitate the task. Alternatively, there may be an interaction between spontaneous and evoked activities such that the FC differences between resting-state and the task reflect correlational changes in both types of activity. I wondered which of these scenarios was most likely. Initially, I hypothesized that the FC difference would largely be due to the task-evoked activity based on the findings of several landmark studies demonstrating the independence of spontaneous and task-evoked activities and that they linearly superimpose (Arieli et al., 1996; Fox et al., 2006b).

Prior studies have established some valuable analysis methods to disentangle sources of spontaneous and task-evoked activity that provide improved reliability and manageability over temporally averaging a very large number of subjects and/or sessions (Henriksson et al., 2015; Kim et al., 2017). Simony et al. (2016) proposed the use of inter-subject functional connectivity (ISFC) during a recorded narrative to isolate correlations from task-evoked networks without contributions from ongoing activity or non-neuronal noise. This technique builds off of the Hasson et al. (2004) study, which demonstrated that natural vision gave rise to reliable responses that were reproducible across individuals. A similar strategy is to assess the inter-regional correlation across different sessions of the same stimuli for the same subject, which gives rise to enhanced reproducibility over inter-subject correlations (Lu et al., 2016; Wilf et al., 2017). Therefore, after implementing an inter-session approach to isolate task-evoked activity from spontaneous sources, I set out to explore the rest-task interaction at the whole brain level using a natural vision task (Chapter 2).

1.5 White-Matter fMRI

Historically, fMRI has not been considered to be detectable in white matter tissue (see Gawryluk et al. (2014) for review). The two main reasons white matter fMRI is controversial are (1) that the cerebral volume and flow in white matter is three to seven times lower in white matter, resulting in a substantially smaller signal-to-noise ratio (Helenius et al., 2003; Jensen et al., 2006; Preibisch and Haase, 2001; Van Osch et al., 2009), and (2) that the primary source of fMRI signal is more commonly attributed to post-synaptic potentials non-existent in white matter (Logothetis and Wandell, 2004) (though this point remains slightly controversial, see). Furthermore, although

fMRI studies have in fact produced activation in white matter, most commonly in the corpus callosum (Aramaki et al., 2006; D'Arcy et al., 2006; Fabri et al., 2011; Tettamanti et al., 2002) and internal capsule (Gawryluk et al., 2011b; Mosier et al., 1999); many argue that this activation is not a "true" representation of neural activity. Moreover, Ding et al. showed that resting-state fMRI signals in white matter were correlated over the optic radiations and corpus callosum, as well as locally, in a similar anisotropic manner as observed with diffusion tensor imaging (DTI) (2013). Further, the white matter-fMRI signal was recently shown (Ding et al., 2016) to be blood oxygenation level dependent (BOLD) through multi-echo acquisitions (Kundu et al., 2012)

Given the morbidity and mortality associated with known white-matter disorders (e.g. multiple sclerosis and traumatic brain injury), as well as the unknown role of white matter pathology in existing neurological disorders (e.g. Alzheimer's disease), a tool to non-invasively characterize the functional dynamics of white matter could provide considerable insight. However, a major challenge in characterizing white activity is the substantially lower signal-to-noise ratio inherent in the tissue type; when traditional univariate or multivariate time-series analyses are applied to gray matter and white matter voxels together, the signal variance and structure are dominated by voxels in gray matter. One potential way to deal with this issue is to separate white matter from gray matter and establish a criterion to distinguish signal from noise (via reproducibility or otherwise). Once signal and noise are separated, conjoint evaluation of the roles of white matter and gray matter networks in various tasks may be conducted. Thus, after establishing a methodology through which fMRI in the white matter may be characterized, I sought to explore and compare the functional organization of the WM in resting-state and during a naturalistic visual task (Chapter 3).

1.6 Functional Changes in the Brain due to Alzheimer's Disease

Alzheimer's Disease (AD) is the most common form of dementia and affects one in three people aged 85 and older (Galvin et al., 2012). Further, it is the only top 10 cause of death that cannot be prevented, cured, or slowed (Alzheimer's Association, 2017). The most common initial clinical symptom is episodic memory impairment (Hodges, 2006), and, as the disease progresses, cognitive decline across widespread neuroanatomical systems becomes marked. Over time, patients experience declines in language/semantic ability (Henry et al., 2011; Leyton et al., 2017) visuospatial deficits (Cronin-Golomb and Hof, 2004; Risacher et al., 2013), attentional and

executive difficulties (Perry and Hodges, 1999; Wong et al., 2014) and neuropsychiatric/behavioral disturbances (De Souza et al., 2009; Hodges, 2006). Eventually, patients exhibit loss of control over bodily functions, and, typically, complications from immobility, swallowing disorders, and malnutrition lead to patient mortality (Alzheimer's Association, 2017).

Researchers and clinicians have become increasingly focused on early detection and characterizing the earliest clinical stages of the disorder – when future interventions could make the greatest impact. Amnestic Mild Cognitive Impairment (aMCI) is often regarded as a "prodromal" or "preclinical" AD state (Villemagne et al., 2013). Mild cognitive impairment (MCI) is defined as "cognitive decline greater than that expected for an individual's age and education level but that does not interfere notably with activities of daily living" (as measured by various cognitive performance tests), and the amnestic subtype primarily involves a memory complaint (Henry et al., 2011). These patients are important to study because they convert to a diagnosis of AD at a faster rate than cognitively healthy controls (Small et al., 2007).

There is increasing evidence that individuals with cognitive complaints, even with normal performance on cognitive tests, also have an increased likelihood of biomarker abnormalities consistent with AD pathology and an increased risk for future cognitive decline and AD dementia (see Jessen et al. (2014) for review). A continuum of Alzheimer's disease makes intuitive sense; pathologically, neurofibrillary tangles (NFTs), which consist of misfolded Tau protein in neurons, begin to accumulate in the transentorhinal region (Braak and Braak, 1995; Morrison and Hof, 1997). From here, the pathology spreads to the entorhinal region, the hippocampus, and then to the neocortex (Braak and Braak, 1995). Thus, cognitive complaints, or subjective cognitive decline (SCD), may in fact indicate the very first effects of AD pathology on cognitive function, between completely intact functioning and first detectable decline.

AD patients have demonstrated alterations in both task activations and resting-state connectivity compared to healthy controls (HC). Task activation studies have consistently revealed reduced activations in medial temporal lobe structures in AD patients compared to controls (Golby et al., 2005; Kato et al., 2001; Machulda et al., 2003; Rombouts et al., 2000; Sperling et al., 2003), with some reports of compensatory hyperactivations in the prefrontal cortex (Grady et al., 2003). FC studies have shown decreased DMN connectivity (Damoiseaux et al., 2012; Greicius et al.,

2004; Jones et al., 2011), increased prefrontal connectivity (Agosta et al., 2012), and increased salience network connectivity (Zhou et al., 2010) in AD patients.

However, research in MCI patients has generated conflicting results. Some groups have shown that MCI patients mostly mirror the medial temporal lobe hypo-activations and reduced connectivity found in AD populations (Machulda et al., 2003; Petrella et al., 2007; Rombouts et al., 2005; Sorg et al., 2007), whereas others have encountered paradoxical hyper-activations and hyper-connectivity of these same regions (Bai et al., 2011; Dickerson et al., 2005; Kircher et al., 2007). To disentangle this difference, a nonlinear trajectory of neurovascular changes has been proposed. In the early stages of MCI, hyperactivity occurs as the brain attempts to compensate for the impaired signaling, which is then followed by a loss of activity as the disease progresses to the later stages of MCI, echoing the functional deficits seen in AD patients (Celone et al., 2006).

Reports of functional changes due to cognitive complaints or SCD are much sparser; nevertheless, we know that changes in hippocampal volume and visual contrast sensitivity are intermediate between healthy aging adults and patients with MCI (Risacher and Saykin, 2013; Saykin et al., 2006). Moreover, Wang et al. (2013) demonstrated that among MCI, SCD, and HC patient groups, significantly different FC of the DMN was localized to the hippocampus; further, the number of significantly different voxels appeared to have a direct relationship with disease progression. So far, neuroimaging-based evidence does appear to show that SCD brain changes are transitional between HC and MCI conditions, but more work is needed in this area.

There are several important motivations for establishing activation and/or correlational differences that occur in SCD and MCI patients. First, an improved understanding of brain changes that occur with SCD, which is postulated to precede MCI, may help us better appreciate the progression of changes that occur in MCI and subsequently, AD. Second, such findings may help give credence to theorized non-linear courses of disease progression or otherwise help resolve conflicting reports. Third, movement toward an imaging-based biomarker for SCD and MCI may allow for pharmacological treatments and other interventions at even earlier stages, when they may have the greatest possible impact. Hence, I sought to relate changes in task activations using a scene-encoding task (Detre et al., 1998) and resting-state functional connectivity to MCI and/or SCD status using participants from a longitudinal study of brain aging and memory (Indiana Memory and Aging Study) (Chapter 4).

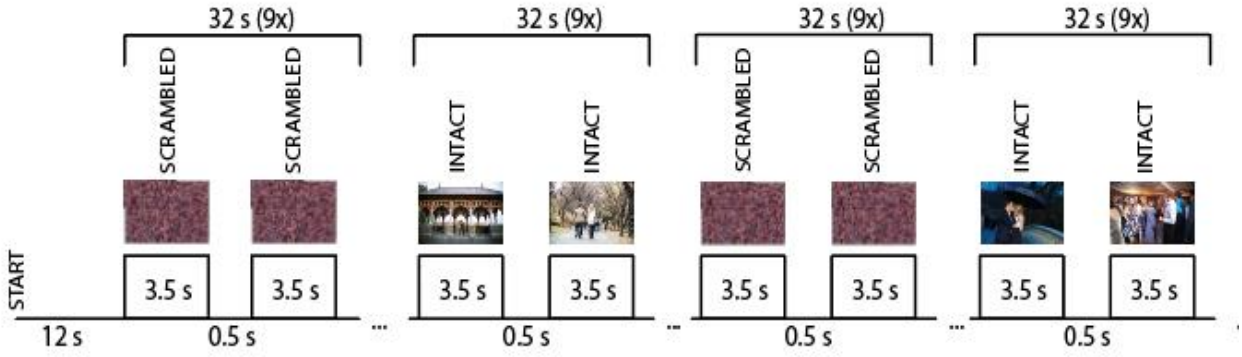

Figure 1.1. Example Block-Design Paradigm. Alternating periods of a task (intact images) are compared against a control condition (scrambled images). (This paradigm was used for the scene-encoding task activation data in Chapter 4.)

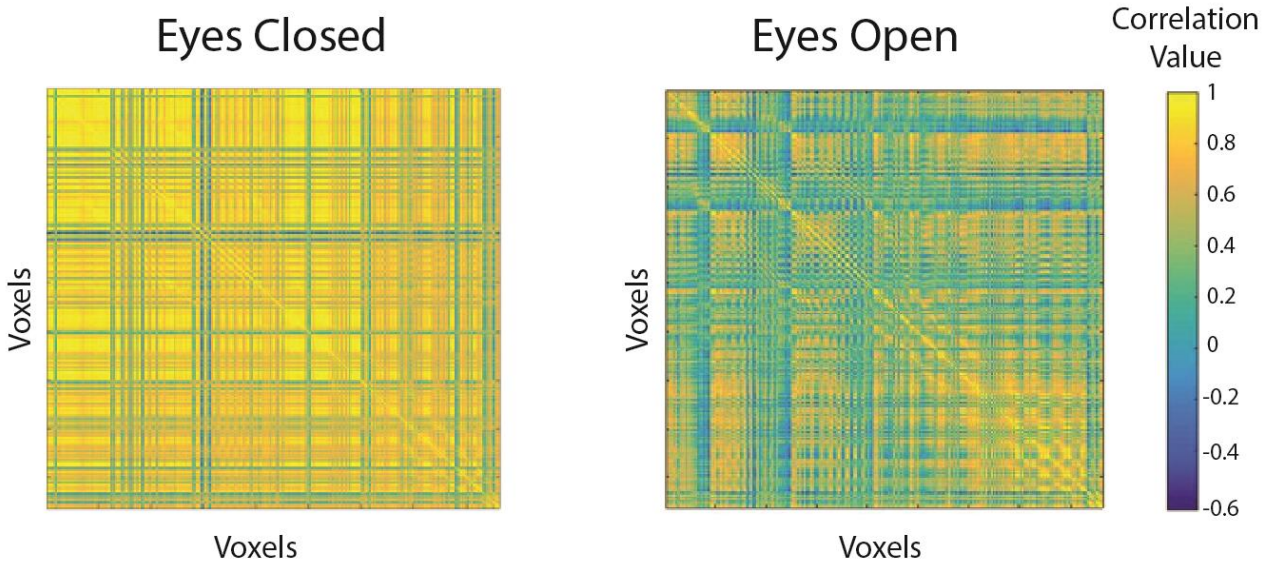

Figure 1.2. Showing the correlation values of voxels in the optic tracts using an eyes-open resting state (left) and an eyes-closed resting-state (right). Yellow is used to indicate high correlation values, blue is used to indicate low correlation values. Both resting-state paradigms were conducted in the dark.

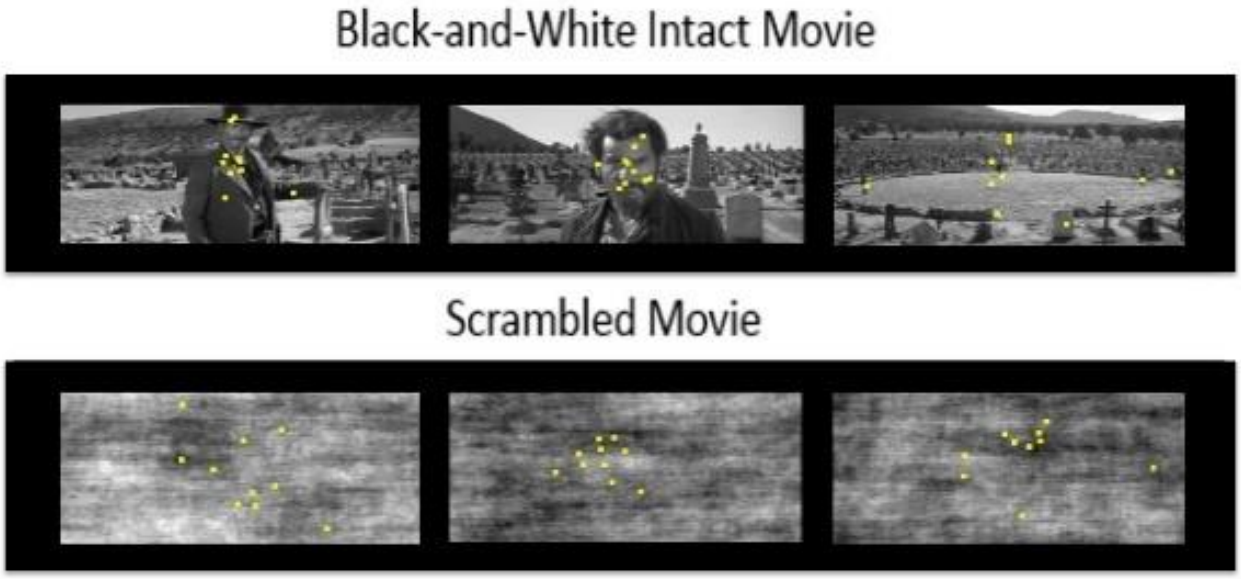

Figure 1.3. Showing the scrambling of the original black and white movie clip (top) via phase shuffling with the image power preserved (bottom), with eye tracking data as a circular pattern of dots. The clip was taken from *The Good, the Bad, and the Ugly*, 1966, from 162:54 to 168:33 min. in the film. Eye movements had little effect on reproducible fMRI responses (see Lu et al. (2016)). (Figure adapted from Lu et al. (2016).)

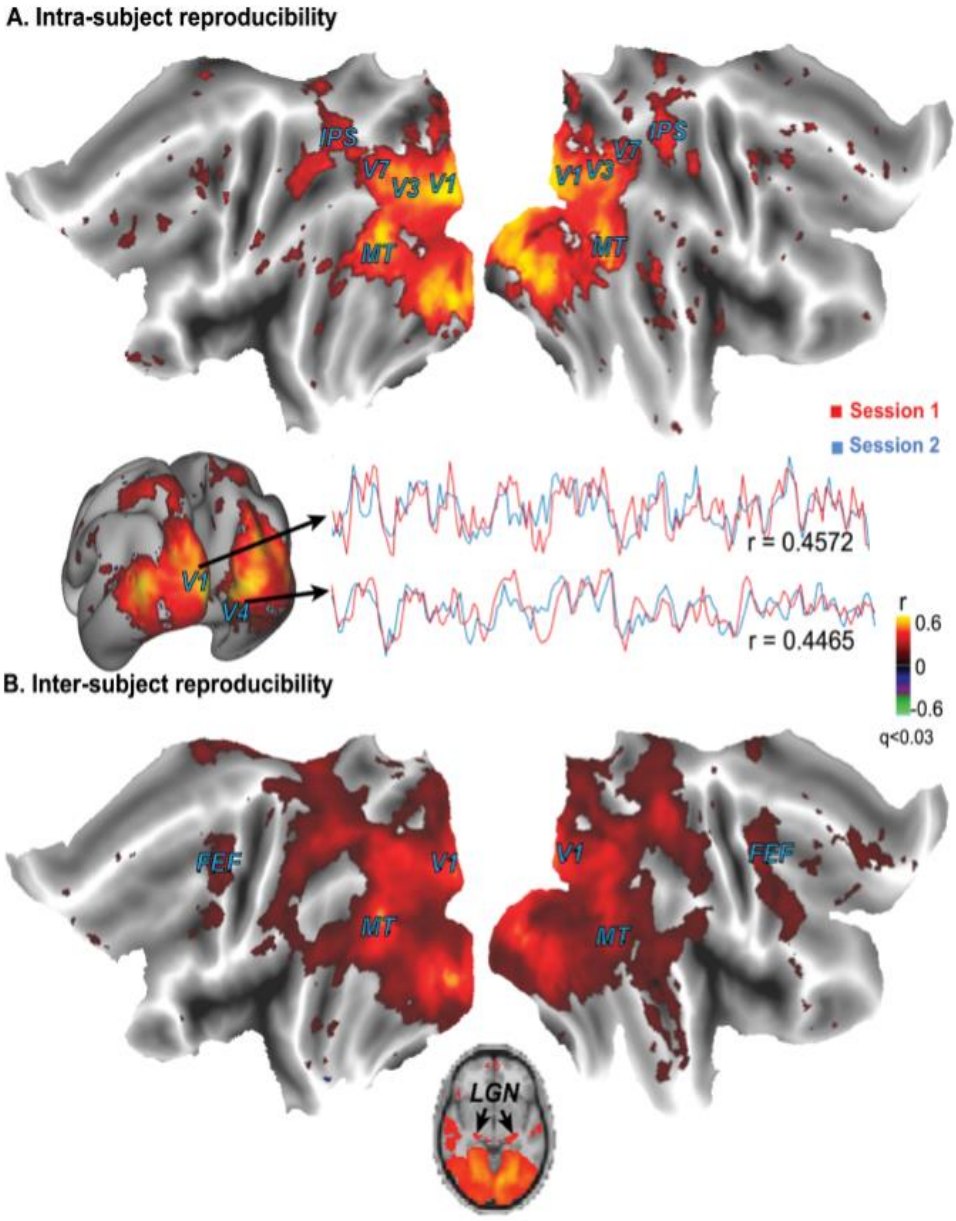

Figure 1.4. Brain activations with the intact movie were found at regions that showed significant intra-subject (A) and inter-subject (B) correlations in cortical activity during free movie watching. The mapping results were based on data from nine subjects. From a single subject, the fMRI signals from two voxels within the primary visual cortex (V1) and the lateral occipito-temporal gyrus (V4) are shown as examples to illustrate the intra-subject reproducibility in cortical activity. The color indicates the cross correlation. (Figure adapted from Lu et al. (2016).)

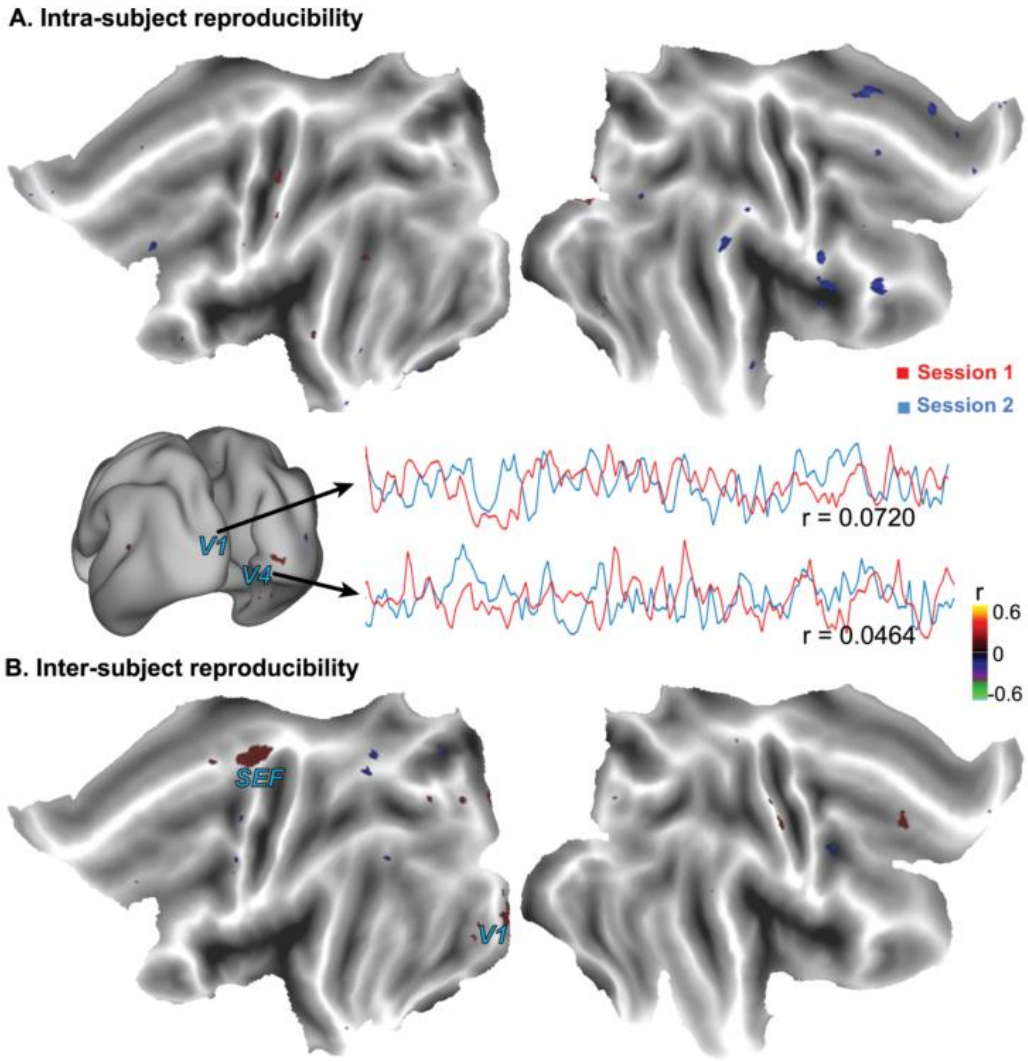

Figure 1.5. Cortical activations with the scrambled movie were reduced and confined to V1, as revealed by the intra-subject (A) and inter- subject (B) reproducibility of the fMRI signal. The mapping results were based on data from nine subjects. From a single subject, the fMRI signals from two voxels within the primary visual cortex (V1) and the lateral occipito-temporal gyrus (V4) are shown as examples to illustrate the relatively low intra-subject reproducibility in cortical activity. The color indicates the cross correlation. (Figure adapted from Lu et al. (2016).)

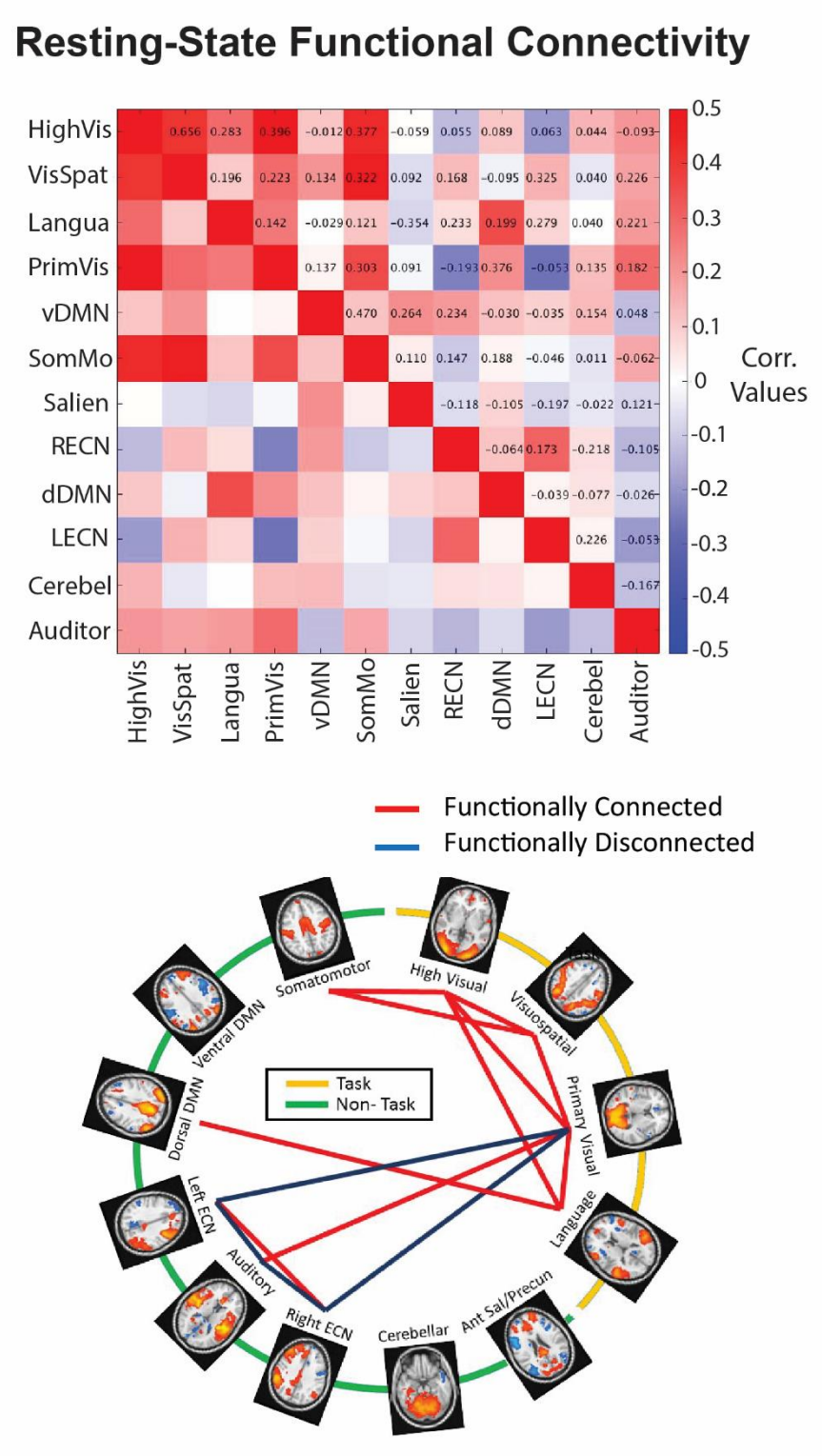

Figure 1.6. Functional Connectivity of Networks in Resting-State. Top: Correlation matrix depicting the temporal correlations of 12 networks derived using independent component analysis (ICA). Bottom: Circle graph illustrating significant correlations among the networks. A Bonferroni correction for multiple comparisons was applied. Adapted from Marussich et al. (2015).

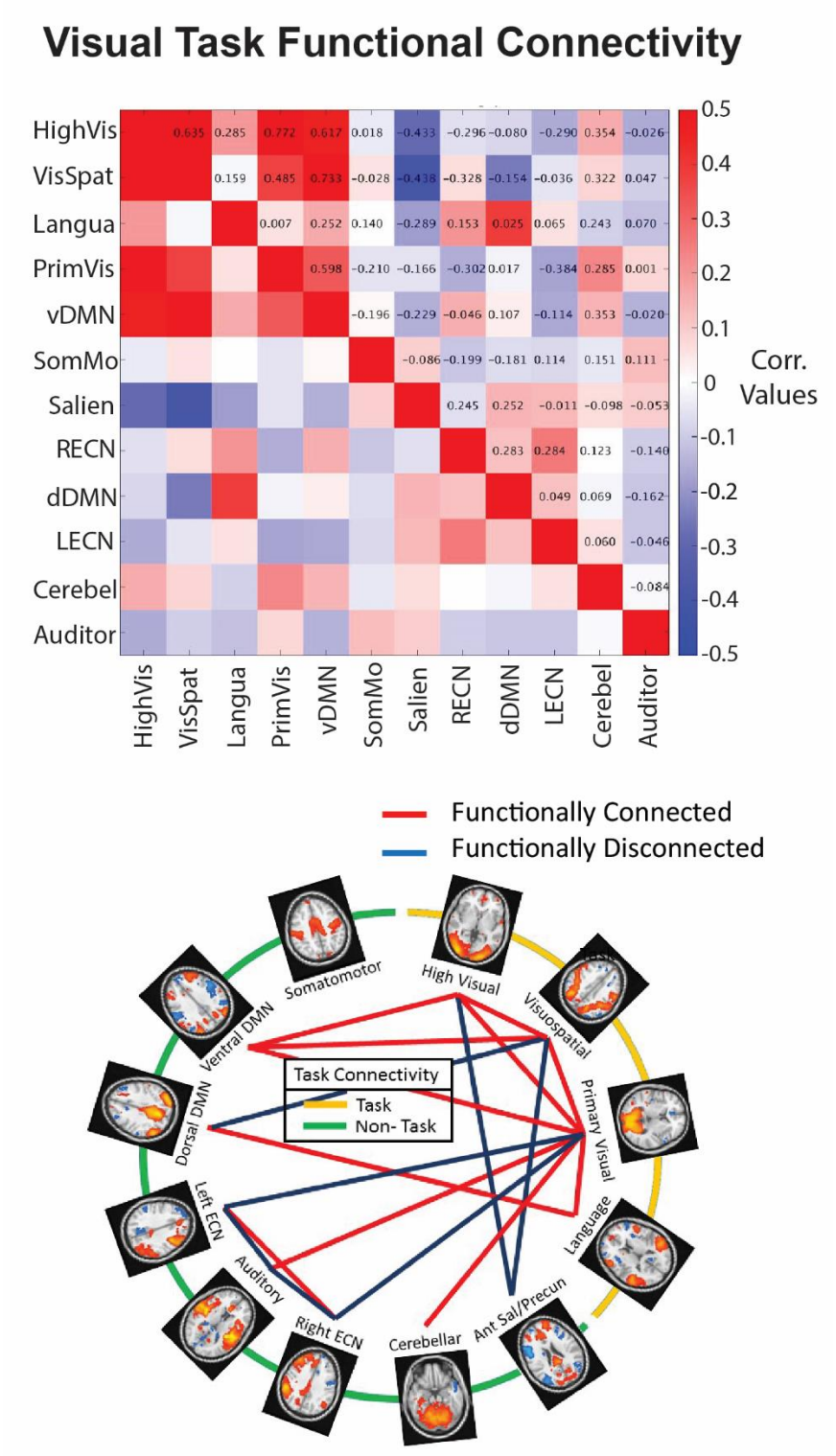

Figure 1.7. Functional Connectivity of Networks During the Visual Task. Top: Correlation matrix depicting the temporal correlations of 12 networks derived using independent component analysis (ICA). Bottom: Circle graph illustrating significant correlations among the networks. A Bonferroni correction for multiple comparisons was applied. Adapted from Marussich et al. (2015).

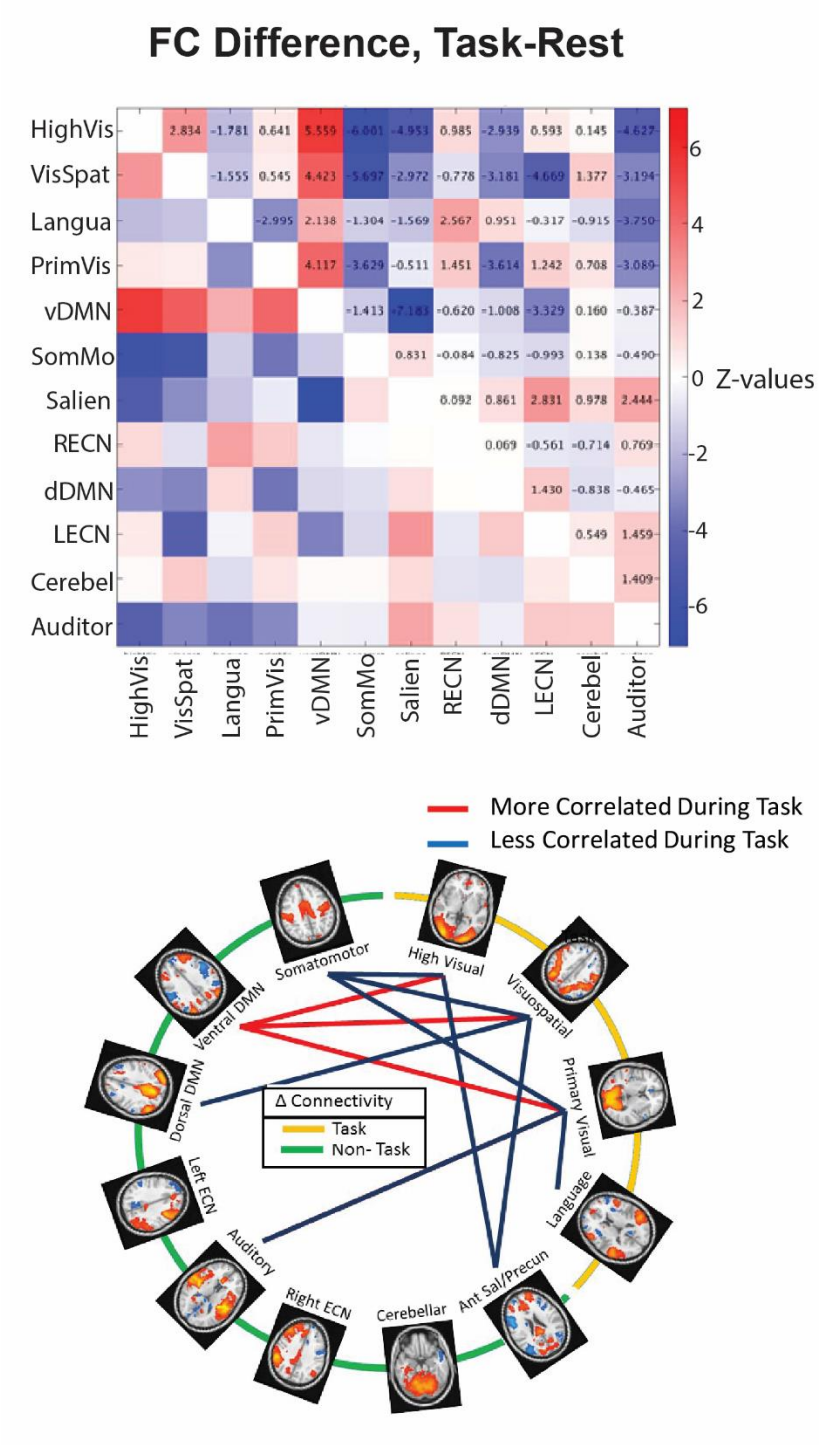

Figure 1.8. Difference between Task and Rest using T-Values (top) and Connectivity Diagram (bottom). Red indicates increased strength of connectivity during the task relative to resting-state, Blue indicates decreased connectivity during the task relative to resting-state. Connectivity was measured by cross-correlations followed by a Fischer's R-to-Z transform, in which t-values were computed. A Bonferroni correction for multiple comparisons was applied. Adapted from Marussich et al. (2015).

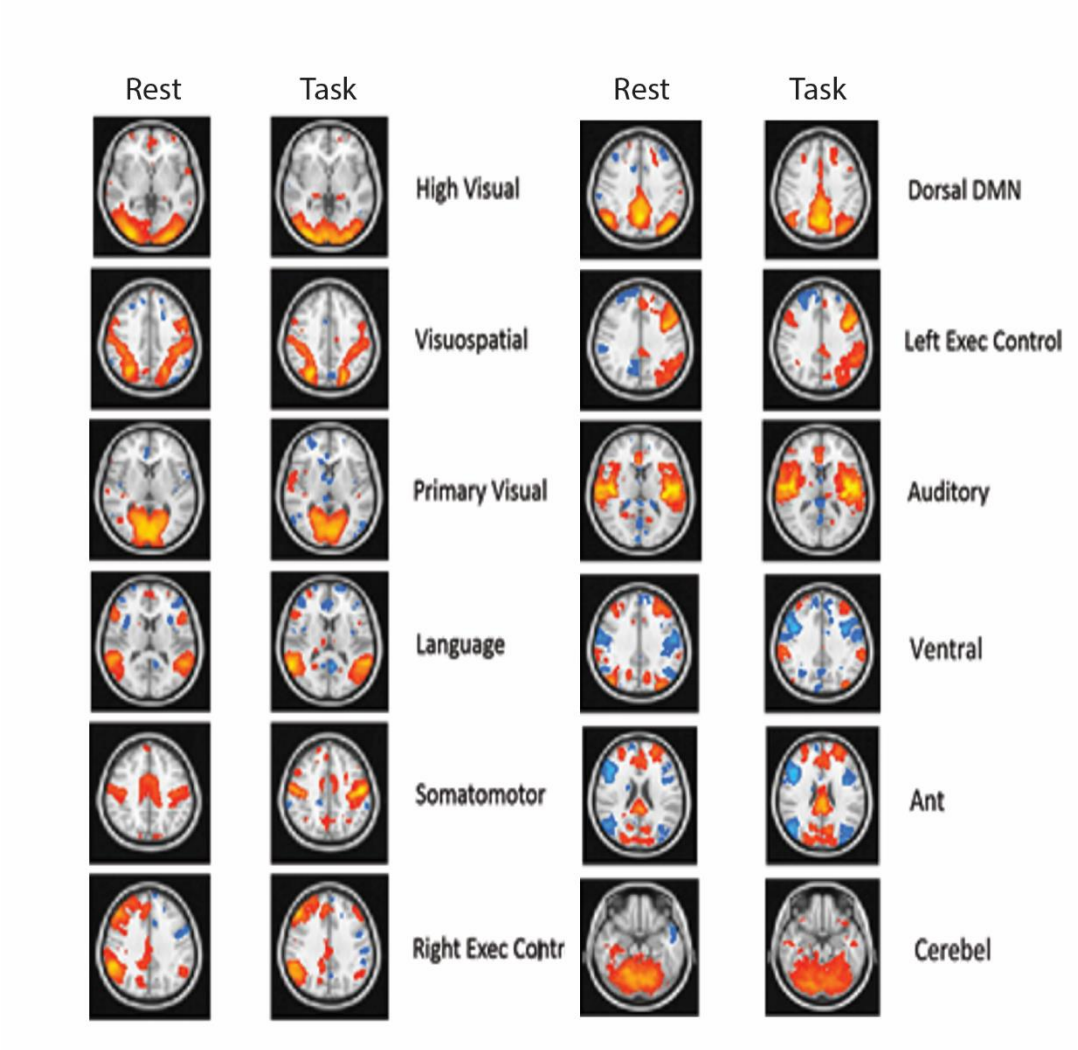

Figure 1.9. Consistent spatial configuration of task and resting-state networks derived from spatial independent component analysis (ICA).

2. MAPPING WHOLE BRAIN FUNCTIONAL ORGANIZATION AT REST AND DURING NATURALISTIC VISUAL PERCEPTION

*The contents of this chapter have been submitted for review with *Human Brain Mapping*

2.1 Rationale

Functional connectivity (FC) captures the correlation of different networks or regions of the brain. Its structure and dynamics have been useful in characterizing the brain's functional organization. Patterns of FC are similar across distinct states of consciousness (Horovitz et al., 2008; Vincent et al., 2007), and they are also largely conserved during the performance of various tasks (Arfanakis et al., 2000; Cole et al., 2014; Fair et al., 2007; Gratton et al., 2016; Harrison et al., 2008; Krienen et al., 2014). However, increasing evidence suggests that FC is altered within and between brain states (Buckner et al., 2013; Hutchison et al., 2013; Mennes et al., 2013; Rehme et al., 2013; Sepulcre et al., 2010; Van Dijk et al., 2010). It leads to the potential use of FC as a network signature of how the brain engages itself in various behavioral or cognitive tasks, e.g. watching a movie. In fact, FC signatures have been used to accurately classify a multitude of brain states (Gonzalez-Castillo et al., 2015), leveraging this notion.

During a task, brain activity measurements reflect a mixture of spontaneous and evoked activities. Disentangling their differential contributions to the pattern of apparent FC is essential to proper interpretation of any FC difference between a task and resting-state, or between different tasks. If the task-dependent FC is due to the task-evoked activity, its pattern reflects the network interactions directly involved in information processing for task execution. If the task-dependent FC is attributed to ongoing activity, its pattern is driven by the brain's functional re-organization or adaption to facilitate the task. Alternatively, evoked activity may interact with spontaneous activity. As such, the task-dependent FC should reflect correlational changes in both task-evoked networks and spontaneously emerging networks.

There is a lack of consensus on the relationship between evoked and ongoing activities. Some prior studies suggest that task-evoked activity is independent from spontaneous neural processes (Arieli et al., 1996; Mäkinen et al., 2005; Tsodyks et al., 1999). Initial evidence has led

to the notion that spontaneous and evoked processes linearly sum to yield the activity observed during a task (Arieli et al., 1996; Azouz and Gray, 1999; Becker et al., 2011; Fox et al., 2006b; Saka et al., 2010). There are, however, other reports to the contrary. Using electrophysiology, several groups have shown a reduction in neural variability following the onset of a stimulus, suggesting that the task suppresses ongoing activity during the task (Borg-Graham et al., 1998; Churchland et al., 2010; Finn et al., 2007; Oram, 2011; Ponce-Alvarez et al., 2013). Using fMRI, He (2013) also found a negative interaction between spontaneous activity and task-evoked activity during a visual attention task. However, how (and whether) such an interaction may occur with respect to functional connectivity has not been fully investigated.

Prior studies have established some valuable analysis methods to address this question. Simony et al. proposed the use of inter-subject functional connectivity (ISFC) during sustained and natural stimulation to extract task-evoked networks without contributions from ongoing activity or non-neuronal noise (Simony et al., 2016). For any given pair of regions, cross-correlation between one subject's time series in one region with the mean time series from all other subjects in the other region was only attributable to task-evoked activity. This technique builds off of the Hasson et al. (2004) study, which showed that natural stimulation gave rise to reliable responses reproducible across individuals. Like ISFC, a similar strategy is to assess the inter-regional correlation across different sessions of the same stimuli for the same subject (Lu et al., 2016; Wilf et al., 2017), while further discounting the variation across subjects.

Using this strategy in this study, we sought to examine whether task-evoked networks were additive to spontaneous networks and were able to explain the change in FC during movie watching relative to the resting state (or the "task-rest FC" difference for simplicity). To address these questions, we began with examining the seed-based correlations for exploratory analysis, and subsequently performed systematic analysis of functional connectivity among brain parcels or networks.

2.2 Methods and Materials

2.2.1 Subjects

Thirteen healthy volunteers (20 – 31 years old, 6 females, 10 right-handed, normal or corrected to normal vision) participated in this study in accordance with a protocol approved by

the Institutional Review Board at Purdue University. Three subjects were excluded because they either were self-reported to fall asleep or had excessive head motion during the experiment.

2.2.2 Experimental Design

Each of the remaining 10 subjects underwent four fMRI sessions with two conditions. Two sessions were obtained in the eyes-closed resting state, and the other two sessions occurred during free-viewing of an identical movie clip (The Good, the Bad, and the Ugly, 1966, from 162:54 to 168:33 min. in the film), as used in prior studies (Hasson et al., 2004; Lu et al., 2016). The visual stimulus was presented using the MATLAB Psychophysics Toolbox (Brainard, 1997; Pelli, 1997); it was delivered to the subjects through a binocular goggle system (NordicNeuroLab, Norway) mounted on the head coil. The display resolution was 800×600; through the goggle system, the visual field covered by the movie was about 26.9°×20.3°. No sound was presented during the movie. Each movie-stimulation session began with a blank gray screen presented for 42 s, followed by the movie presented for 5 min and 37 s, and ended with the blank screen again for 30 s. The resting-state sessions had the same duration as the movie-stimulation sessions. The session order was randomized and counterbalanced across subjects. For simplicity, hereafter the resting-state and movie-stimulation sessions were referred to as the "rest" and "task" conditions, following the general notions in a broader context (Cole et al., 2014).

2.2.3 Data acquisition

Whole-brain structural and functional MRI images were acquired using a 3-Tesla Signa HDx MRI system (General Electric Health Care, Milwaukee, USA). As described previously (Marussich et al., 2017), the fMRI data were acquired using a single-shot, gradient-recalled (GRE) echo- planar imaging (EPI) sequence (38 interleaved axial slices with 3.5mm thickness and 3.5 × 3.5 mm^2 in-plane resolution, TR=2000 ms, TE=35 ms, flip angle=78°, field of view=22×22 cm^2). T1-weighted anatomical images covering the whole head were acquired with a spoiled gradient recalled acquisition (SPGR) sequence (1×1×1mm^3 voxel size, TR/TE=5.7/2ms, flip angle=12°). A 16-channel receive-only phase array coil (NOVA Medical, Wilmington, USA) was used for image acquisition.

2.2.4 Pre-Processing

Pre-processing of the fMRI images was carried out with a combination of AFNI (Cox, 1996), FSL (Smith et al., 2004), and MATLAB (Mathworks, Natick, MA). T_1-weighted anatomical images were non-linearly registered to the Montreal Neurological Institute (MNI) brain template using a combination of *flirt* and *fnirt* in FSL (Smith et al., 2004). T_2*-weighted functional image time series were corrected for slice time variations using *slicetimer* in FSL, co-registered to the first volume within each series to account for head motion using *mcflirt* in FSL, restricted to within-brain tissues using *3dcalc* in AFNI (Cox, 1996), aligned to the T_1-weighted structural MRI using FSL's Boundary Based-Registration (BBR) function (Greve and Fischl, 2009), and registered to the MNI space with 3-mm isotropic voxels using *applywarp* in FSL. The first six volumes in the fMRI data were discarded to avoid any pre-steady-state longitudinal magnetization.

For the task sessions, we only analyzed the fMRI data during the movie while excluding any transient fMRI response during the first few seconds since the start of the movie. Thus, we excluded the first eight seconds and the last fourteen seconds of the movie. For each session and each voxel, the voxel time series was detrended by regressing out a third-order polynomial function that modeled the slow trend; the detrended signal was bandpass filtered (0.0001 - 0.1 Hz). Spatial smoothing was applied by using a Gaussian kernel (FWHM=6 mm), and the spatially smoothed voxel time series were demeaned and normalized to unit variance. The global signal, i.e. the time series averaged across all brain voxels, was regressed out in all subsequent analyses except for the ICA-based whole-brain parcellation.

2.2.5 Seed-Based Functional Connectivity in Rest Versus Task

We first explored the difference in seed-based correlation patterns between the resting state and the task state. For this purpose, seed voxels were selected from the primary visual cortex (V1), the middle temporal visual area (V5), precuneus (PCu), and primary motor cortex (M1); each of these regions of interest was defined in an independent study (Shirer et al., 2012). The MNI coordinates of these seed regions were (0, -54, 30) for PCu, (0, -87, 9) for V1, (48, -78, 0) for V5, and (39, -18, 57) for M1. These seed locations were chosen because they are representative of major functional systems activated by visual (V1 and higher visual areas) or motor tasks (M1), or deactivated by cognitive tasks (PCu as a part of the default-mode network).

Within either a rest or task session, the correlation between the seed voxel's time series and every other voxel's time series was calculated (after global signal regression), and the correlation coefficient was converted to a z-score using the Fisher's transform. The voxel-wise z-score was averaged across all rest (or task) sessions from all subjects. The significance of the mean z-score (against zero) was evaluated by using one-sample t-test (df = 19) corrected at the false discovery rate (FDR) $q<0.05$. The above analysis was performed separately for the rest and task conditions.

To determine the task-rest FC difference, the mean z-score of the movie sessions was then compared to the mean z-score of the resting-state sessions using a paired t-test (df = 19, $p<0.001$, uncorrected). Then, to determine the task-evoked FC, the seed voxel's time series in session 1 was cross-correlated with the time series of all voxels in session 2 for each subject; the resulting Pearson correlation values were z-transformed to allow for parametric statistical testing. This process was repeated was repeated using seed voxels in session 2 with cross-correlations to all voxels in session 1. To determine the statistical significance of the results, the mean z-score was compared to zero using one-sample t-tests for the task-evoked connectivity (df = 19, $q<0.05$, FDR corrected). This process is illustrated in Fig. 2.1.

2.2.6 Whole Brain Functional Connectivity

To compare the task-rest FC difference to the task-evoked FC in a systematic manner encompassing the whole brain, neural activity was decomposed into smaller networks and/or regions using three different methods: 1) using a 17-network atlas (Yeo et al., 2011), 2) via networks obtained using spatial independent component analysis (ICA), and 3) using a fine-grained, 246-region functional atlas (the Brainnetome Atlas) (Fan et al., 2016) (Fig. 2.2). The 17-network atlas was from http://surfer.nmr.mgh.harvard.edu/fswiki/CorticalParcellation_Yeo2011 and the 246-region Brainnetome Atlas was obtained from http://atlas.brainnetome.org/. Using the 17-network and 246-functional parcellation atlases, the mean intensity of brain regions over time was regressed from the signal.

Group spatial ICA using the Infomax algorithm (Bell and Sejnowski, 1995) was applied to data after two additional processing steps. Prior to ICA, the data was concatenated across all subjects, sessions, and conditions; principal component analysis (PCA) was applied to the data such that 95% of the variance was retained. After ICA was applied to this result, 30 independent

components were obtained; of those, 24 networks corresponded to canonical resting-state networks (RSNs) (Beckmann et al., 2005; De Luca et al., 2006; Power et al., 2011). One component with a global pattern was excluded from the analysis. Then each session's time course was obtained by regressing the group spatial map into the session's 4D dataset.

Large-scale FC was assessed within the resting-state and within the movie task ("mixed" FC). To create the within-session resting-state and movie FC, the correlations between each pair of networks or regions calculated based on based on their corresponding time series, and then the correlation coefficient was converted to the z-score. Significant correlations were identified using one-sample t-tests for each pair of regions in each condition (df = 19), FDR-corrected at $q < 0.03$. Then, task-rest FC differences were evaluated by subtracting the resting-state z-scores from the movie z-scores for each pair of regions. Significant differences were evaluated using paired t-tests (df = 19), FDR corrected at $q < 0.03$. Finally, to obtain the task-evoked FC, the cross-correlations between each network/region's mean time series in session 1 (rows) and the mean time series in session 2 (columns) were determined and z-transformed. We also included the transposes of the task-evoked matrices (i.e. cross-correlation of session 2's time series (rows) with session 1's time series (columns)) for each subject, yielding two task-evoked FC matrices per subject. This was done in order to generate a complete and symmetric result after hypothesis testing; individually, each matrix was not symmetric because the parcels' time series from session 1 to session 2 were not identical. We then evaluated significant correlations using one-sample t-tests (df = 19), FDR-corrected at $q < 0.03$. Because our focus was on the functional connectivity between regions or networks, we ignored the correlation within the exact same region or network itself in our analysis.

In order to further characterize the similarity of the FC profiles, we performed a session-wise cross-correlation analysis of the FC matrices prior to hypothesis testing. Spatial cross-correlations between the resting-state FC matrices and the movie FC matrices were calculated for each pair of sessions (e.g. Subject 1 Rest Session 1 with Subject 1 Movie Session 1, and so on). Lower triangular elements (from one element below the diagonal) were used in these correlation calculations to represent only unique, meaningful information from these symmetric matrices. Then, spatial cross-correlations were calculated between the task-rest FC difference matrices and the task-evoked FC matrices. In this case, the lower triangular elements of the first session's FC difference (e.g. Subject 1 Movie Session 1 cross-correlation matrix – Subject 1 Rest Session 1 cross-correlation matrix, a symmetric matrix) were cross-correlated with the lower triangular

elements of that subjects' first task-evoked FC matrix (e.g. Subject 1 Movie Session 1's time series cross-correlated with Subject 1 Movie Session 2's time series, not a symmetric matrix), and the second session's difference (e.g. Subject 1 Movie Session 2's cross-correlation matrix – Subject 1 Rest Session 2's cross-correlation matrix) was correlated with the lower triangular elements of the transpose of the task-evoked FC matrix (e.g. Subject 1 Movie Session 2's time series cross-correlated with Subject 1 Movie Session 1's time series). This was done to maximize the information obtained from individual subjects because, at each pair of parcels (an element in an FC matrix), there were two possible FC results: Parcel 1 Session 1's time series cross-correlated with Parcel 2 Session 2's time series and Parcel 1 Session 2's time series cross-correlated with Parcel 2 Session 1's time series.

2.2.7 Comparing Significant Task-Rest FC Differences with Task-Evoked FC

The specific functional connectivity implicated in the task-rest FC difference and the task-evoked FC were investigated using the fine-grained, 246-region parcellation's information. To test the significance of the functional connectivity between each pair of regions and/or networks, the average z-score was compared against zero by performing one- sample t-test on the z-score of every pair regions ($q < 0.03$, FDR corrected). The significant correlations for each analysis method were then compared in terms of reproducibility.

2.2.8 Explaining the Task-Rest FC Differences with Task-Evoked FC

To determine the extent to which the task-evoked FC explains the task-rest FC difference, we used the task-evoked FC matrices as regressors for the task-rest FC difference matrices at the session-level. This was performed separately using 1) the Yeo et al. 17-network atlas (2011), 2) the previously obtained 24 spatial ICs, and 3) the 246-region Brainnetome Atlas (Fan, et al., 2016). For each subject, the lower triangular elements (from one element below the diagonal) of task-evoked FC matrix were used as regressors for the lower triangular elements of the first session's FC difference matrix (i.e. Subject 1 Session 1 Task cross-correlation matrix – Subject 1 Session 1 Rest cross-correlation matrix). Then, using the transpose of the task-evoked FC matrix, the resulting lower triangular elements were taken as regressors for the second session's lower triangular elements of the FC difference matrix (i.e. Subject 1 Session 2 Task cross-correlation matrix – Subject 1 Session 2 Rest cross-correlation matrix). After obtaining regression coefficients

for each session, the estimated lower triangular elements of the task-rest FC difference matrix for that session were obtained by multiplying the calculated regression coefficients with the corresponding lower triangular elements of the task-evoked FC matrix. Then, the variance of the lower triangular elements of each session's estimated task-rest FC difference matrix was divided by the variance of the lower triangular elements of the same session's measured task-rest FC difference to yield the percentage of the task-rest FC difference that was explained by the task-evoked FC.

2.3 Results

2.3.1 Seed-Based FC Distributions

Seed voxels from the PCu, V1, V5, and M1 were used to assess voxel-wise FC at rest, voxel-wise FC during the naturalistic visual task (i.e. the "mixed" FC), the difference between these two states, and the task-evoked FC (Fig. 2.3, findings projected onto the surface).

FC patterns in the resting-state and during the movie were mostly consistent among the four seeds, but there were some differences between the two conditions. Although the PCu seed exhibited similar, positive distributions in both conditions, the anti-correlated voxels were more widespread during the movie task (Fig. 2.3A, far left and left middle columns). In the resting-state, the V1 seed (Fig. 2.3B, far left and left middle columns) was coupled not only to higher visual areas more laterally, but also to the superior/medial motor cortex; during the movie task, the broad primary visual cortex indeed was significantly correlated, but no coupling to other regions was observed. In addition, the V5 seed was more correlated to more medial visual areas (e.g. fusiform gyri) during resting-state (Fig. 2.3C, far left and left middle columns). Finally, the M1 seed elicited FC with visual regions at rest, but such correlations were more narrowly confined during the movie task (Fig. 2.3D, far left and left middle columns).

The task-evoked and task-rest FC difference distributions were largely very different. Using FDR-corrected thresholds, task-evoked FC was observed using the V1 and V5 seeds but not using the PCu and M1 seeds, in line with the findings of others (Kim et al., 2017; Wilf et al., 2017). Thus, the V1 and V5 seeds allowed for more in-depth analysis in that they were significantly activated by the naturalistic visual task. The positively connected voxels to V1 in the task-evoked FC (Fig. 2.3B, far right column), were, in fact, more weakly connected to the seed during the

movie than at rest (Fig. 2.3B, right middle column). Voxels which were more strongly correlated to the V1 seed during the movie than resting-state tended to instead lie within frontoparietal control networks (Niendam, et al., 2012). Moreover, the positively correlated voxels to the V5 seed arising from task-evoked activity (Fig. 2.3C, far right column) were not significantly different between the movie task and resting-state (Fig. 2.3C, right middle column) despite qualitatively appearing stronger during the movie (Fig. 2.3C, far left and left middle columns). Instead, with this seed, the movie condition elicited significantly more negative FC between motor and precuneus regions as compared to rest, with some more positive FC during the movie in the right lateral frontal cortex (Fig. 2.3C, right middle column). Instead, with this seed, the movie condition elicited significantly more negative functional connectivity between motor and precuneus regions as compared to rest, with some more positive connectivity in the right lateral frontal cortex and scattered through some white matter regions (Fig. 2.3C, right middle column).

When comparing the task-evoked networks from the V1 and V5 seeds (Figs. 2.3B and 2.3C, far right columns) to the corresponding resting-state networks (Figs. 2.3B and 2.3C, far left and left middle columns), we observed that these regions were more restricted using an inter-session approach than they were within-session during both the movie task and resting-state. Overall, there was little coupling of the primary and higher visual cortices to other parts of the visual system, let alone to other cortical regions.

2.3.2 Whole-Brain Differences Between Task and Rest Conditions

Whole brain patterns of resting-state FC, task FC (still containing spontaneous activity), the task-rest FC difference, and task-evoked FC were evaluated in a systematic manner using three different atlases: 1) a 17-network atlas (Yeo et al., 2011), 2) networks obtained using spatial independent component analysis (ICA), and 3) a 246-region functional atlas (the Brainnetome Atlas) (Fan et al., 2016). Because the ICA components used were derived in-house, we have provided them in Fig. 2.6; the 24 ICs that were used corresponded to 40.1% of the variance of the signal present in the concatenated data. Based on this more systematic approach, similar overall findings were observed to those we had uncovered with the previous seed-based approach (Fig. 2.4A).

Similarity between the within-session resting-state and mixed (task-evoked + spontaneous) FC profiles was again made apparent, although the resting-state again showed more widely

distributed FC (Fig. 2.4A). There was stronger functional connectivity from visual areas (all methods), the dorsal attention network (17-network atlas), and dorsal default mode network (dDMN) (ICA) to other networks during resting-state. Within-visual functional connectivity (e.g. Vis1 to Vis2) were surprisingly weaker during the movie as compared to rest. At the $q < 0.03$ level, the 17-network atlas yielded no significantly different correlations among visual regions, ICA gave rise to 3 significantly different correlations ($t = -5.2323$ to -5.2042, $q = 0.0072$-0.0081), and the 246-region parcellation resulted in 4 significantly different correlations ($t = -7.9544$ to -6.3931, $q = 0.0046$-0.0196).

Moreover, non-visual sensory networks (e.g. somatomotor, auditory networks) exhibited weaker FC strengths with visual areas during the movie. With respect to visual-somatomotor FC, the 17-network atlas gave rise to 3 significantly different correlations ($t = -7.0622$ to -4.5202, $q = 0.0008$-0.0250), ICA resulted in 6 significantly different correlations ($t = -8.0592$ to -4.7280, $q = 0.0003$-0.0147), and the 246-region parcellation yielded 14 significant correlations ($t = -7.0389$ to -5.8485, $q = 0.0129$-0.0291). Auditory regions were included within the Som2 region in the Yeo et al. parcellation (2011); therefore, we were unable to evaluate the visual-auditory FC using this atlas. However, we observed 4 significantly weaker visual-auditory correlations during the movie using ICA ($t = -6.5712$ to -4.4074, $q = 0.0012$-0.0259) and 23 significantly weaker correlations using the 246 region parcellation ($t = -11.0213$ to -5.8682, $q = 0.0004$-0.0291).

In addition, frontoparietal networks (i.e. executive control networks) displayed stronger FC with visual regions during the movie. Using the 17-network atlas, we observed 4 significantly different visual-frontoparietal correlations ($t = 4.3116$-4.5027, $q = 0.0228$-0.0281), no significantly different correlations with ICA ($q<0.03$), and 12 significantly more positive correlations using the 246-region parcellation that all involved the right inferior frontal junction (IFJ R) ($t = 5.9733$-9.2107).

Finally, by cross-correlating the resting-state and movie FC profiles, it was evident that baseline connectivity patterns in the two states were highly similar, though not entirely so (mean $\pm$ SD: 17-network: $r = 0.6064 \pm 0.1100$; ICA: $r = 0.5503 \pm 0.0900$; 256-region: $r = 0.5086 \pm 0.0928$) (Fig. 2.4B).

2.3.3 Whole-Brain Patterns: Task-Rest FC Difference Versus Task-Evoked FC

Using the different parcellations, we also uncovered additional similar results to what we had observed using seed-based FC: that the task-evoked FC and task-rest FC differences were strikingly different. Task-evoked FC gave rise to 5 significant correlations using the 17-network parcellation (3.67%), 3 significant correlations using ICA (1.21%), and 174 significant correlations using the 246-region parcellation (0.577%). Examining the task-rest FC difference while using the 17-network atlas, only two of these five correlations (40%, Vis1-Som1 and Som2-dAt1) were found to be both significant and in the same direction (i.e. both more connected or more disconnected during the movie) as in the task-evoked profile. None of the significant task-evoked correlations found using ICA were also significant in the task-rest FC difference (0%). Finally, only four of the significant task-evoked correlations found using the 246-region parcellation (2.30%) were also significant and in the same direction in the task-rest FC difference (A37mv L to A1/2/3tru R, A39c R to G R, A1/2/3tru R to rLinG R, and G R to mOccG L). In fact, two significant task-evoked correlations were significant with the opposite sign in the task-rest difference (rCunG R to cCunG R and msOccG R to msOccG L).

This result is surprising considering the comparable number of significant correlations with respect to the task-rest difference: 10 correlations using the 17-network atlas (7.35%), 21 correlations using ICA (7.31%), and 140 correlations using the 246-region parcellation (3.05%). Overall, the significant functional connectivity found using task-evoked FC were not at all reproduced by the task-rest difference (Fig. 2.4A). Finally, the correlation analysis further quantitatively validated that the task-rest FC difference and task-evoked FC had very little similarity (mean ± SD: 17-network: $r = 0.2330 \pm 0.1923$; ICA: $r = 0.1487 \pm 0.1120$; 256-region: $r = 0.1413 \pm 0.0771$) (Fig. 2.4C).

2.3.4 Specific Differences Between Task-Evoked FC and the Task-Rest FC Difference

In the interest of revealing more in-depth information about the fine-scale differences between the FC profiles elicited by the task-evoked FC and the task-rest FC difference, the significant correlations were plotted in connectivity circle graphs and compared (Fig. 2.3). Indeed, these graphs are vastly different, with very little overlap. Visual regions using the fine-scale 246-region parcellation were considered to consist of areas in the lateral occipital cortex, medioventral occipital cortex, and fusiform gyrus.

Task-evoked FC indicated that visual regions were positively coupled with one another due to the movie task using all three methods (Fig. 2.4A). Using the 17-network Yeo et al. atlas (2011), the Vis1 to Vis2 functional connectivity was significant (t = 7.5001, q = 0.0003). In addition, we discovered that there were three significant correlations involving the Vis1, Vis2, and Vis 5 ICA networks (t = 6.8589-7.9547, q = 0.0005-0.0009). The 246-network Brainnetome parcellation (2016) gave rise to 280 significant correlations within visual areas (t = 5.7474-17.2342, q = 1.5347×10^{-7}-0.0291); every parcel within the Lateral Occipital Cortex, MedioVentral Occipital Cortex, and Fusiform Gyrus was positively connected with at least one other parcel within those regions. However, the areas implicated in these correlations were actually more positively coupled with one another during resting-state than during the movie, eliciting mostly negative, but largely not significant, t-values in terms of the task-rest FC difference using all three parcellations. The Vis1 to Vis 2 functional connectivity in the 17-network atlas fit this pattern, though the difference was not statistically significant (t = -1.9711, q=1.0535). Similarly, using ICA, the Vis1 to Vis 2 correlation was marginally weaker during the movie (t = -2.0315, q=0.8544), but the Vis1 and Vis2 to Vis 5 correlations were slightly, but not significantly, positive (t = 0.4500-2.8524, q = 0.2491-4.8305). Using 246-region parcellation, 81.43% of the significant (and entirely positive) task-evoked correlations in fact gave rise to negative task-rest FC differences. Of these, two correlations were statistically significant (t = -7.9544 to -6.6811, q = 0.0046-0.0159). The results of the 246-region parcellation can be more easily appreciated using the circle graphs (Fig. 2.3); the within-visual correlations that dominate the task-evoked FC connectivity graph (Fig. 2.3B) were almost completely non-existent with respect to the task-rest FC difference (Fig. 2.3A). The spatial locations of these regions are shown in Fig. 2.8.

Additionally, when assessing task-evoked FC, we were largely unable to observe the previous finding that sensory regions not recruited by naturalistic visual stimulation (e.g. somatomotor, auditory regions) were more negatively coupled with visual regions. The 17-network atlas demonstrated only one significant task-evoked correlation between Vis1 and Som1 (t = -4.9515, q = 0.0165) that was reproduced in the task-rest FC difference (t = -6.0447, q = 0.0020), and there were no significant task-evoked correlations with visual to auditory and visual to somatomotor regions found using ICA (t = -4.6912-1.622, q = 0.0680-6.0868). Using the 246-region parcellation (Fig. 2.4A – right column, Fig. 2.5), there were 3 significant task-evoked correlations between visual and auditory areas, which all involved TE1.0/TE1.2 R and TE1.0/1.2

L in the superior temporal gyrus (t = -6.8119 to -5.8406, q = 0.0049-0.0246). These specific correlations were not observed to be significant in the task-rest FC difference (t = -4.2848 to -5.1558, q = 0.0533-0.1310). Additionally, there were 6 significant task-evoked correlations between visual and somatomotor areas involving A1/2/3tru R and A1/2/3tru L in the post-central gyrus and A4ul R in the pre-central gyrus (t = -7.7223 to -5.8511, q = 0.0049-0.0246) (Fig. 2.3B); of these, only two (A37mv L to A1/2/3tru R and rLinG R to A1/2/3 R) were reproduced in the task-rest difference (t = -6.6699 to -6.5433, q = 0.0156-0.0179) (Fig. 2.3A).

Frontoparietal networks (i.e. executive control networks) were not observed to have significant task-evoked FC with visual networks using the 17 network parcellation and ICA, in contrast with positive FC differences that were observed. The 246-region parcellation yielded 4 positive task-evoked visual correlations with frontoparietal regions, specifically with A7c (Superior Parietal Lobule) and A39c (Inferior Parietal Lobule) (t = 6.0503 – 7.2768, q = 0.0022-0.0170) (Fig. 2.3B). None of these correlations were significant at the q < 0.03 level in the task-rest FC difference (t = 2.8834-5.2753, q = 0.0478-0.7629) (Fig. 2.3A). Moreover, the positive visual functional connectivity from visual areas to the inferior frontal junction (IFJ) that were strongly evident in the task-rest FC difference graph were not at all observed in the task-evoked FC at the q < 0.03 level (t = 0.0241 – 5.4687, q = 0.0472-10.8194) (Fig. 2.3).

We also observed stronger visual-to-thalamus FC within-session during the movie than at rest; these differences were not observed during the task-evoked FC (Fig. 2.3). The 17-network parcellation and ICA networks did not include any thalamus-specific networks (Fig. 2.4A, left + middle), but the Brainnetome parcellation was fine-grained enough to more reliably segregate relationships regarding the basal ganglia and thalamus (though it did not provide classical thalamic nuclei, such as the lateral geniculate nucleus). Eleven significant correlations were uncovered from visual regions to the thalamus when investigating the task-rest FC difference (t = 5.8489-6.4350, q = 0.0191-0.0293) (Fig. 2.3A). Conversely, there were zero significant task-evoked correlations between any visual and thalamus regions (t = -3.3433-4.1352, q = 0.3524-10.8733) (Fig. 2.3B).

2.3.5 How Much of the Task-Rest FC Difference Is Explained by the Task-Evoked FC?

After linearly regressing the task-evoked FC from the task-rest FC difference using 1) the Yeo et al. 17-network atlas (2011), 2) the previously obtained 24 spatial ICs, and 3) the 246-region Brainnetome Atlas (Fan et al., 2016), we determined that the mean percent variance explained by

the task-evoked FC for the 17-network atlas was 15.86 ± 3.30%, 5.19 ± 1.25% for the ICA maps, and 3.55 ± 0.73% for the 246-region atlas (all values: mean ± SEM); the mean value was calculated across sessions. Taking the mean percent variance of these three methods yielded an overall value of 8.20 ± 1.40% across both sessions and methods. Thus, only about 3-15% of the task-rest FC difference can be explained by the task-evoked FC.

2.4 Discussion

We have shown that the difference between FC at rest and during a task, which contains an unknown mixture of task-evoked and spontaneous signals, cannot be explained by separating the task-evoked FC from the connectivity profile. The results lead to the following findings: 1) connectivity between resting-state and task states is mostly conserved; 2) during the resting-state, non-visual sensory-related functional networks (e.g. somatomotor, auditory) were more coupled to visual networks than during the natural movie; 3) the task-evoked FC was predominantly characterized by positive and restricted correlations among regions within the visual system, and 4) task-evoked FC accounted for only 3-15% of the FC difference between task and rest conditions. Therefore, the results suggest that the task-evoked FC and the spontaneous FC are neither linear nor additive, which was somewhat surprising to us.

2.4.1 FC Is Mostly Conserved During a Task and at Rest

Consistent with several prior studies (Cole et al., 2014; Gratton et al., 2016; Krienen et al., 2014), we also identified a relatively high degree of similarity between the apparent FC during resting-state and the task using both seed-based and whole-brain methods (Pearson correlation values of 0.5-0.6, Fig. 2.4B). This is likely due to the presence of dominating spontaneous, ongoing sources in both conditions that strongly contribute to the signals correlated with one another in FC fMRI. Despite this similarity, however, we observed more widespread connectivity in the resting-state, as well as stronger within-visual coupling as compared to during the movie task.

2.4.2 Apparent FC Differences Between Rest and Task Are Not Explained by Task-evoked Correlations

Task-evoked FC was only observed within task-related, visual regions. These areas appeared to be more restricted and less coupled to other regions than in the resting-state or during

the task (Fig. 4.1). In contrast, the connectivity differences involving visual regions between the two conditions were predominantly negative and/or not significant. Instead, we found widespread negative differences between task-related networks and non-visual sensory areas (e.g. somatomotor, auditory cortices). In addition, thalamic regions, which have not often been incorporated in analyses of FC changes, were more anti-correlated with one another and more positively correlated to portions visual cortex during the movie task. Finally, positive functional connectivity from the occipital cortex and fusiform gyrus to the inferior frontal junction (IFJ) resulted from the subtraction that also were not reproduced; functionally, the IFJ has been implicated in attentional circuits and in cognitive control (Baldauf and Desimone, 2014; Sundermann and Pfleidferer, 2012). Overall, these differences between rest and task FC were largely not represented in the task-evoked FC patterns.

The fact that the task-evoked FC did not reveal the difference between the FC during the task and the FC at rest (i.e. spontaneous FC) suggests that correlations in ongoing, spontaneous activity are driving this difference. Other studies have found that modulations in task state functional connectivity may be driven be changes in intrinsic networks, and that flexible "hubs", typically within the frontoparietal network, dorsal attention network, and/or default mode network, are thought to be flexible across tasks and play a role in "linking" different networks to facilitate different behavioral states (Bray et al., 2015; Cole et al., 2013; Dixon et al., 2017; Gilson et al., 2017). Therefore, it is likely that this intrinsic activity drives the coupling of task-evoked networks to other regions.

2.4.3 Rest and Task Correlations Negatively Interact

The task-evoked FC explained less than 15% of the FC differences between the task and resting-state. Therefore, it seems that the task-evoked FC and spontaneous FC are neither independent nor linearly additive. Beyond this, however, we would like to tease apart the nature of the rest-task interaction: is the task suppressing spontaneous activity or amplifying it? Our observations that the movie-watching task reduced the extent and strength of FC suggest that the task suppresses spontaneous correlations. This can be explained mathematically:

If X_o is the spontaneous activity and X_e is the task-evoked activity, and if the two sources are independent, the measured activity during the task, X_m, would be described by

$$X_m = X_o + X_e$$

if X_o and X_e are independent. Rearranging, the inequality becomes

$$X_m - X_o = X_e$$

However, if instead the spontaneous activity is suppressed during the task, the equation then becomes

$$X_m < X_o + X_e$$

rearranging to

$$X_m - X_o < X_e$$

Therefore, the difference may yield smaller and/or more negative values than actually reported by the task-evoked activity.

This can be re-written using covariances to reflect FC relationships for locations 1 and 2:

$$cov(X_{m1},X_{m2}) = cov(X_{o1}+X_{e1},X_{o2}+X_{e2}) = cov(X_{o1},X_{o2}) + cov(X_{e1},X_{e2})$$

if X_o and X_e are independent. (Random signal theory allows the distribution of covariances.) Rearranging,

$$cov(X_{m1},X_{m2}) - cov(X_{o1},X_{o2}) = cov(X_{e1},X_{e2})$$

If instead the spontaneous correlations during the task are suppressed,

$$cov(X_{m1},X_{m2}) < cov(X_{o1},X_{o2}) + cov(X_{e1},X_{e2})$$

Rearranging,

$$cov(X_{m1},X_{m2}) - cov(X_{o1},X_{o2}) < cov(X_{e1},X_{e2})$$

Covariances and correlations are related by a scaling factor of the standard deviations of the signals involved. We standardized the resting-state signals X_o and the mixed signals during the task X_m such that they have equal variance; therefore, a negative sign for the left side of this inequality cannot explain a positive sign in the right side (e.g. Fig. 2.3, right middle and far right columns).

Thus, the suppression of spontaneous correlations during the task may be the driving force behind what we have observed, particularly with respect to the different parts of the visual cortex.

He (2013) and several others (Churchland et al., 2010; Monier et al., 2003; Ponce-Alvarez et al., 2013), also suggest a negative task-rest interaction. Initial evidence suggests that this negative interaction may help facilitate the task execution (Boly et al., 2007; Deneux and Grinvald, 2017; Hesselmann et al., 2008) (see Northoff et al. (2010) and Ferezou and Deneux (2017) for review), or may increase with task difficulty (Garrett et al., 2014; Szostakiwskyj et al., 2017). As such, it may bear functional significance.

The negative task-rest interaction may or may not hold true for all tasks. Passive versus active task engagement may not equally affect spontaneous signals (Ferezou et al., 2006; Otazu et al., 2009). Crochet and Petersen (2006) found that active and conscious engagement in a task gave rise to more desynchronization of ongoing activity than passive or conscious states (e.g. in the anesthetized states). In our natural vision task, subjects actively engaged in the movie with free eye movement. Speculatively, cognitively engaging in the task itself, rather than simply having a visual experience, explains the nonlinear interaction between spontaneous and evoked functional connectivity. However, this remains to be tested.

Using natural vision, we noticed that the suppression of spontaneous correlations during the task was not consistent throughout the brain. The greatest magnitude of this change was within the components of the visual system; these regions exhibited the greatest dissimilarity between task-evoked FC and the apparent FC difference between the movie and resting-state conditions. These findings may be mediated simply by 1) reduced spontaneous activations in visual areas relative to other regions, or 2) by a reduced synchrony of cortical oscillations in task-related regions. In EEG, alpha band oscillations are postulated to stem from the rhythmic fluctuations of inhibitory neurons, and engaging in certain tasks such as eye-opening, desynchronizes the alpha-band power (see Klimesch et al. (2007) for review). Other reports relate resting-state inhibitory neurotransmitter concentrations, such as GABA (Muthukumaraswamy et al., 2009; Northoff et al., 2007) or anesthetics thought to modulate GABA (Maandag et al., 2007), to task-induced changes in specific regions. Here, we cannot disentangle whether location differences in spontaneous FC suppression are mediated by region-specific reduced activations or de-coupling of neuronal oscillations, but this is certainly an area for future investigation.

2.4.4 Is Resting-State Really a "Second" Cognitive State?

Another possible explanation for why the task-evoked FC did not match the task-rest FC difference lies in the mischaracterization of resting-state as a proxy for spontaneous activity. Over the last decade, the field of fMRI has been dominated by studies of the brain in the so-called resting state: a 'task-free' paradigm in which subjects are asked to lie still in the MR scanner with their eyes opened or closed (with little consensus as to which is preferred, see Patriat et al. (2013)) (Fox and Raichle, 2007; Raichle, 2015). However, as researchers in the field of dynamic functional connectivity have astutely identified, during resting-state, subjects actually engage in a variety of introspective tasks that are not temporally controlled. Using post-experiment questionnaires, Delamillieure et al. (2010) demonstrated that, during resting-state, subjects engage in visual mental imagery, inner language experiences, somatosensory awareness, inner musical experiences, and the inner processing of numbers; the average percent time reported in these different activities were 40 ± 22% (mental imagery), 30 ± 19% (inner language), 19 ± 16% (somatosensory awareness), 23 ± 17% (inner musical experiences), and 12 ± 10% (inner processing of numbers), further proving the heterogeneity of resting state. These different "mini-cognitive states" have also been shown to modulate fMRI findings (Doucet et al., 2012), and exhibit similar functional profiles to those regions active while subjects engage in internally directed mental operations (Spreng et al., 2008). Additionally, it is worth noting that this assortment of mind-wandering states during rest has also been posited as the sources of the "spontaneous multi-stability" hypothesis that attempts to reconcile increased variability during resting-state as compared to task states (Ponce-Alvarez et al., 2015).

If "resting-state" does not represent spontaneous activity, but is instead a second cognitive state, the FC difference between these two conditions may actually represent the difference between task-evoked activity and mental imagery, inner monologues, or somatosensory awareness, etc. If the FC within different parts of the visual cortex is more strongly positive during these various activities than is positive during the movie, for example, the task-rest FC difference would elicit negative values in these regions, in spite of the positive FC values obtained during the movie. However, upon close inspection of prior fMRI studies of subject-driven cognitive states, we failed to uncover strongly negative resting-state FC within parts of the visual cortex or from visual to other task areas (somatomotor, auditory) consistent with our findings (Chou et al., 2017; Doucet et al., 2012; Shirer et al., 2012). Though mind-wandering is a nearly impossible to control potential

confound in all fMRI studies using resting-state protocols, we feel it is unlikely to have driven the findings obtained in this study for those reasons.

2.4.5 Methodological Considerations

Indeed, naturalistic stimuli (Hasson et al., 2004) are of particular significance in studies of rest-task interaction. Natural stimuli provide a rich behavioral context reflective of the activities of daily life (e.g. viewing natural scenes with sharp, moving edges or engaging in conversation) that unfold over relatively long time scales (Hasson et al., 2010). It has experimentally been proven that neural responses to naturalistic stimuli are reliable and widespread (Hasson et al., 2010; Jääskeläinen et al., 2008; McMahon et al., 2015; Mukamel et al., 2005), and the connectivity patterns that appear during naturalistic activations better reflect spontaneously emerging patterns in the resting-state as compared to controlled, artificially designed stimuli (Wilf et al., 2017). Further, it has been shown that naturalistic stimuli reduce head motion, improve arousal, and lead to more stable and more individualized estimates of FC (Vanderwal et al., 2017). The high-level natural content of such movies is necessary for reproducible responses; by spatiotemporally scrambling the natural stimulus, widely distributed and highly reproducible fMRI responses cannot not be well demonstrated (Lu et al., 2016). Therefore, naturalistic visual stimuli provide rich task-evoked information about neural dynamics as compared to more traditional psychophysical stimuli (e.g. Gabor filters).

Unlike our study, Simony et al. (2016) observed default mode network FC to a seed in the Precuneus during a naturalistic auditory task. Therefore, the lack of DMN FC to the precuneus seed in Fig. 1 of this study may be surprising to some readers. However, in Supplementary Fig. 5 in Simony et al. (2016), the authors compared two different naturalistic auditory conditions and found that “belief” content (relating to inferring the beliefs held by different protagonists, found using a “Theory of Mind” localizer) was necessary for the DMN to be observed. Such content likely relates to more to introspective processes thought to relate to DMN function (Andrews-Hanna et al., 2014; Buckner et al., 2008). The control condition, in which with narratives describing photographs and maps with no belief content were presented, instead yielded a null functional connectivity result with the seed in the Precuneus. Like this control condition, the natural movie task presented little opportunity for inference about beliefs or introspection, and thus may be the source of the lack of DMN FC observed.

Optimally isolating the task-evoked activity from the unknown mixture of spontaneous activity and task-evoked activity obtained during fMRI scans is important for comprehensive studies of the difference between resting-state and task states. The presence of intrinsic activity in both conditions often leads to over-estimation of the similarity of FC estimates between rest and task (Kim et al., 2017). One way of reducing the variability present in fMRI signals from intrinsic activity is through temporal averaging; however, a very large number of subjects and/or sessions is needed to achieve appropriate statistical power. Even with a great number samples, the efficacy of simple averaging in removing spontaneous activity has been shown to be inferior to that of inter-session or inter-subject correlations (Henriksson et al., 2015; Kim et al., 2017). Moreover, using inter-session correlations allows one to generate task-evoked FC specific to each subject, which cannot be accomplished through averaging. Along these lines, between inter-session (i.e. "intra-subject") and inter-subject approaches, inter-session correlations have shown enhanced reproducibility (Henriksson et al., 2015; Lu et al., 2016). An earlier approach uses the general linear model (GLM) to construct a trial-to-trial series of activation parameters (β) for each voxel that can be cross-correlated (Mennes et al., 2013; Rissman et al., 2004); however, whether this method more effectively removes intrinsic activity than inter-session and inter-subject approaches has yet to be shown.

Further, the extent to which global signal regression (GSR) may have impacted results is a potential concern. GSR improves the spatial specificity of FC fMRI maps, but there are concerns about whether it artificially introduces anticorrelations among certain networks (Fox et al., 2009; Murphy et al., 2009; Weissenbacher et al., 2009). In addition, others have shown evidence that there may indeed be neural contributions of the global signal (Wen and Liu, 2016; Wong et al., 2013). Therefore, we repeated this analysis without performing the global signal regression step (Fig. 2.9-2.11). Overall, the same overall conclusion was formed: the task-evoked functional connectivity did not explain the FC difference between rest and task conditions. We observed stronger global correlations in the resting-state than during the task; this is most likely because there are no additional contributions from a task-evoked signal that may otherwise reduce this effect. Because of this, it was more difficult to disentangle the difference between task FC and resting-state FC. However, global correlations did not appear to have much of an effect on the task-evoked functional connectivity (comparing Figs. 2.1-2.3 with Figs. 2.9-2.11), suggesting that they are likely unrelated to visual task-related neural processing. Consequently, an additional

potential advantage of inter-session and inter-subject correlations is that the confounding effects of physiological and motion variability that are so challenging to remove from typical within-subject FC analyses are effectively reduced (Simony et al., 2016). It may be beneficial for others studying FC to consider such approaches when investigating the veridical "task" FC over traditional within-session FC analyses.

We opted not to regress head motion from subjects' fMRI signals to avoid potentially removing physiologically relevant signals. Although the majority of variation across subjects in functional connectivity subjects is not attributable to head motion, there can be significant systematic effects on estimates of coupling between different networks, particularly if the amount of motion is large (Power et al., 2012; Van Dijk et al., 2012). In general, head motion has been shown to increase estimates of FC between local regions, while reducing estimates of FC between distant regions or functionally unrelated networks(Van Dijk et al., 2012). A recent study of high frequency oscillations in fMRI, which are particularly sensitive to both head motion and the regression of related artifacts, found that group-level head motion regression had little effect on between-condition high frequency oscillation results when head motion was very small across subjects (Yuan et al., 2016). We also tightly restricted head motion allowances for included subjects such that subjects with >1 mm of translational motion or >0.035 radians of rotational motion were excluded. In addition, the time series of the seeds and parcels also did not show signal drift or abrupt changes that typically arise from head motion.

Overall, inter-session and inter-subject correlation methods have been understudied in neuroimaging, and new studies using these methods provide an additional vantage point from which we may learn about the brain. In this work, our focus was on whether the difference between the resting-state and the mixed FC observed during the task reflected the task-evoked FC. It did not, but we shed light on a suppression of correlations of spontaneous activity that occurs to facilitate a task. However, a consensus regarding this phenomenon still needs to be formed for additional researchers to fully disentangle its origins and purpose.

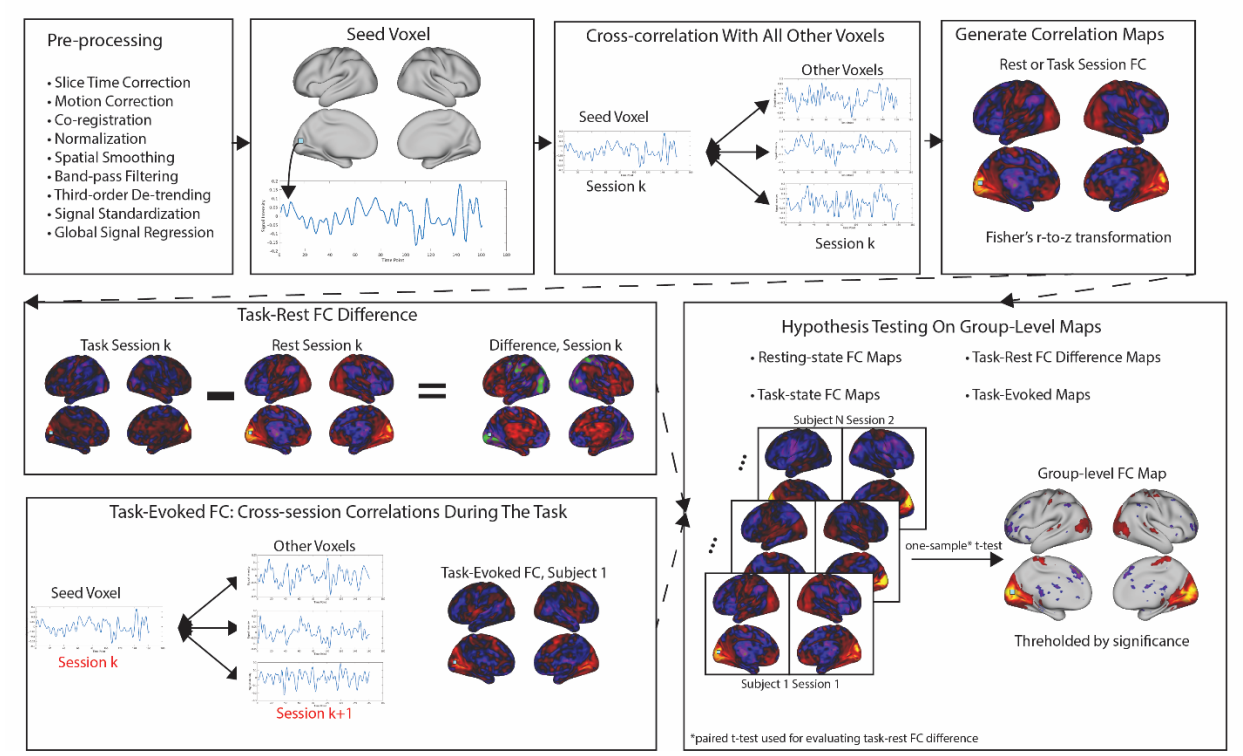

Figure 2.1. Pipeline Illustration for Seed-based Analysis. After pre-processing, a seed voxel is chosen, whose time series is correlated with that of all other voxels within that session to generate the session-level FC map for either resting-state or task conditions. The session-level resting-state FC maps are subtracted from the session-level task maps to create the FC difference maps for that session. To determine task-evoked FC maps, a seed voxel's time series in one session is correlated with all other voxels from the other session for that subject. Finally, group-level maps are determined by applying t-tests (one-sample for the resting-state, task, and task-evoked FC; paired for the task-rest FC difference) to the session-level data.

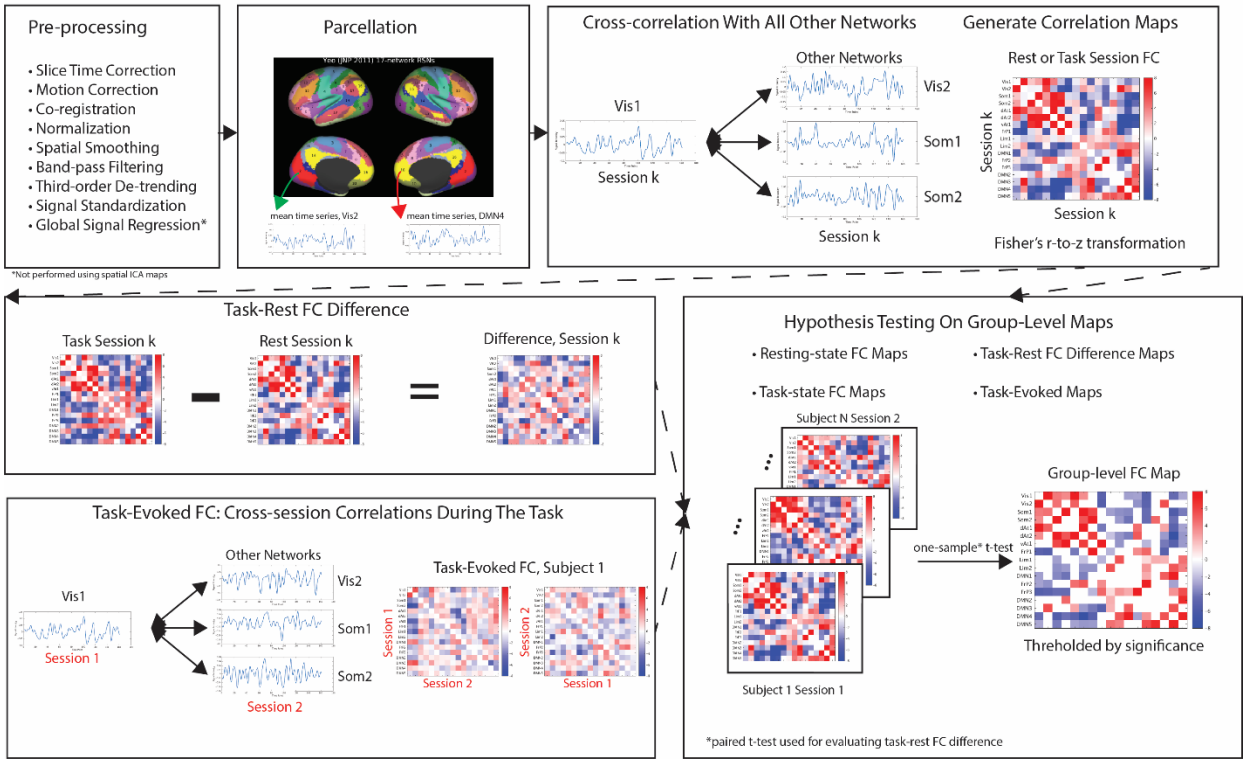

Figure 2.2. Pipeline Illustration for Parcellation-based Analysis. After pre-processing, mean time-courses for the voxels within each network are cross-correlated with one another to generate session-level FC matrices. The session-level resting-state FC matrices are subtracted from the session-level task matrices to create the FC difference matrices for that session. To determine task-evoked FC maps, the networks' mean time series in one session are correlated with the networks' mean time series from the other session for that subject. Finally, group-level maps are determined by applying t-tests (one-sample for the resting-state, task, and task-evoked FC; paired for the task-rest FC difference) to the session-level data.

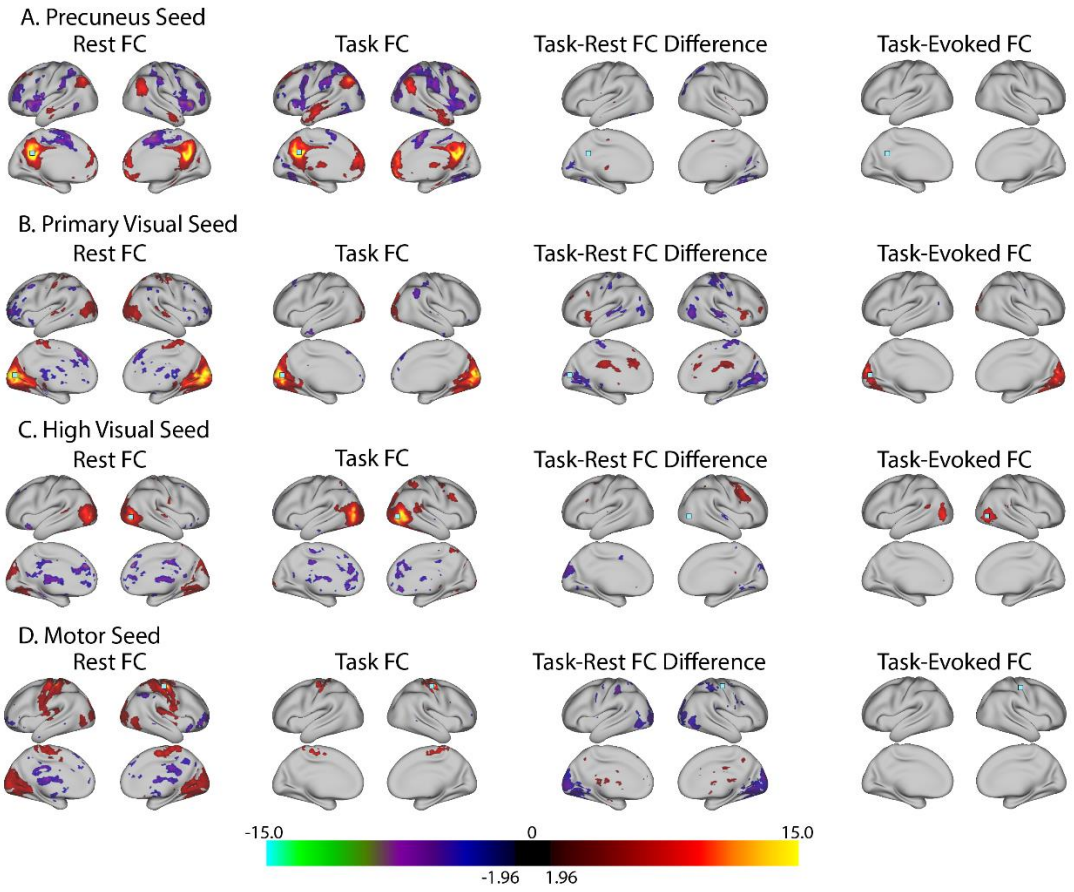

Figure 2.3. Seed-based functional connectivity ($q<0.05$, FDR-corrected for all except for within-session FC differences (right middle), uncorrected at $p<0.001$) using a seed in A) PCu, B) V1, C) V5, and D) M1. Each panel shows the result for within-session FC during eyes-closed resting-state (left), within-session FC during the movie task (left middle), the within-session FC difference during the movie relative to rest (right middle), and the task-evoked FC computed using inter-session correlations (right). The seed voxel is shown as a light blue square in each image. The color bar indicates t-values.

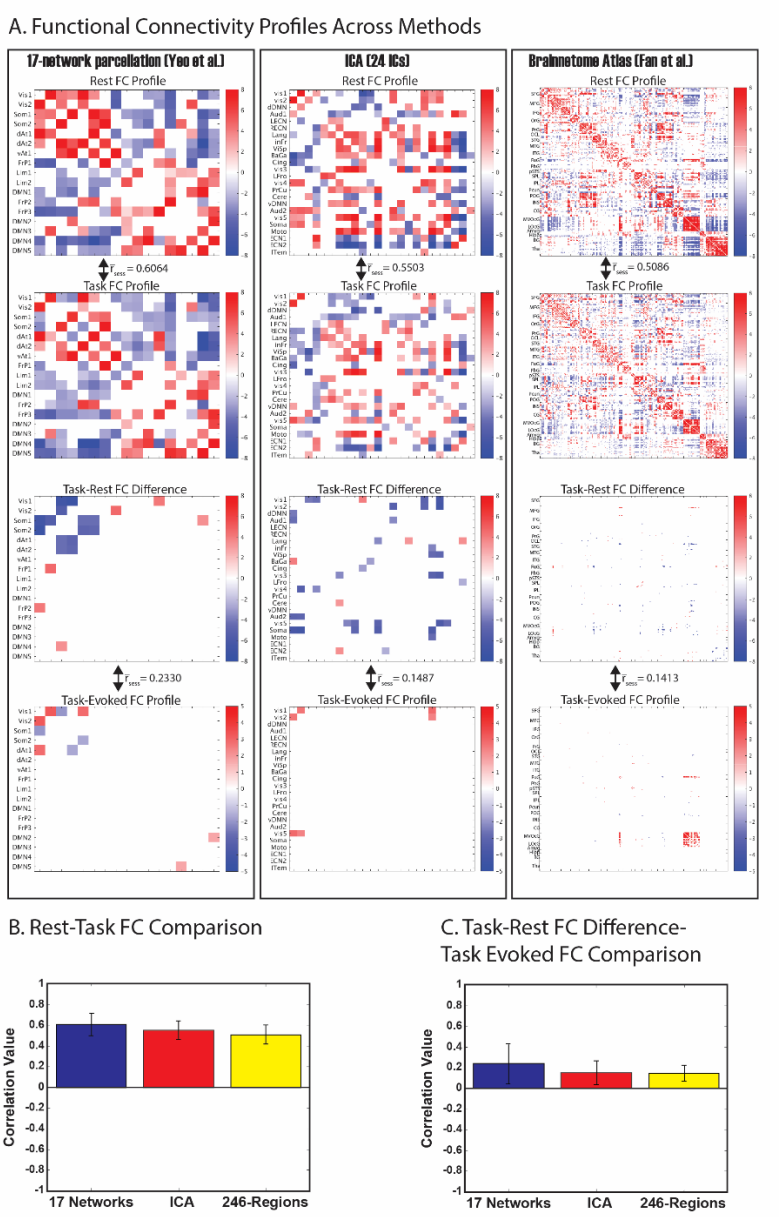

Figure 2.4**.** Functional Connectivity Profiles Across Methods. A) Here, we show correlation matrices corresponding to the FC profiles during resting-state (top) and the movie task (top middle), the FC difference during the movie relative to rest (bottom middle), and the task-evoked FC computed using the inter-session approach (bottom). Profiles were calculated using the Yeo et al. 17-network parcellation (left), ICA using 24 components corresponding to the canonical RSNs (middle), and the Fan et al. Brainnetome Atlas 246-region functional parcellation (right). The color bar indicates mean z-transformed cross correlation values; only significant connections ($q<0.03$) are displayed. We have listed mean session-wise correlation coefficients between the resting-state and movie tasks for each of the three methods in the white space between the matrices, as well as between the task-rest FC difference and the task-evoked FC. B) The mean correlations between movie FC and rest FC are plotted on the bar graph. Error bars indicate SD. C) The mean correlations between the task-rest FC difference and task-evoked FC are plotted on the bar graph. Error bars indicate SD.

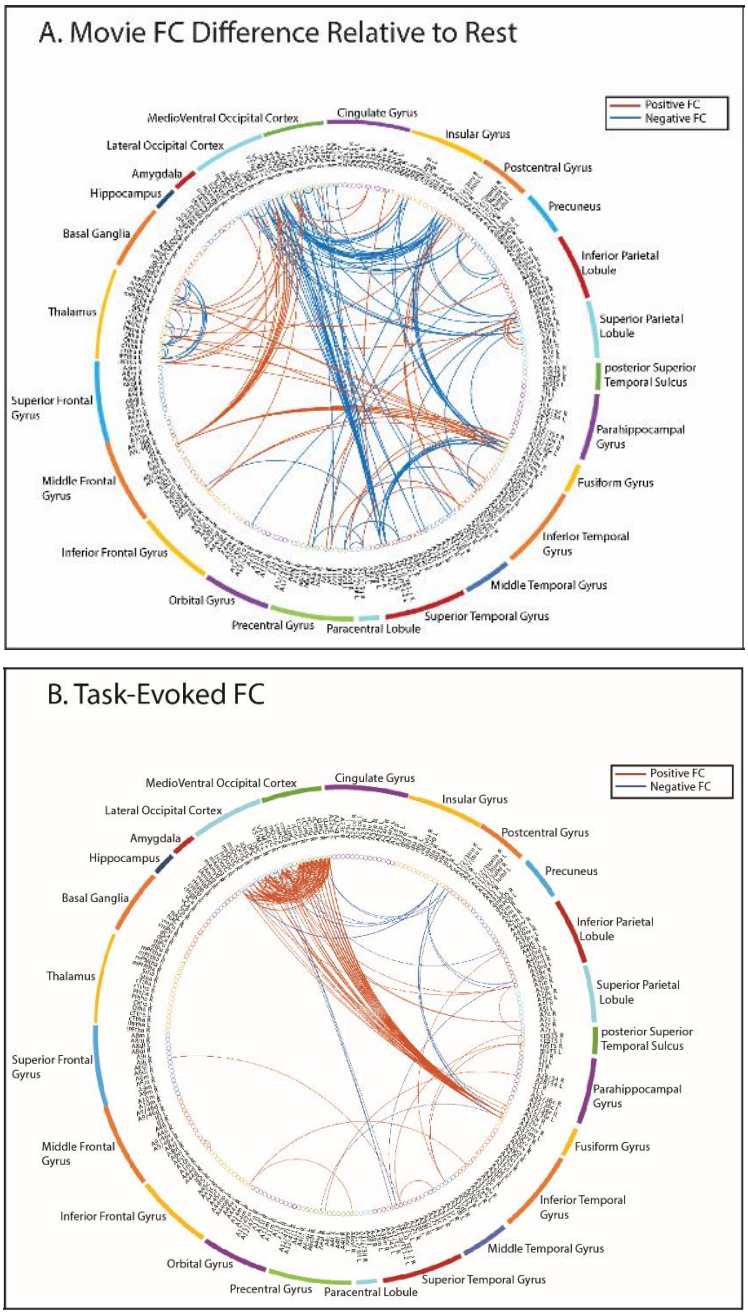

Figure 2.5. Functional Connectivity Findings- Comparing the Task-Rest FC Difference to the Task-Evoked FC. The circle graphs indicate significant FC findings ($p>0.03$, FDR-corrected). Abbreviations of regions are based on the Brainnetome Atlas. A) Significant Task-Rest Difference Connections. Positive connections during the movie relative to rest are noted with red lines; negative connections during the movie relative to rest are noted with blue lines. B) Significant Task-Evoked Connections. Positive connections across two repeated viewings of the natural movie are denoted with red lines; negative connections across two viewings of the movie are denoted with blue lines.

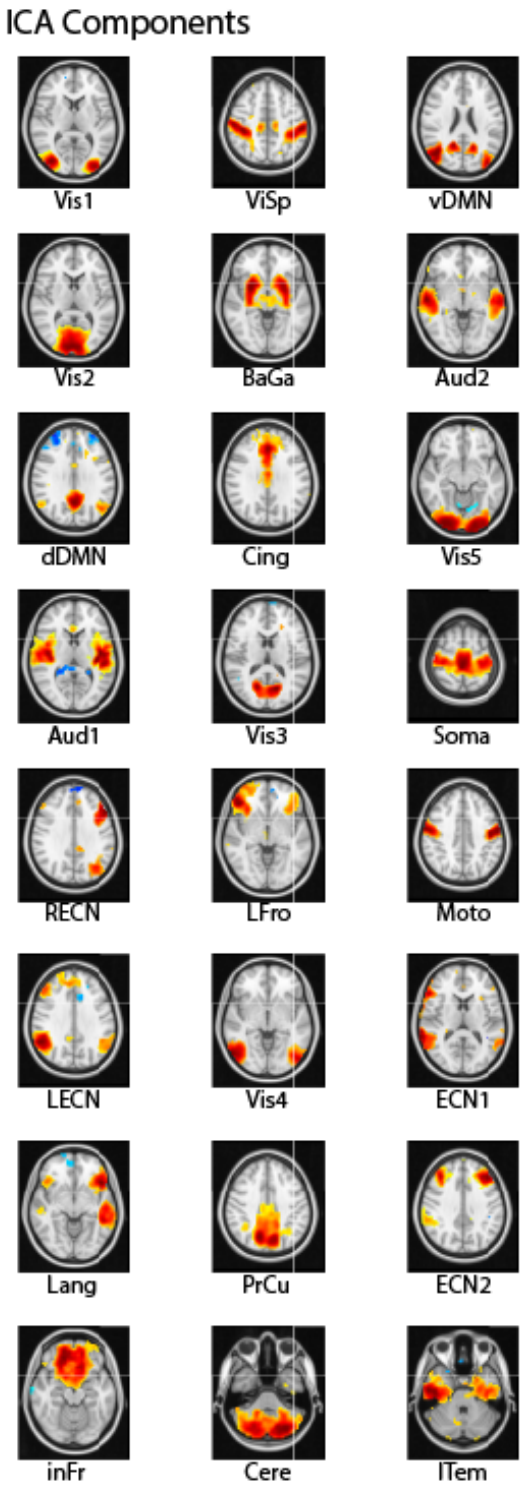

Abbreviations from top-to-bottom, left-to-right are as follows: Visual Network 1 (Vis1), Visual Network 2 (Vis2), dorsal Default Mode Network (dDMN), Auditory Network 1, Right Executive Control Network (RECN), Left Executive Control Network (LECN), Language Network (Lang), inferior Frontal Network (inFr), Visual-Spatial Network (ViSp), Basal Ganglia (BaGa), Cingulate Network (Cing), Visual Network 3 (Vis3), Lateral Frontal Network (LFro),Visual Network 4 (Vis4), Precuneus (PrCu), Cerebellum Network 1 (Cer1), ventral Default Mode Network (vDMN), Auditory Network 2 (Aud2), Visual Network 5 (Vis5), Somatosensory Network (Soma), Motor Network (Moto), Executive Control Network 1 (ECN1), Executive Control

Figure 2.6. Maps obtained using group-level spatial ICA. The thresholding for display purposes only was determined according to the voxel-wise posterior probability equal to 0.6, per a Gaussian Mixture Model; ICA maps used in any calculations were not thresholded.

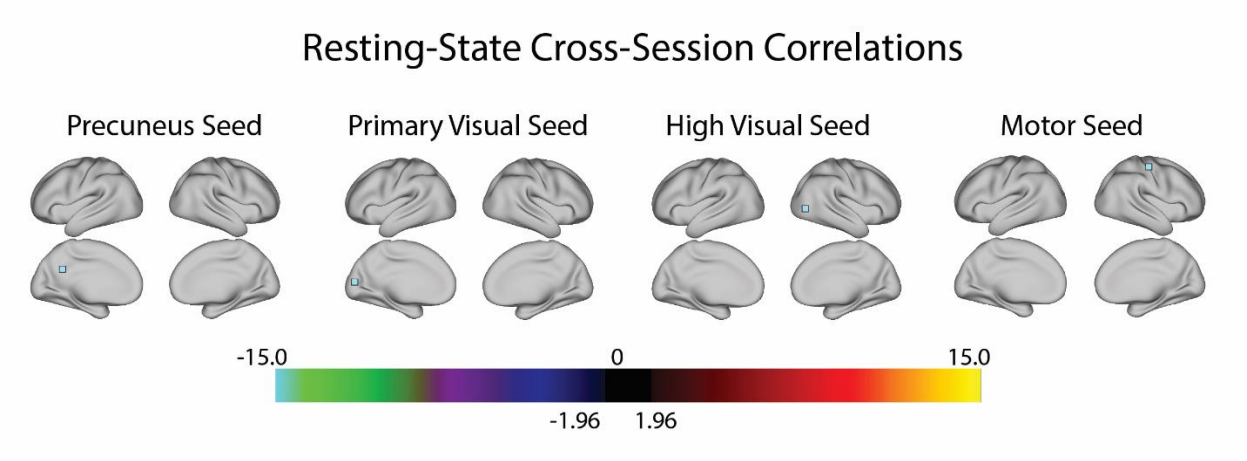

Figure 2.7. Resting-state inter-session correlations. By showing that there are no significant voxels correlated to the seed voxel across two sessions of the same stimulus, we demonstrate the efficacy of inter-session correlations in isolating task-evoked activity. The seed voxels were the same as in Fig. 2.5 and were derived from the precuneal (left), B) primary visual (left middle), C) high visual (right middle), and D) motor cortices (right), respectively. The color bar indicates z-transformed cross correlation values.

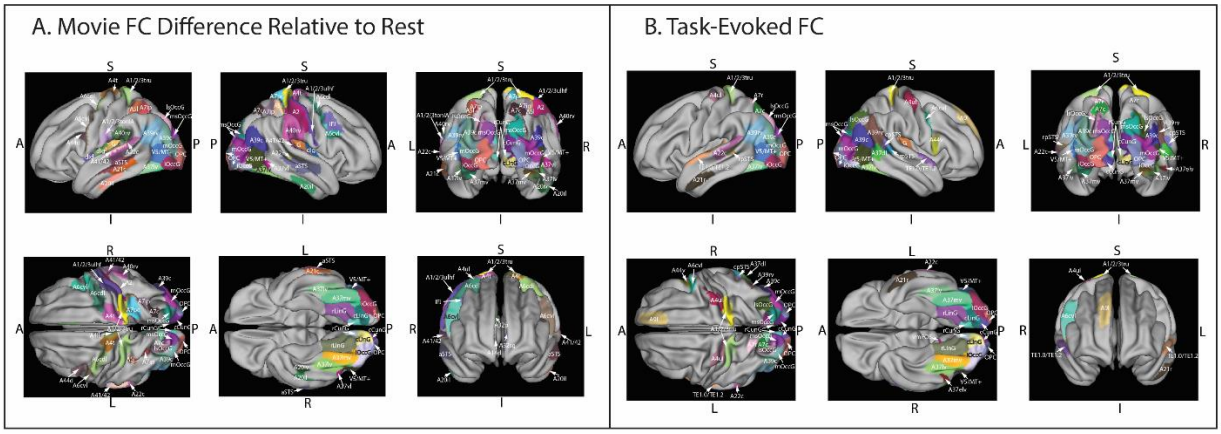

Figure 2.8. Visualization of functional connectivity findings- comparing the task-rest FC difference to the task-evoked FC. Significant regions in Fig. 2.5 were visualized using MRICron software (http://people.cas.sc.edu/rorden/mricron/index.html). Abbreviations of regions are based on the Brainnetome Atlas. A) Significant Task-Rest Difference Connections. B) Significant Task-Evoked Connections.

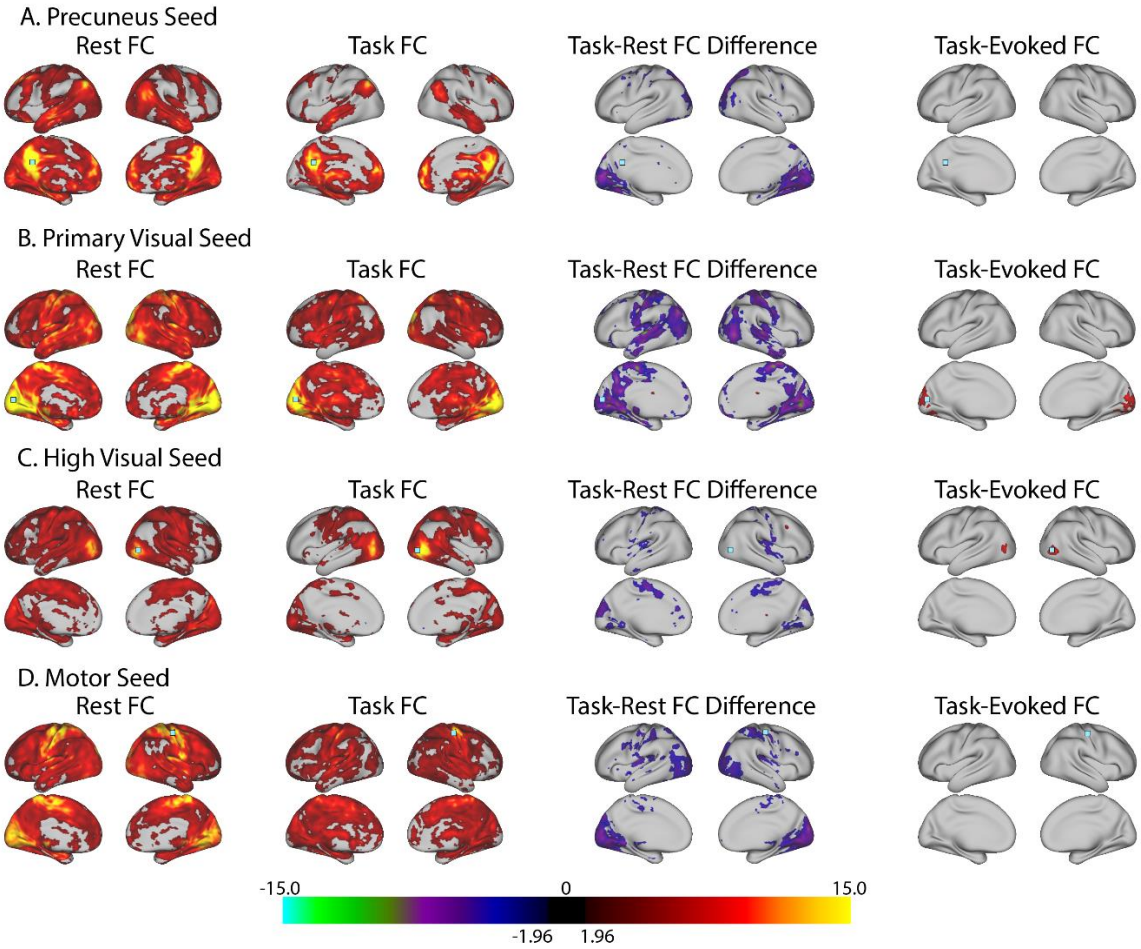

Figure 2.9. Seed-based FC Findings without Global Signal Regression. Seed-based functional connectivity ($q<0.05$, FDR-corrected for all except for within-session FC differences (right middle), uncorrected at $p<0.001$) using a seed in A) PCu, B) V1, C) V5, and D) M1. The global signal regression step was not performed prior to analysis. Each panel shows the result for within-session FC during eyes-closed resting-state (left), within-session FC during the movie task (left middle), the within-session FC difference during the movie relative to rest (right middle), and the task-evoked FC computed using inter-session correlations (right). The seed voxel is shown as a light blue square in each image. The color bar indicates t-values.

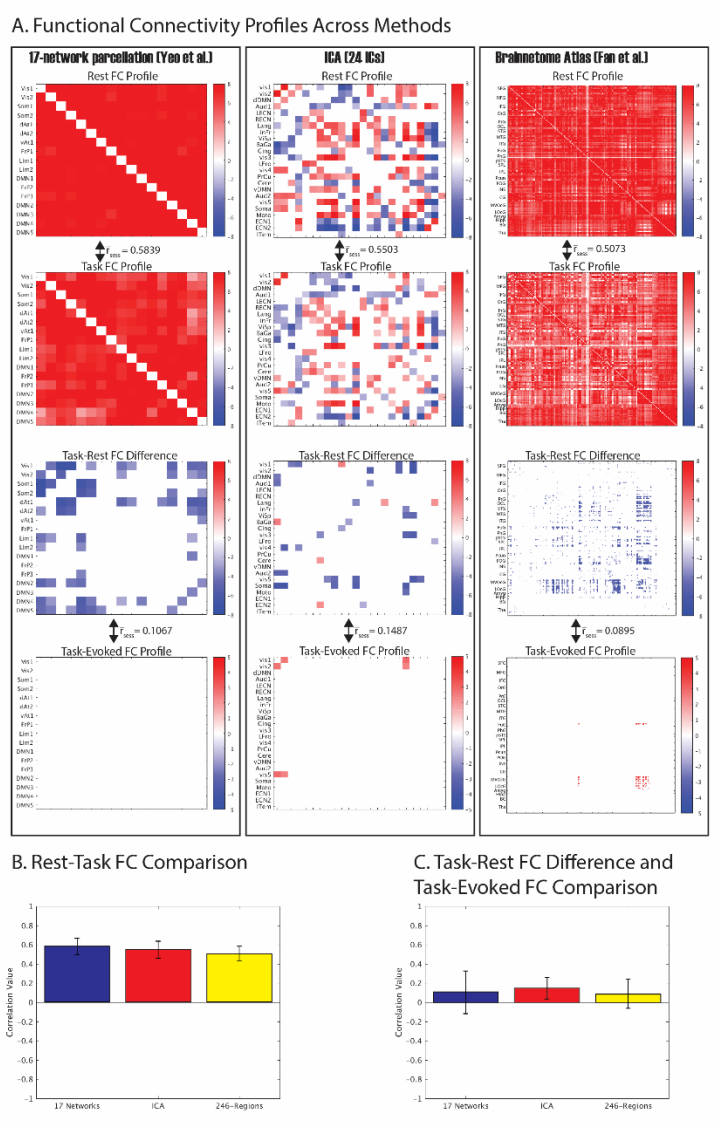

Figure 2.10. Functional Connectivity Profiles Across Methods without Global Signal Regression. A) Correlation matrices corresponding to the FC profiles during resting-state (top) and the movie task (top middle), the FC difference during the movie relative to rest (bottom middle), and the task-evoked FC computed using the inter-session approach (bottom). The global signal regression step was not performed prior to analysis. Profiles were calculated using the Yeo et al. 17-network parcellation (left), ICA using 24 components corresponding to the canonical RSNs (middle), and the Fan et al. Brainnetome Atlas 246-region functional parcellation (right). The color bar indicates mean z-transformed cross correlation values; only significant correlations ($q<0.03$) are displayed. We have listed mean session-wise correlation coefficients between the resting-state and movie tasks for each of the three methods in the white space between the matrices, as well as between the task-rest FC difference and the task-evoked FC. B) The mean correlations between movie FC and rest FC are plotted on the bar graph. Error bars indicate SD. C) The mean correlations between the task-rest FC difference and task-evoked FC are plotted on the bar graph. Error bars indicate SD. See Fig. 2 caption for Yeo parcellation abbreviations, Fig. 4 for ICA abbreviations, and Fan et al. (2016) for Brainnetome atlas abbreviations.

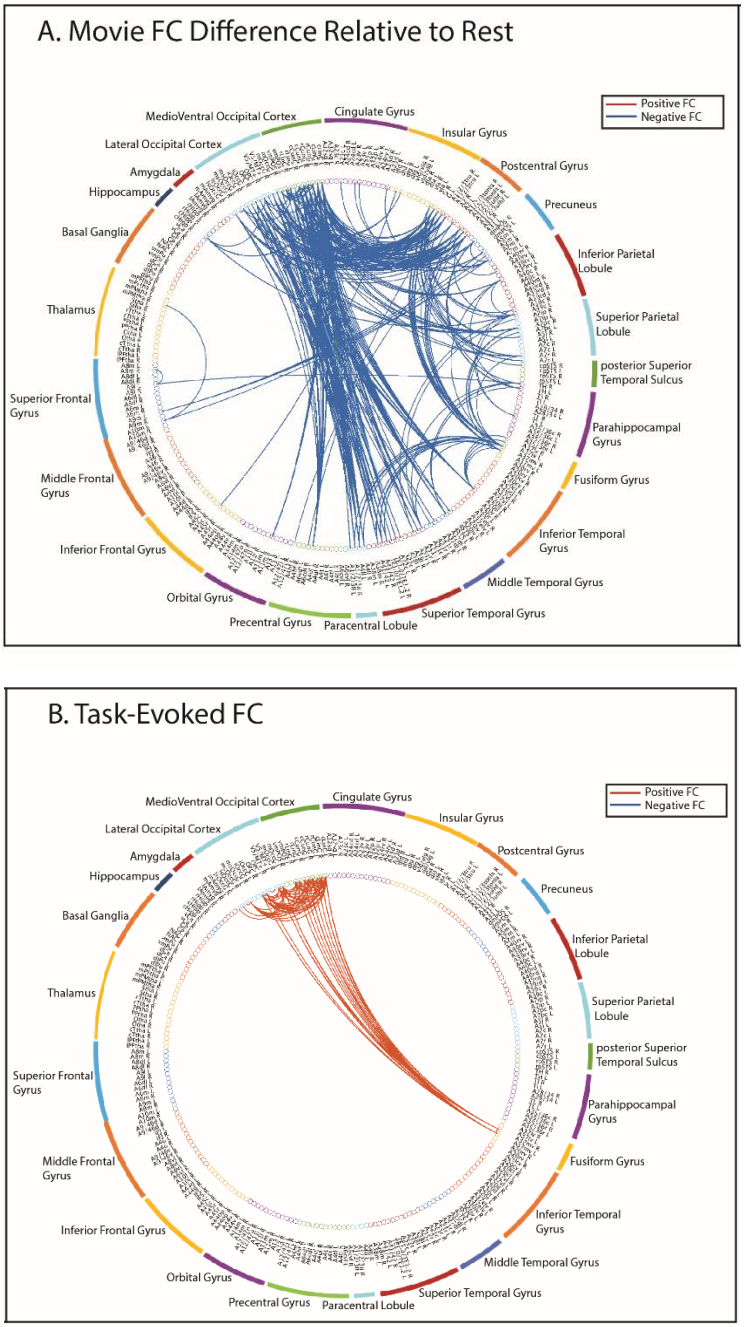

Figure 2.11. Functional Connectivity Findings: Comparing the Task-Rest FC Difference to the Task-Evoked FC without Global Signal Regression. The circle graphs indicate significant FC findings (q>0.03, FDR-corrected). The global signal regression step was not performed prior to analysis. Abbreviations of regions are based on the Brainnetome Atlas. A) Significant Task-Rest Difference Functional Connectivity. Positive correlations during the movie relative to rest are noted with red lines; negative correlations during the movie relative to rest are noted with blue lines. B) Significant Task-Evoked Functional Connectivity. Positive correlations across two repeated viewings of the movie are denoted with red lines; negative correlations across two viewings of the movie are denoted with blue lines.

3. MAPPING WHITE-MATTER FUNCTIONAL ORGANIZATION AT REST AND DURING NATURALISTIC VISUAL PERCEPTION

*Formatted for dissertation from the article published in *NeuroImage*. (Marussich et al., 2017)

3.1 Rationale

Since its inception, functional magnetic resonance imaging (fMRI) has been focused on mapping activations and connections in the cerebral gray matter (GM) (Bandettini et al., 1992; Biswal et al., 1995; Fox and Raichle, 2007; Kwong et al., 1992; Ogawa et al., 1992). It has had limited use in investigating the functional dynamics and organization of the cerebral white matter (WM) (Gawryluk et al., 2014). This paucity of WM-fMRI literature is disproportional considering that WM occupies about half of the human brain volume, contains structural pathways for long-range signaling (Sporns et al., 2005), and has critical implications for numerous neurological diseases (Ffytche and Catani, 2005).

It has been often assumed that WM lacks the typical hemodynamic changes driven by neural activity (Logothetis and Wandell, 2004). Relative to GM, WM has much lower cerebral vascular density (Lierse and Horstmann, 1965), blood volume (Jensen et al., 2006), and blood flow (Van Osch et al., 2009). Moreover, energy consumption in WM is about one fourth that of GM overall (Logothetis and Wandell, 2004), with more energy used on action potentials rather than synapses (Harris and Attwell, 2012). While neurometabolic and neurovascular coupling in WM is also unclear (Logothetis and Wandell, 2004), previous findings about the relationship between neural and hemodynamic activities are all based on signals specific to GM (Logothetis et al., 2001; Smith et al., 2002). It is problematic to simply extrapolate such findings either for or against the validity of WM-fMRI. Furthermore, artifacts of motion (Johnstone et al., 2006), partial-volume (Jo et al., 2010), and physiological origin (Makedonov et al., 2015) are also of concern in WM-fMRI. Hence, the fMRI signal in WM has an unclear basis and an inherently low signal-to-noise ratio (SNR); as such, it has been dismissed from analysis or interpretation in the vast majority of fMRI studies.

However, increasing evidence has shed light on the feasibility of using fMRI to map WM activation and connectivity. See Gawryluk et al. (2014) for a review. Previous studies showed that

inter-hemispheric transfer tasks could induce fMRI activations in the corpus callosum (Fabri et al., 2011; Gawryluk et al., 2011a; Tettamanti et al., 2002), through which activated cortical regions were structurally connected across hemispheres (Mazerolle et al., 2010). Such callosal activations may have a metabolic basis, since local cerebral metabolic rate for glucose was found to depend on neural activity in the corpus callosum given graded intra-cortical electrical stimuli (Weber et al., 2002). Beyond the corpus callosum, WM activations have rarely been reported in fMRI studies (Mazerolle et al., 2013; Mosier et al., 1999). Astafiev et al. (2015; 2016) have demonstrated that symptomatic chronic mTBI subjects show abnormal neural activation during visual tracking tasks in a common set of subcortical and white matter regions using BOLD fMRI acquisitions. Moreover, Ding et al. reported that resting-state fMRI signals in WM were correlated over long distances, as well as locally in a similar anisotropic manner as observed with diffusion tensor imaging (DTI). Although all prior studies that reported WM- fMRI activations were based on T_2^*-weighted MRI sequences, the WM-fMRI signal and its correlational structure were recently shown to be blood oxygenation level dependent (BOLD) (Ding et al., 2016). This finding is important since T_2^*-weighted signal fluctuation may arise from both BOLD and non-BOLD origins: the former reflects changes in R_2^*, the latter may reflect changes in initial signal intensity (S_0) likely due to nuisance effects, e.g. motion artifacts and physiological noise (Kundu et al., 2012). Collectively, these studies suggest that there is no fundamental barrier for which fMRI is doomed to fail for functional imaging in WM, paving the way for an emerging domain of fMRI methodologies and applications.

Perhaps the most critical and practical challenge is the much lower dynamic range in WM (i.e. versus that in GM). When univariate or multivariate time-series analyses are applied to GM and WM voxels together, signal variance and structure are dominated by voxels in GM, whereas activity and connectivity patterns in WM are likely under-detected or mistaken as noise. One potential way to deal with this issue is to separate WM from GM and use data-driven analysis, e.g. independent component analysis (ICA), to characterize the spatiotemporal patterns of signal versus noise exclusively in the WM. This is helpful especially for the resting state, since the absence of any overt task makes it more difficult to discriminate signal from noise without any presumed temporal characteristics. A plausible criterion to distinguish signal from noise is based on their expected difference in reproducibility within and across subjects. The brain's structural and functional organization is generalizable and stable, serving as the underlying constraint for the signal characteristics; this is not so for noise. Once signal and noise are separated, a new stage may

be formed to further assess the network patterns of WM activity, as well as their relationships with cortical networks. This may also allow for the conjoint evaluation of the roles of WM and GM networks in perceptual, behavioral, and cognitive tasks.

Taking this strategy, we set out to characterize WM-fMRI signals in the resting state and also during free viewing of a natural movie. The natural-vision paradigm provides a dynamic and realistic behavioral context. As in the resting state, brain activity in this task state is seemingly complex and unpredictable, yet it exhibits coordinated cortical network patterns that support visual perception (Hasson et al., 2004). Here, we further asked whether the patterns of functional connectivity in the white matter would differ between the resting state and the natural-vision state. The answer to this question was expected to shed light on the functional relevance of white-matter fMRI. Briefly, high-dimensional ICA was used to decompose and de-noise WM-fMRI signals in the resting state and during a natural-vision task. From the de-noised data, we found that WM-fMRI signals were patterned into clusters and hierarchically organized in the resting state, whereas naturalistic visual stimuli drove more coherent signal fluctuations within the optic radiations, as well as the coupling between the WM pathways and the GM networks engaged in visual processing and perception.

3.2 Methods and Materials

3.2.1 Subjects

Thirteen healthy volunteers (25 ± 3 years old, 6 females, 10 right-handed, normal or corrected to normal vision) participated in this study in accordance with a protocol approved by the Institutional Review Board at Purdue University. Two subjects were excluded because they were self-reported to fall asleep during the sessions.

3.2.2 Experimental Design

Each subject underwent four fMRI sessions with two conditions. Two sessions were in the eyes-closed resting state, and the other two were during free-viewing of an identical movie clip (The Good, the Bad, and the Ugly, 1966). We chose this movie because it was previously used to obtain interesting findings on cortical gray-matter activity during natural vision (Hasson et al., 2004). Every movie-stimulation session began with a blank gray screen presented for 42 s, followed by the movie presented for 5 min and 37 s (from 162:54 to 168:33 min. in the film), and

ended with the blank screen again for 30 s. No sound was played during the movie. The resting-state sessions had the same duration as the movie-stimulation sessions. The session order was randomized and counterbalanced across subjects. The scanner environment was darkened to minimize external light exposure. Hereafter, we also refer to the movie stimulation condition as the task state, in contrast to the resting state.

3.2.3 Data Acquisition

Whole-brain structural and functional MRI images were acquired using a 3-Tesla Signa HDx MRI system (General Electric Health Care, Milwaukee, USA). A 16-channel receive-only phase array coil (NOVA Medical, Wilmington, USA) was used during all acquisitions. The fMRI data were acquired using a single-shot, gradient-recalled (GRE) echo- planar imaging (EPI) sequence (38 interleaved axial slices with 3.5mm thickness and 3.5×3.5 mm^2 in-plane resolution, TR=2000 ms, TE=35 ms, flip angle=78°, field of view=22×22 cm^2). T_1-weighted anatomical images covering the whole head were acquired with a spoiled gradient recalled acquisition (SPGR) sequence (1×1×1mm^3 nominal resolution, TR/TE=5.7/2 ms, flip angle=12°).

3.2.4 Pre-Processing

Pre-processing of the fMRI images was carried out with a combination of AFNI (Cox, 1996), FSL (Smith et al., 2004), and MATLAB (Mathworks, Natick, MA). In brief, T_1-weighted anatomical images were non-linearly registered to the Montreal Neurological Institute (MNI) brain template, using a combination of *flirt* and *fnirt* in FSL. T_2^*-weighted functional image time series were corrected for slicetiming (using *slicetimer* in FSL), co-registered to the first volume within each series to account for head motion (using *mcflirt* in FSL), had non-brain tissues masked out (using *3dAutomask* in AFNI), aligned to the T_1-weighted structural MRI (using *align_epi_anat.py* in AFNI), and registered to the MNI space with 3-mm isotropic voxels (using *applywarp* in FSL, and *3dresample* in AFNI).

The first six volumes in the fMRI data were discarded to avoid any pre-steady-state longitudinal magnetization. Each session's data was subjected to third-order de-trending and low-pass filtering (< 0.1 Hz) using the regression and filtering toolboxes in MATLAB. For the movie sessions, we excluded data acquired during the blank gray screen presentation and further removed

the first 6 volumes and the last 7 volumes of the movie to avoid any transient fMRI response during the movie stimulation.

Following the pre-processing steps, data analysis for the fMRI data was twofold: analysis within the WM-only and analysis within the GM- only. This was achieved by creating and applying a WM mask to the normalized fMRI images to isolate WM-only voxels. The WM mask was created from the LONI Probabilistic White Matter template in the MNI space (Shattuck et al., 2008) by setting a probabilistic threshold to a level of 0.85. This threshold was chosen to be very conservative to avoid possible partial volume effects close to GM/WM junctions; hence, the mask covered most but not all WM voxels. The thalamus was not included in the WM mask. The GM mask was derived by finding the intersection of the complement of the WM mask and the brain mask in the MNI template. Both the WM and GM masks were restricted to voxels within axial slices from $z=-15$mm to z=51 mm. Linear spatial smoothing (FWHM=6 mm) was then performed separately within the WM or GM voxels to avoid partial volume effects between them. Effectively, the voxels outside the mask were set to null, and thus did not contribute to the smoothed voxel intensity, while the spatially smoothed voxel time series was demeaned and variance normalized before any subsequent analysis.

3.2.5 De-Noising via Independent Component Analysis (ICA)

For each condition (i.e. the resting state and the task state), the fMRI data were separated into two sets for each of the two sessions from every subject. In a total of four sets of fMRI data, two were from resting state and the other two were from the task state with naturalistic visual stimuli. The fMRI data were then temporally concatenated across subjects for each of the sets. The four concatenated fMRI time-series data allowed us to evaluate the test-retest reproducibility of the group-level ICA maps in the resting state and the task state. Group spatial ICA using the Infomax algorithm (Bell and Sejnowski, 1995) was applied to each set of the concatenated data. This gave rise to 70 spatially independent components (ICs) with distinct temporal basis functions that yielded a sparse representation of the data; as such, voxels were considered to be synchronized (i.e. functionally related) within each component. To evaluate the test-retest reproducibility of each of the 70 ICs, we calculated the spatial cross correlations between the two sets of ICs for each condition. An IC in one set was assumed to be reproducible if there was a corresponding IC in the other set that was spatially correlated with this IC. We calculated the absolute values of the

correlation coefficients and found the optimal pairing by maximizing the sum of the pair-wise absolute cross-correlation values. Here, the absolute cross-correlation value was used because spatially consistent ICA components might appear 180° out of phase from one another. Upon visual inspection, non-reproducible components were regarded as noise and discarded, whereas the remaining components were re-assembled to generate the de-noised fMRI data for every session and every subject. For each condition, the de-noised fMRI data were further concatenated across the two sessions for each of the eleven subjects, giving rise to 22 sessions in total. Then, group ICA was applied again to the de-noised and concatenated data, generating about 30 ICs that characterized the WM-fMRI signals in the resting state or during the natural visual stimulation.

Following group ICA, we used dual regression (Filippini et al., 2009) against each subject's fMRI data to extract subject-specific ICA maps in order to capture inter-subject differences (Tavor et al., 2016). Briefly, the first (multiple) regression was applied to the spatial domain, using the group-level ICA maps as regressors to get individual time series for each subject and each component; the second regression was applied to the time domain, using the obtained individual time series as regressors to get individual-level ICA maps.

3.2.6 Hierarchical Clustering Based on Temporal Correlations

In both the resting state and the task state, the ICs of WM-fMRI signals were progressively grouped into clusters based on the cross-correlations of their corresponding time series and a complete-linkage hierarchical clustering algorithm (Dasgupta and Long, 2005). At the beginning of the algorithm, each component was in a cluster of its own. These clusters were then progressively combined into larger clusters until all components ended up in the same cluster. At each step, the clusters separated by the ‘shortest distance' (i.e. the largest temporal cross correlation) were combined. Such hierarchical clustering was visualized as a dendrogram, which showed the sequence of clusters merging and the distance at which each fusion took place (Cordes et al., 2002; Dasgupta and Long, 2005; Wang and Li, 2013).

3.2.7 Comparison Between the Resting and Task States

We also compared the reproducibility of WM-fMRI ICA components in the resting state versus the task state. For this purpose, the test-retest reproducibility (i.e. spatial cross correlations between repeated sessions of the same condition) was compared between the resting state and the

task state. Specifically, after pairing the ICA components between session 1 and session 2 of either the resting state or the task state as mentioned previously, the pairwise correlation coefficients were transformed into z-scores. The z-scores were compared between the two states, and the significance of their differences was evaluated by using a two-sample independent t-test with a significance level of 0.05.

We further compared the WM-fMRI ICA maps in the resting state with those in the task state. Specifically, we calculated the spatial cross correlations between every component in the resting state and every component in the task state. Then, individual components in the resting state were optimally paired to those in the task state to maximize the sum of cross correlations between all paired components. After pairing, the pair-wise cross correlations were further tested for statistical significance. To calculate the p-value from the correlation coefficient, we used an approximate estimate of the spatial degree of freedom (DF), as previously described elsewhere (Smith et al., 2009). The voxels were not independent samples due to spatial smoothing. For a conservative approximation, we considered independent samples as larger (than a voxel) cubes that included five voxels in each direction, given that the voxel size is 3mm and the smoothing filter has FWHM=6 mm. For a total of 7990 voxels in WM, this approximation yielded an estimated DF of 64. To be even more conservative, we used a DF of 50 to account for other potential spatial dependency in data acquisition or processing. Although seemingly arbitrary, the above procedure yielded a reasonable approximate of the spatial degree of the freedom.

3.2.8 Functional Relationship Between GM and WM Networks

Furthermore, we assessed the functional relationships between WM and GM networks at rest or during task. For this purpose, we first identified a number of functional networks within the cortical gray matter during the resting or task state. Specifically, GM-fMRI data were concatenated across all sessions from all subjects in the resting or task state. For either state, ICA was applied to the concatenated data to produce 70 spatially independent components, among which ~45 cortical networks were recognizable as previously reported resting state networks (Shirer et al., 2012), and retained for subsequent analyses. We evaluated the temporal cross correlations between ICA components in WM and those in GM. The activity time series of every WM and GM component was extracted from each of the 22 sessions separately for the resting state and the task state. For every session of the resting or task state, temporal cross correlations were calculated

between every GM component and every WM component, and then transformed to z-scores. To test the significance of the cross correlation, the average z-score was compared against zero by performing one- sample t-test to every pair of GM and WM components ($p < 0.05$, DF=21).

3.2.9 Comparison with Diffusion MRI

For both resting-state and task conditions, we thresholded the spatial ICA maps to delineate the shapes of WM structures revealed in individual components using the method described in Beckmann and Smith (2004). Briefly, we first calculated the z-statistic for each voxel and each ICA map by dividing the ICA maps by the estimated standard deviations of the voxel-wise residuals. We further modeled the null distribution of each z-statistic map with a mixture of two Gaussian distributions (i.e. Gaussian Mixture Model (GMM)), and then calculated the voxel-wise posterior probability based on the estimated GMM. We then thresholded the ICA maps according to the voxel-wise posterior probability, which was set to 0.6. For each condition, we then used the thresholded ICA maps to create a set of WM structures. Such structures, obtained with WM- fMRI in the resting or task state, were visualized in the open-source 3D Slicer toolkit (http://www.slicer.org) (Fedorov et al., 2012), and were compared with a diffusion tensor imaging atlas, the ICBM-DTI-81 white-matter labels atlas (Mori et al., 2008; Oishi et al., 2008).

3.3 Results

3.3.1 Spatially Independent Components of WM-fMRI Signals

We explored the spatiotemporal patterns of WM-fMRI data in the resting state by using ICA. 70 spatially independent components were extracted from all WM voxel time series, after data were temporally standardized and concatenated across all subjects and separately for the two repeated resting-state sessions (referred to as session 1 and session 2). Components from the two sessions were optimally matched into distinct pairs based on the spatial cross correlation between each component from session 1 and its corresponding component from session 2. This pair-wise cross-correlation provided the measure of intra-subject reproducibility for each component. Twenty-eight out of the 70 components were found to exhibit relatively high intra-subject reproducibility ($r = 0.4028 \pm 0.0276$) and were paired between the two repeated sessions. Fig. 3.1 shows the spatial patterns of five example components that were found to be reproducible between session 1 (Fig. 3.1, left) and session 2 (Fig. 3.1, middle). Many of the reproducible components

appeared to be cluster-like (or non-fiber-like), showing spatial distributions confined to focal regions in WM (e.g. Fig. 3.1 IC 1 and IC 6). In contrast, some components were readily observed as a fiber-like distribution over a long distance, as in the optic radiations (e.g. Fig. 3.1, IC 2 and IC 13) and the corpus callosum (e.g. Fig. 3.1 IC 8).

We discarded components as "noise" that were spatially inconsistent between the two repeated sessions in order to improve the SNR of WM-fMRI data. The discarded components had either relatively lower reproducibility ($r = 0.1879 \pm 0.0147$), or spatially non-specific distribution most likely due to artifacts. Thus, we attributed the 28 reproducible components to the "signals" likely of neural origin, and attributed the 42 non-reproducible components to "noise". Such "signal" vs. "noise" components accounted for 33.98% and 66.02% of the variance in WM-fMRI, respectively.

After excluding all noise/artifact components, the signal components were reassembled to give rise to presumably de-noised WM- fMRI data. The de-noised data were then concatenated across the two resting-state sessions, and further decomposed into 31 spatially independent components for subsequent analyses. Here, a buffer (+3 ICs) was provided to account for the variation between the two sessions. Among the 31 components, two components were not consistent to the spatial maps produced by ICA in either session 1 or session 2; they were further discarded, leaving a total of 29 components for subsequent analyses. Some example components extracted from the de-noised data are shown in Fig. 3.1 (right). All of the 29 components in the resting-state are shown in Fig. 3.2A.

3.3.2 Hierarchical Organization of WM-fMRI Components

We assessed the temporal relationships between different components of the de-noised WM-fMRI data. These components, although spatially independent, were temporally correlated with each other to a varying degree, with the absolute correlation coefficients ranging from 0 to 0.27 (Fig. 3.2B, bottom). These temporal cross-correlations were used to progressively merge the individual components into a hierarchical organization based on hierarchical clustering (Fig. 3.2B, top). For example, bilateral optic radiations emerged from progressively merging multiple ICs: two adjacent ICs were first grouped into a unilateral fiber bundle connecting LGN to V1, which were then paired with the homologous fiber bundle from the opposite hemisphere (Fig. 3.2C). Similarly, adjacent segments in the corona radiata (Fig. 3.2A – IC 17 and IC 28) were clustered to

construct the overall fiber bundle (Fig. 3.2B). For comparison, we also applied the same hierarchical clustering analysis to cortical networks. Results showed that cortical networks were more tightly correlated and clustered than the white-matter components (Fig. 3.8).

3.3.3 Spatiotemporal Structure of WM-fMRI During Natural Vision

Following this result, we asked whether the above intrinsic patterns and the hierarchical structure of WM-fMRI signals were preserved during complex, dynamic, and realistic visual experiences. To address this question, we analyzed the WM-fMRI data during naturalistic visual stimulation using the same method applied in the resting state. Similar to the test-retest reproducibility evaluated for the resting-state components (Fig. 3.3A, left), some ICA components were reproducible across the two repeated movie stimulation sessions (Fig. 3.3A, middle). Twenty- seven components were reproducible ($r = 0.5867 \pm 0.0323$) and were kept as signals, while other components were attributed to noise or artifacts and thus removed. The signal and noise/artifact components accounted for 34.69% and 65.31% of the variance in WM-fMRI, respectively, which was comparable to that of those in the resting state. Overall, the components during the visual task were more reproducible than those in the resting state (Fig. 3.3A, right) ($p < 0.0001$, two-sample t-test). As done for the resting state, we also concatenated the de-noised WM-fMRI data across the two movie sessions, and decomposed the concatenated data into 30 spatially independent components. Two components were not consistent with any of the components produced by ICA in either session 1 or session 2; the other 28 components were kept for subsequent analyses.

The task-state WM ICs mostly resembled those in the resting state (Fig. 3.3B). Twenty-one out of the 28 components observed during the visual task were also observed in the resting state, giving rise to one-to- one matched pairs with significantly correlated spatial patterns ($|r| = 0.5306 \pm 0.0298$, $p < 10^{-5}$ to $p=0.0207$, uncorrected). For example, IC 3, IC 10, IC 27 were three ICA maps in the task state that were matched to IC 8, IC 14, IC 6 in the resting state (Fig. 3.3B). Four components were not matched ($|r|=0.0868\pm 0.0182$, $p=0.3208$ to $p=0.8611$, uncorrected) in a one-to-one manner. For an example, see Fig. 3B, IC 1 (task) versus IC 13 (rest).

To further characterize the consistency (and inconsistency) between the resting and task states, we compared the hierarchical relationships between spatially independent components in these two states. See Fig. 3.4A for all 28 components in the task state. The independent components

that were matched between the task and resting states were also found to bear a similar hierarchical organization in both states (Fig. 3.4D). For example, the corona radiata began to emerge from clustering its three segments (IC 8, IC 23, and IC 17) through two hierarchical steps (Fig. 3.4B). Among the components that were not matched between the task and resting states, a single component (IC 1) in the task state was found to encompass the bilateral optic radiations connecting LGN and V1 (Fig. 3.4C). This observation, that the bilateral optic radiations manifested themselves as a single component, suggests that activity fluctuations within the optic radiations were more coherent during visual stimulation than in the resting state, during which the optic radiations were segregated into multiple pieces (Fig. 3.2C). Also note that during the task, the optic radiations (IC 1) were further clustered with a component corresponding to an anterior segment in the right inferior longitudinal fascicular (ILF) (IC 13), which is located near and posterior to the optic radiations (see Fig. 3.4A and D) and contains connections between associative visual areas and anterior temporal structures (Catani et al., 2003).

While the above results were obtained with group ICA, we also used dual regression to obtain the corresponding ICA maps from individual subjects. For both the resting state and the task state, the individual- level ICA maps were generally consistent with the group-level ICA maps (Fig. 3.5).

3.3.4 Interactions Between WM and GM Networks

To further explore the functional role of the coherent signal within the optic radiations, we evaluated its coupling with cortical visual networks in GM by computing their temporal cross correlations. For this purpose, 70 spatially independent components were extracted from all GM voxel time series after concatenating every session and every subject for the visual task; among those, 47 components were recognizable as established intrinsic functional networks (Shirer et al., 2012). We identified four cortical networks that had the highest (and significant) positive cross-correlations with the optic radiations ($p=0.01–0.047$, one-sample t-test, uncorrected). As shown in Fig. 3.6A, all of these four networks were parts of the visual system: namely, the primary visual area (IC 4), higher order visual networks (IC 1 and IC 3), and a medial visual network (IC 2). These areas are involved in natural visual processing, as shown in previous studies (Hasson et al., 2004).

We performed this analysis on the resting-state data to assess the temporal relationships between the optic radiations and intrinsic cortical visual networks in the absence of the visual task. In Fig. 3.9, we identified four cortical networks in the resting state as the counterparts to those vision-related components shown in Fig. 3.6A. The optic radiations resting-state component was formed from a sum of the three optic radiations components (IC 11, IC 13, and IC 2) shown in Fig. 3.2C; the time series was formed from the mean of those of the three components. However, unlike the task state (Fig. 3.6B, left), the resting state did not exhibit any significant temporal cross correlations between the optic radiations and cortical visual networks ($p=0.1003– 0.9526$, uncorrected) (Fig. 3.6B, right).

However, head motion was a potential confounding factor to the above findings. We found that the head motion parameters (translations and rotations) exhibited, on average, 2.3 and 3.5 times greater standard deviations in the resting state than in the task state, respectively. This difference was significant ($p < 0.00001$, Wilcoxon rank sum test). Despite the significantly different head motion between the two states, this difference was less likely to account for the spatially and functionally specific findings about WM components and their interactions with GM networks. We noted that the time courses of the WM and GM components of interest did not show the slow drift or abrupt changes that characterized the head motion. In addition, we addressed the concern that head movements in the task condition might be task related; i.e. that common movements between sessions would occur at particular moments in the movie at particularly suspenseful or surprising points. To effectively capture sudden movements while ignoring slow drifts, we evaluated the time derivative of every motion-correction parameter and calculated its correlation between the repeated movie sessions within each subject. Only margin- al correlations were found ($r < 0.08$) for all six motion parameters. Therefore, head motion was not a confound of major concern.

3.3.5 Relationships with White-Matter Structure

Finally, we asked whether the ICA maps obtained with WM-fMRI in the resting state and the task state were distributed along the axonal fiber tracts. For this purpose, we compared the thresholded ICA maps with white-matter tracts based on diffusion MRI using the ICBM-DTI- 81 white-matter labels atlas (Mori et al., 2008; Oishi et al., 2008) (Fig. 3.7). Qualitatively, for both the resting and task states, most of the ICA components of WM-fMRI data covered only segments

of individual fiber tracts, without extending the full tract length. However, some components appeared to align well with major fiber bundles (e.g. the optic radiations, the corpus callosum, and the internal capsule). It suggests a complex structure-function relationship in the white matter when observed with white-matter diffusion and functional MRI.

3.4 Discussion

Using data-driven analysis methods, we examined the spatiotemporal characteristics of fMRI time series in the cerebral white matter both in the resting state and during naturalistic visual perception. The results led to the following findings: 1) spatially independent components of resting-state fMRI signals in WM revealed reproducible either cluster-like or fiber-like structures with synchronized spontaneous fluctuations within each structure; 2) different components were temporally correlated in a hierarchical manner, leading us to report the intrinsic hierarchical functional organization of WM fiber tracts; 3) such intrinsic structures and their hierarchical organization were mostly preserved during naturalistic visual stimulation; 4) however, a subset of these structures that were engaged in visual processing showed stronger synchronization within themselves and significant interactions with cortical visual networks. Therefore, fMRI signals in WM, like those in GM, may be utilized to uncover the intrinsic functional organization of WM, and to map axonal pathways that support neural signaling between cortical networks during complex tasks. The WM-fMRI methods as reported here and elsewhere (Ding et al., 2016; Gawryluk et al., 2014), as well as functional DTI methods (Mandl et al., 2008; Spees et al., 2013), may begin to uncover WM functionality in health and disease.

3.4.1 Spontaneous WM-fMRI Signals Reflect the Hierarchical Organization of Axonal Fibers

Spatial ICA has been widely used to map large-scale resting state networks (RSN) (Beckmann and Smith, 2004; Calhoun et al., 2008), especially when one seeks a relatively lower number of components. For a large-scale RSN that typically includes multiple discrete GM regions (e.g. the default-mode network), those regions are temporally correlated (Van Dijk et al., 2010) and structurally inter-connected through axonal fibers (Greicius et al., 2009). In other words, such large-scale RSNs have corresponding structural substrates to support neural signaling between different GM regions in the RSN (van den Heuvel and Sporns, 2013). It is thus tempting to

hypothesize that the WM substrate underlying a GM network carries synchronized activity within itself, whereas the WM substrates underlying different GM networks are temporally distinct in order to support their different functions. If this hypothesis were true, one would expect to be able to use ICA to decompose resting-state WM-fMRI signals into spatially independent and temporally distinct WM sub-systems that consist of axonal fibers connecting regions comprising individual GM networks.

However, spatially independent components of resting-state WM-fMRI signals did not appear as long-range fiber tracts; instead, they were mostly shown as cluster-like (or non-fiber-like) patterns, appearing as local segments of fiber tracts with a varying length. Nevertheless, these seemingly fragmented components were not isolated from each other, but instead exhibited varying levels of temporal cross correlations. These fragments tended to be more correlated if they were parts of the same fiber tract; combining these correlated components gave rise to the entire fiber tract; the combined fiber tract in one hemisphere tended to be correlated with the homologous fiber tract in the opposite hemisphere. As such, functional networks of WM fiber tracts did not readily result from a single-level decomposition of the WM-fMRI signals; instead, they emerged progressively as short segments of fiber tracts were combined into a hierarchical organization based on their temporal relations. The cluster-like appearance and hierarchical organization of the WM-fMRI ICA components might be counter-intuitive given what is known about neuronal structure. While the dendrites and the soma of a neuron occupy a tiny volume in GM, its axon runs a long distance in WM for relaying neuronal spikes. Different locations along the axon carry the same functional information, and thus are expected to be temporally synchronized along a long and continuous pathway in the fMRI time scale. However, the spatial resolution of fMRI is insufficient to resolve axons. An fMRI voxel samples a cubic piece of a large axonal bundle, containing a mixture of neuronal activity along every axon in the bundle. The fact that axons are routed and bundled differently at different voxels is expected to cause discontinuity in the spatial patterns of temporal synchronization in the fMRI signal. We speculate that this discontinuity is a major reason why ICA applied to coarsely sampled WM-fMRI data tend to reveal segments of fiber tracts as opposed to the intact long-range fiber tracts.

Also contributing to the discontinuity and segregation of the WM-fMRI signal is the orientation-dependence of T_2^*-sensitive MRI in WM. Magnetic susceptibility contrast in WM is anisotropic due to the highly oriented water compartments of the axonal bundles (Duyn, 2013; Lee

et al., 2011). This may in part explain why regions with higher densities of parallel axons, such as the corpus callosum, are more reliably detected in previous WM-fMRI activation studies. Interestingly, Ding et al. showed that the tensor of local temporal correlations in WM-fMRI signals demonstrated similar orientations as those observed with diffusion MRI (Ding et al., 2013), and could be specifically altered by tasks (Ding et al., 2016). Combining local and global correlation structures of WM-fMRI is a potentially promising direction for future studies.

3.4.2 Natural-Vision Task Reshapes the WM Functional Organization

It has been increasingly recognized that spontaneously emerging network patterns are functionally relevant since such activity patterns are well preserved from the resting state to various task states (Kenet et al., 2003; Smith et al., 2009; Wilf et al., 2017). Findings from the present study further extend this conclusion from the gray matter to the white matter. During naturalistic visual stimulation, the WM-fMRI signals exhibited reproducible independent components with similar spatial distributions as those observed in the resting state. Therefore, like those in the cortex, resting-state fMRI patterns within WM also reflect intrinsic functional units that are recruited to perform complex tasks. Although intrinsic functional structures in WM were preserved during the naturalistic visual task, the task enhanced the temporal synchronization within the task-related WM structures, as well as between the task-related WM structures and GM networks. The former is supported by the finding that bilateral visual pathways emerge as a single component, as opposed to the multiple hierarchical components found during the resting state; this implies that a stronger level of synchronization between the left and right optic radiations occur along with the tract emanating from LGN. The latter is supported by the finding that the WM component showing optic radiations is significantly correlated with several cortical visual networks during the task, but not during resting-state (also discussed later). Previous studies have shown that natural vision evokes reliable cortical fMRI responses (Hasson et al., 2004; Jääskeläinen et al., 2008) and spiking activity (Belitski et al., 2008; McMahon et al., 2015) within and across subjects. Interestingly, Mukamel et al. (2005) have shown significant correlations between spiking activity and fMRI response between different subjects watching the same movie. Furthermore, Astafiev et al. (2016) have demonstrated a link between BOLD fMRI in the MT+/LO and FA (measured through DTI) in the left optic radiation in mTBI patients. Extrapolating these studies and the findings from this study, we speculate that natural visual perception induces reliable and synchronized WM activity,

which gives rise to spiking activity as the direct effect, and the fMRI signal as the secondary indirect effect. While this speculation is reasonable, it remains to be confirmed, ideally with simultaneous white-matter neural recording and fMRI imaging.

3.4.3 Biophysical and Physiological Origins of WM-fMRI

Here, the so-called "fMRI" signal refers to the temporal variation of voxel intensity in gradient-echo echo-planar imaging (GE-EPI) images that primarily carry the T_2^*-weighted contrast. Multiple sources con tribute to this signal, but those sources may or may not bear any relationship to underlying neural activity (Bianciardi et al., 2009b). For the signals from gray-matter voxels, the source related to neural activity is blood oxygenation level dependent (BOLD) (Ogawa et al., 1990). The BOLD fluctuation reflects the combined effects of cerebral blood flow (CBF), blood volume (CBV), and the metabolic rate of oxygen ($CMRO_2$) (Buxton et al., 1998). Such hemodynamic and metabolic changes are coupled to neural activity in terms of both synaptic input and spiking output (Logothetis et al., 2001; Smith et al., 2002). While the basis of fMRI is complex, as it is a topic of active research and debate (Leopold and Maier, 2012), extra caution should be exercised when interpreting WM-fMRI.

Is the WM-fMRI signal BOLD? Despite a lower density of vasculature, the white matter has the vascular capacity for MRI-detectable hemodynamic changes (Gawryluk et al., 2014). Two defining features of the BOLD mechanism, cerebrovascular reactivity (Ogawa et al., 1990) and echo-time dependence (Kundu et al., 2012), have been both demonstrated for the WM-fMRI signal. The WM vasculature dilates in response to hypercapnia, showing detectable CBF and BOLD responses in the white matter, although the responses have a lower magnitude than in the gray matter (Rostrup et al., 2000; Thomas et al., 2014). The fluctuation and correlation of WM-fMRI signals at rest vary with different echo times, reaching their maxima at a similar echo time as the T_2^* in the gray matter (Ding et al., 2016). In addition, metabolic changes to neuromodulation are observable in the white matter (Weber et al., 2002). Astrocytes, which mediate neurovascular coupling in gray matter (Petzold and Murthy, 2011), are also present in white matter (Rash, 2010; Waxman and Ritchie, 1993). Therefore, all of the necessary machinery for neurometabolic and neurovascular coupling are generally in place in the white matter to give rise to detectable BOLD signals.

If it is BOLD, does the WM-fMRI signal report neural activity? WM-fMRI signals show task-dependent activations as reviewed in (Gawryluk et al., 2014). Their correlational structures are reorganized from the resting state to the task state, as shown in this study, as well as in (Ding et al., 2016). Therefore, the WM-fMRI signals are functionally relevant, and hence report, at least in part, neural activity in the white matter. However, it is not trivial and largely speculative to posit the specific type of neural activity that is coupled with the WM-fMRI signal. The BOLD signal is an indirect measure of neural activity (Logothetis and Wandell, 2004). In the gray matter, the neuronal origin of the BOLD signal may be synaptic activity observed with local field potential (Logothetis et al., 2001; Viswanathan and Freeman, 2007), or spiking activity observed with single or multi-unit activity (Mukamel et al., 2005; Smith et al., 2002). Synaptic activity (neuronal input) and spiking activity (neuronal output) are inherently linked with one another most of the time; their individual couplings with the BOLD signal are in fact comparable (Logothetis et al., 2001). When they have been dissociated under special experimental conditions, the BOLD signal has been found to be more coupled with synaptic activity (Rauch et al., 2008; Viswanathan and Freeman, 2007), although counter-examples have also been demonstrated (Pelled et al., 2009). As such, it is still not quantitatively understood which specific types of neuronal activity drive BOLD-fMRI. It is at least plausible that spiking activity is partly coupled with the BOLD signal, even in the gray matter. In the white matter, neuronal activity is mostly spiking activity propagating along the axon, with little synaptic activity (Gawryluk et al., 2014). This leads us to hypothesize that the WM-fMRI signal is BOLD and indirectly coupled to spiking activity. Nevertheless, this hypothesis is speculative and remains to be tested, while the signaling pathway that potentially links spiking activity to vasodilation also needs to be elucidated. To the best of our knowledge, there is no study directly addressing the relationship between spiking and fMRI signals in the white matter.

3.4.4 Methodological Considerations

We did not observe significant interactions between WM and GM at rest, but during task (Fig. 3.6B). A possible explanation for this observation was that the task might drive greater WM activity fluctuations, and thus a higher SNR. We did not expect the difference in SNR as a major contributor, because the fraction of the data variance explained by the signal versus noise components was comparable for the task state and the resting-state. Given future improvement in

the SNR of WM-fMRI, we anticipate that significant WM-GM correlations may also be observable even at rest, while tasks would further strengthen such correlations.

As mentioned in Introduction, the separation of the WM voxels from the GM voxels is an essential pre-processing step in this work in order to deal with the different dynamic range and correlational structure in WM and GM. When we performed a whole-brain ICA analysis on resting-state fMRI data without WM-GM separation (the number of components was 70), most of the components were gray- matter networks, as previously shown in numerous resting-state fMRI studies. There were a few components for which the spatial distributions were predominantly in the white matter, as opposed to the gray matter, as shown in Fig. 3.11. Given the very small number of white- matter-like components, the components tended to capture the patterns with the strongest degree of coherence (e.g. the global white- matter pattern, the optic radiations, and the corpus callosum). The whole-brain analysis did not allow for finer-grained pattern analysis and hierarchical clustering in the white matter, as enabled by only looking at the white-matter voxels.

Spatial smoothing was also helpful to improve the SNR of WM-fMRI. When we performed the white-matter ICA analysis on data without spatial smoothing, some of the general features were still observed (Fig. 3.10). However, without spatial smoothing, the overall reproducibility of the ICA maps was lower (Fig. 3.10A). Given the same criteria of selecting signal versus noise ICA components, we were only able to identify less than 10 “signal” components in the white matter, making the de-noising process more challenging. However, when we retained an identical number of components, we found qualitatively similar results; for example, components showing optic tracts appeared unilateral in the resting-state (Fig. 3.10B), but bilateral in the task state (Fig. 3.10C). Thus, the spatial smoothing is a helpful pre-processing step, but is not as essential as the WM-GM separation.

Head motion is generally a concern in fMRI (Van Dijk et al., 2012) and is likely a confounding factor in our WM-fMRI findings. In this study, we found that the resting-state sessions had significantly more head motion than the task state, likely because the engagement in the natural movie helped the subjects restrain their heads. Although we could not rule out the potential effects of head motion, we considered it as a minor confound to the WM-fMRI signals for the following reasons. First, the effects of head motion usually occur at the borders of different tissues (e.g. GM versus WM). As mentioned before, we used a conservative WM mask so as to avoid voxels around the GM-WM borders. Second, most of the head motion parameters varied in

time as slow drifts, which were discounted as the WM-fMRI signals were detrended (by removing up to 3rd order polynomial functions). Furthermore, the ICs kept in the ICA-based de-noising procedure were consistent across sessions and subjects, unlikely to be attributable to head motions. The time courses of the "signal" components also did not show either any signal drift or any abrupt change, which typically arise from head motion. Finally, it is worth noting that, overall, our results demonstrate that head movements occurring during the task are unlikely to be task-related.

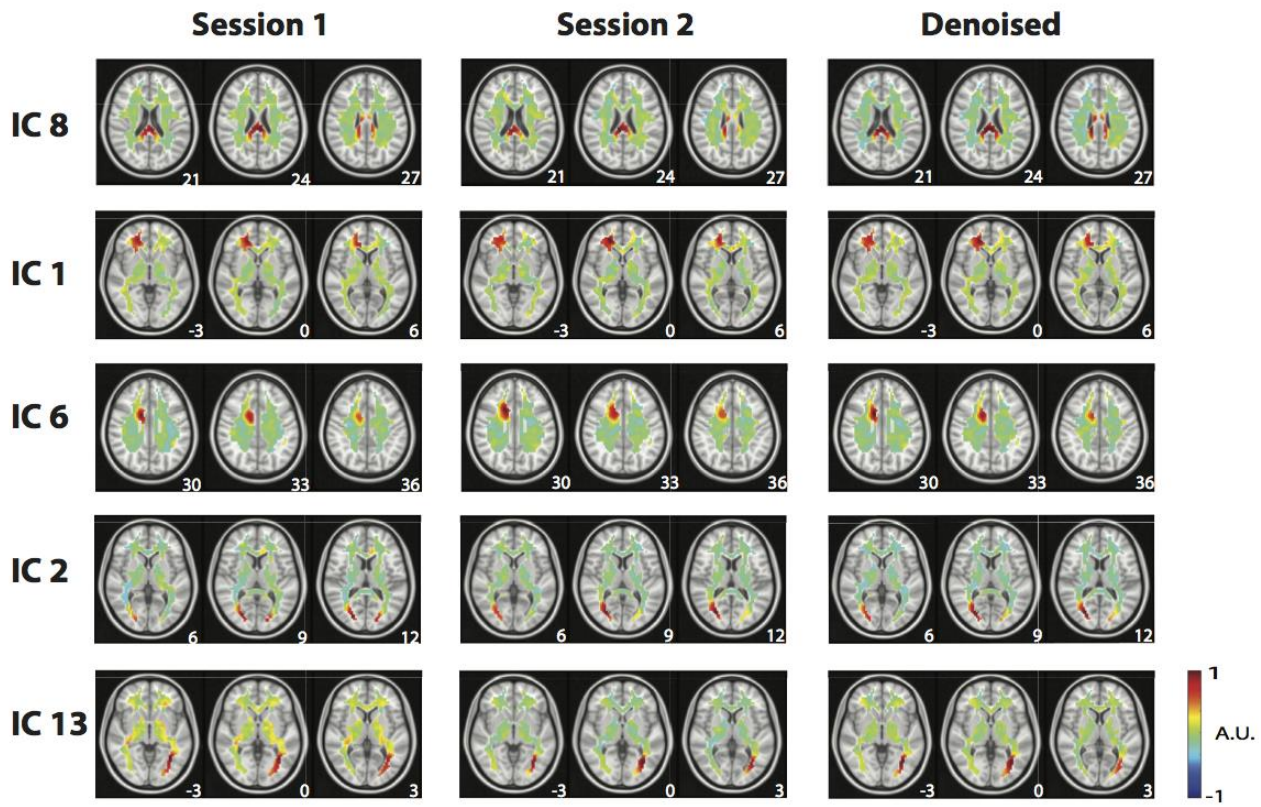

Figure 3.1. Reproducibility. A sample of reproducible resting-state components from Session 1 to Session 2, along with the corresponding de-noised components that consisted of information from both sessions. The z-coordinate (mm) of the position of each axial image is shown in the lower right corner. IC #8 corresponds to the posterior corpus callosum (splenium). IC #1 corresponds to the right forceps minor. IC #6 corresponds to part of the cingulum. IC #2 corresponds to a part of the optic radiations. IC #13 also corresponds to a part of the optic radiations.

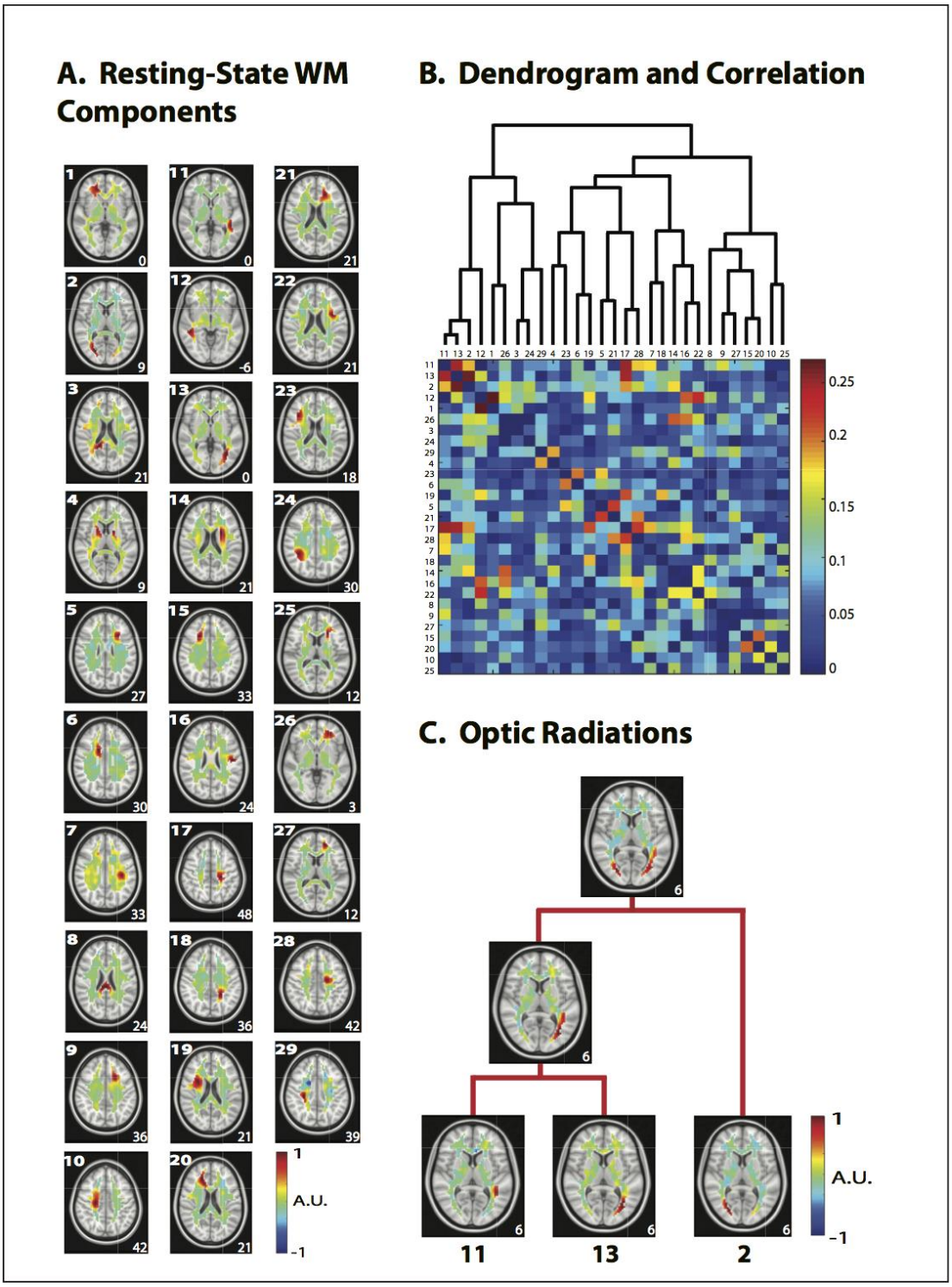

Figure 3.2. Hierarchical clustering of WM ICs in the resting state. A. 29 resting-state components were obtained after de-noising. B. The dendrogram used in the hierarchical clustering (top) with the corresponding temporal correlation values between WM ICs. C. Two portions of the left optic radiation were first clustered together, followed by clustering with a portion of the right optic radiation. For all axial slices in A and C, the z-coordinate (mm) is shown in the lower right corner.

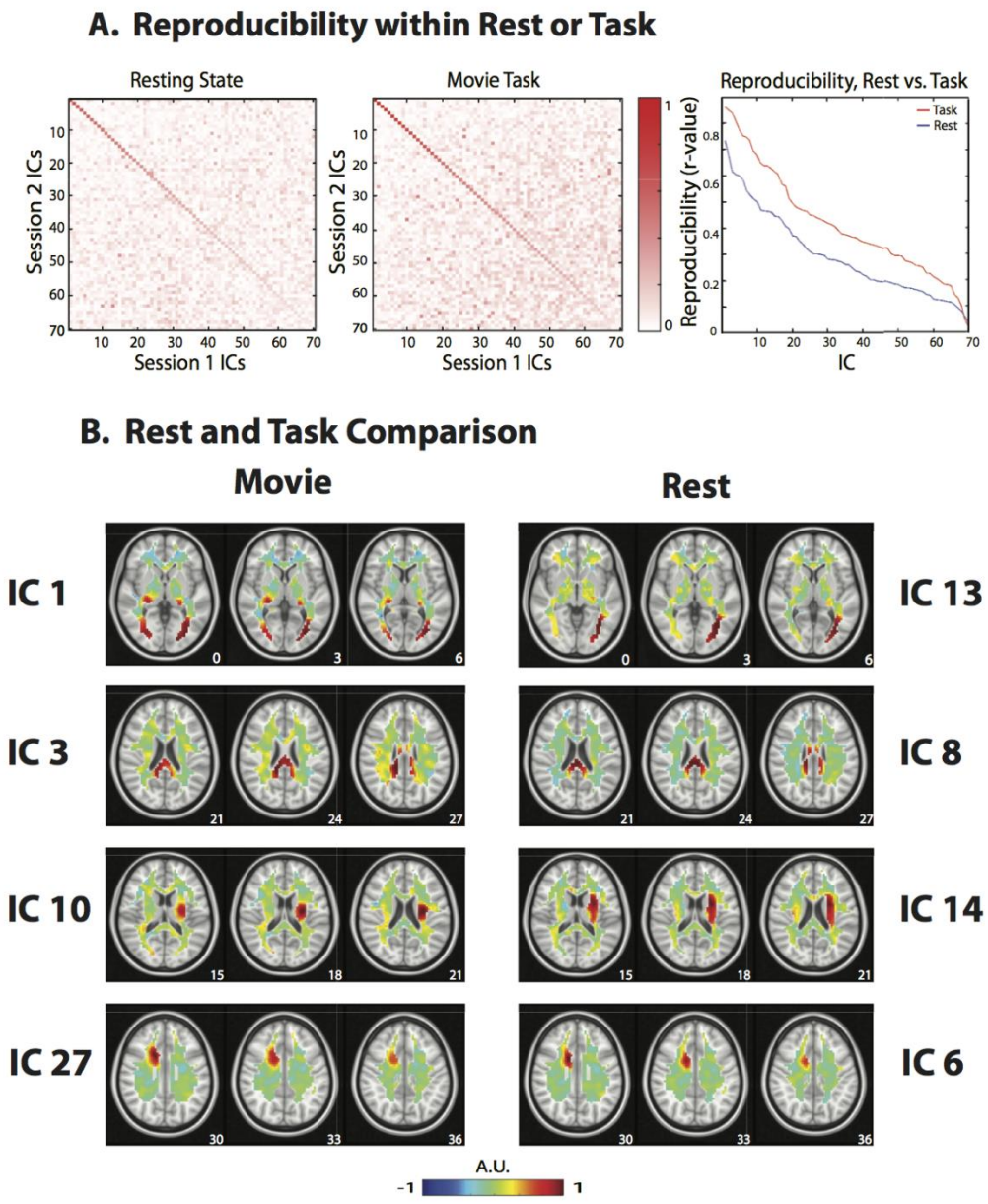

Figure 3.3. Reproducibility of ICA components. A. Reproducibility within the resting state or the task state. The spatial maps between session 1 and session 2 were optimally matched into pairs sorted in descending order of their spatial cross correlations. The matrices show the spatial correlations of one session's 70 components to the other session's 70 components, for either the resting state (left) or the movie task state (middle). The diagonal elements are the spatial correlations between individually 'paired' components. The 'paired' components generated by the movie task demonstrated stronger spatial correlations with one another than in the resting state (right). B. Rest and task comparison of WM components. Four example pairs of components obtained from resting-state (right) and task-state (left) are shown. While the first row shows notably different maps, the other three rows show similar patterns. The z-coordinate (mm) of the position of each axial image is shown in the lower right corner.

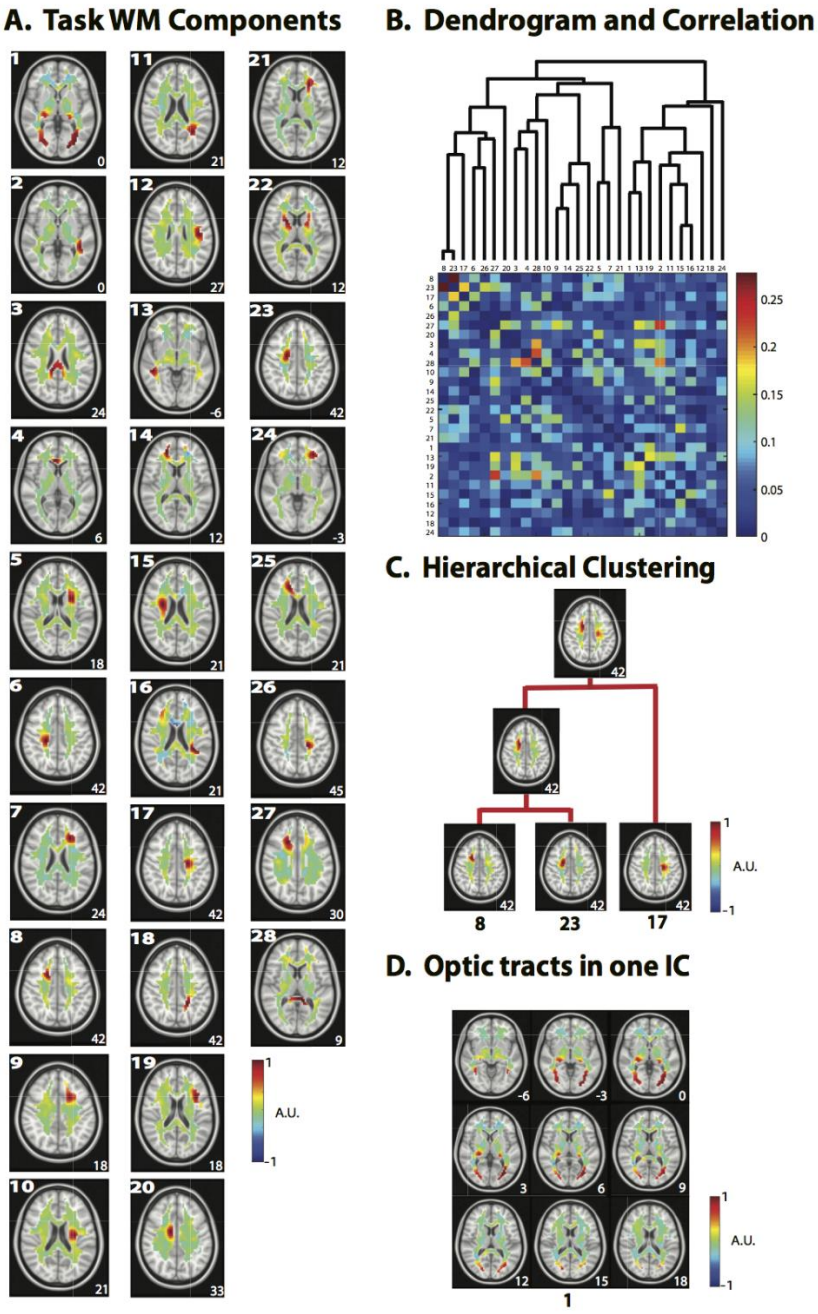

Figure 3.4. Task-state WM activity patterns. A. 28 task components were obtained after de-noising. The component number is shown in the top left corner. B. The dendrogram used in hierarchical clustering (top) with the corresponding temporal correlation values between WM ICs during the naturalistic visual task. C. Hierarchical clustering of task-unrelated components – (right anterior corona radiata). Two portions of a single tract were paired together, which were then paired with a more dorsal portion in the opposite hemisphere. D. Task-related component. One component shows the optic radiations emanating from the LGN. For all axial slices in A, C, and D, the z-coordinate (mm) is shown in the lower right corner.

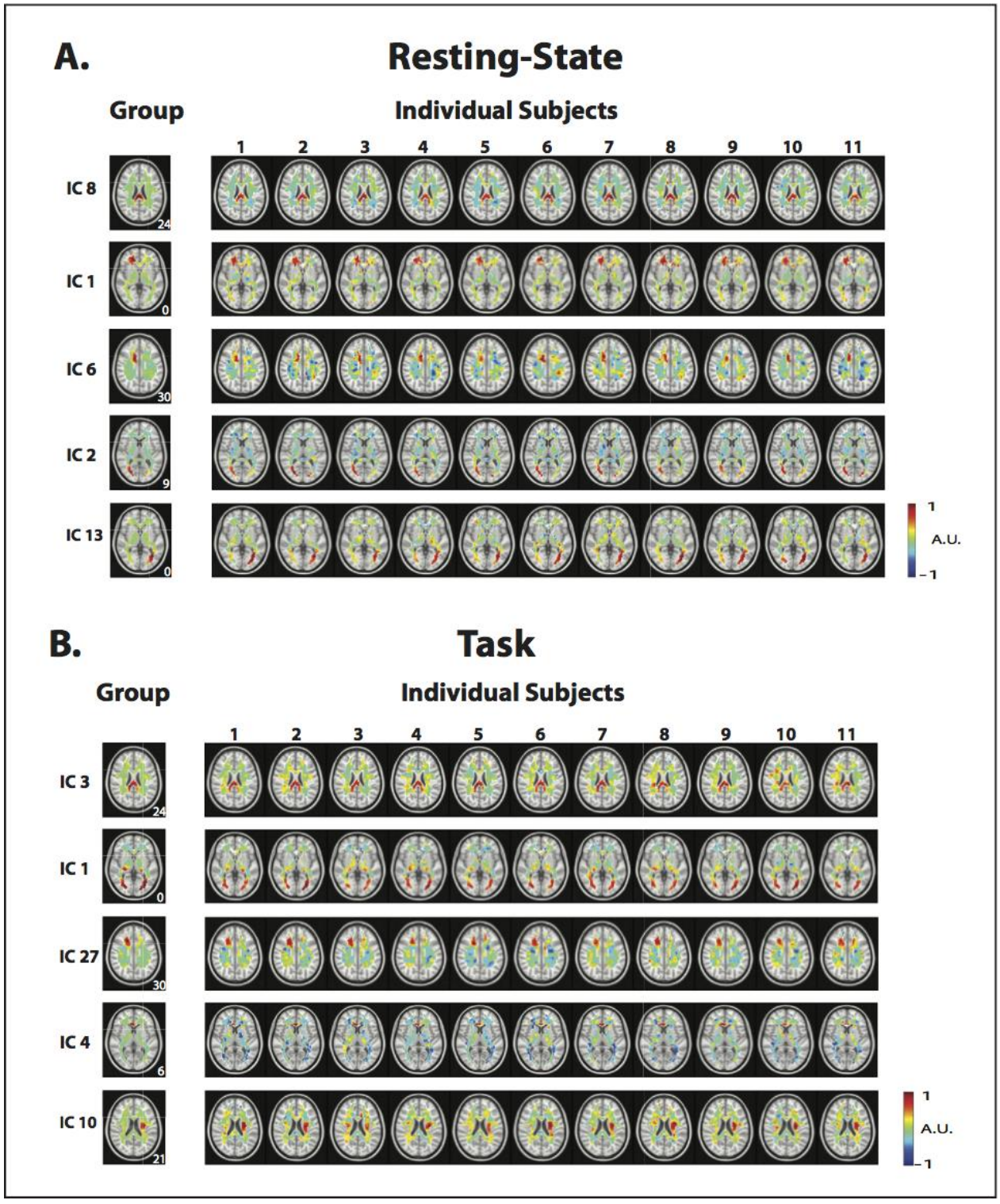

Figure 3.5. ICA maps from individual subjects obtained through dual regression in the resting-state (A) and during the task (B). For each state, the left-most column shows the group level map; the right columns show the maps obtained from individual subjects using this method. The z-coordinate (mm) is shown in the lower right corner.

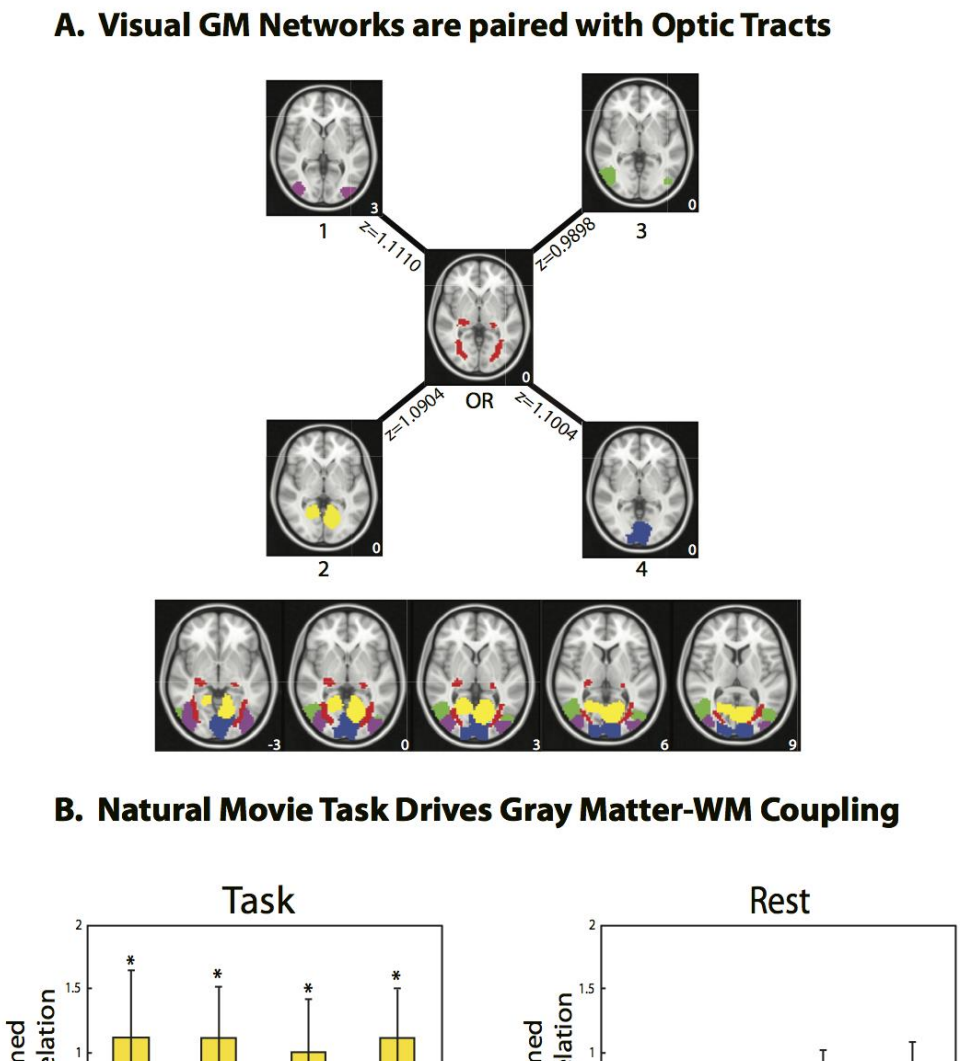

Figure 3.6. Functional relationships between WM and GM networks. A. During natural visual perception, the optic radiations (OR) in WM were temporally correlated with four cortical visual networks in GM (ICs #1, #2, #3, and #4). Shown below each connection is the average z-transformed cross correlation between the corresponding WM and GM regions. The z- coordinate (mm) is shown in the lower right corner. B. Such temporal correlations were statistically significant in the task state (left), but not in the resting state (right). These functional connectivity relationships are presented as OR-1 (i.e. optic radiations cross-correlation with cortical visual IC #1), OR-2, OR-3, and OR-4. The bar height indicates the average z- transformed cross correlation. The error bar indicates the standard error of the mean.

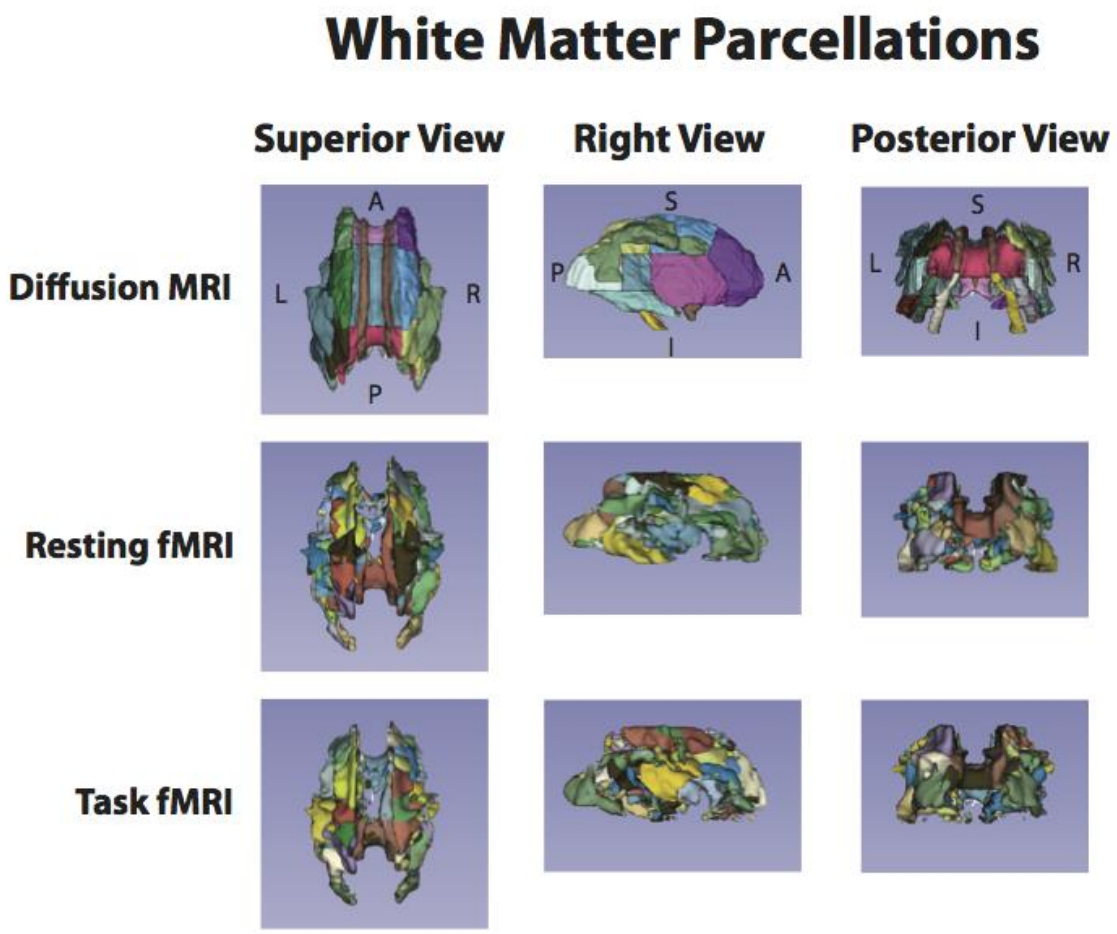

Figure 3.7. Structural vs. functional parcellation of the white matter. The first row shows the white-matter parcellation based on diffusion MRI (JHU ICBM-DTI-81 atlas). The second and third rows show the white-matter structures delineated from the thresholded ICA maps obtained from resting state fMRI or natural-vision task fMRI data, respectively.

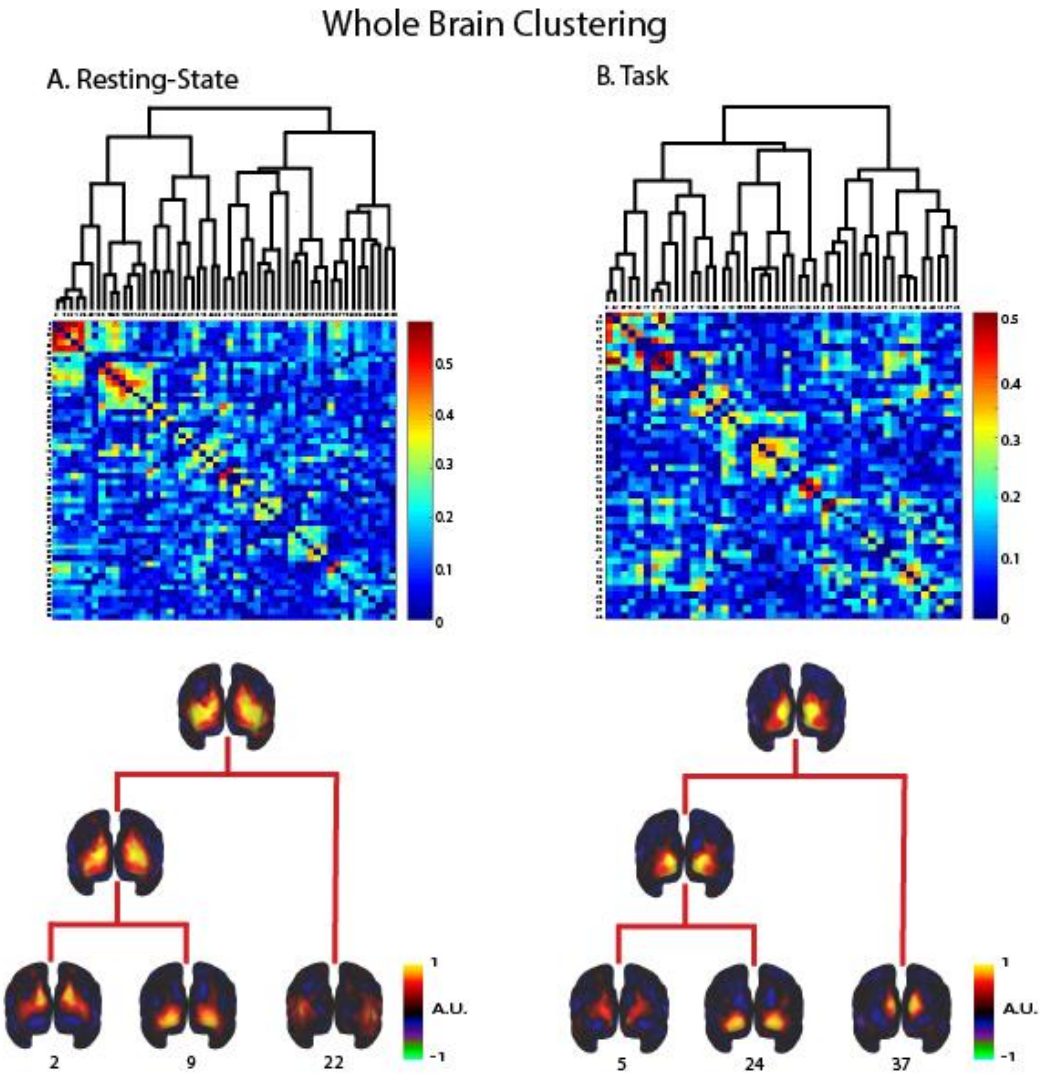

Figure 3.8. Hierarchical clustering of whole-brain (gray-matter) cortical networks during the resting state (A) and the natural vision task (B). For both A) and B), the top shows the dendrogram obtained from hierarchical clustering of spatially independent components; the middle shows the correlation matrix between independent components; the bottom shows the examples of visual cortical networks merging in a hierarchical manner.

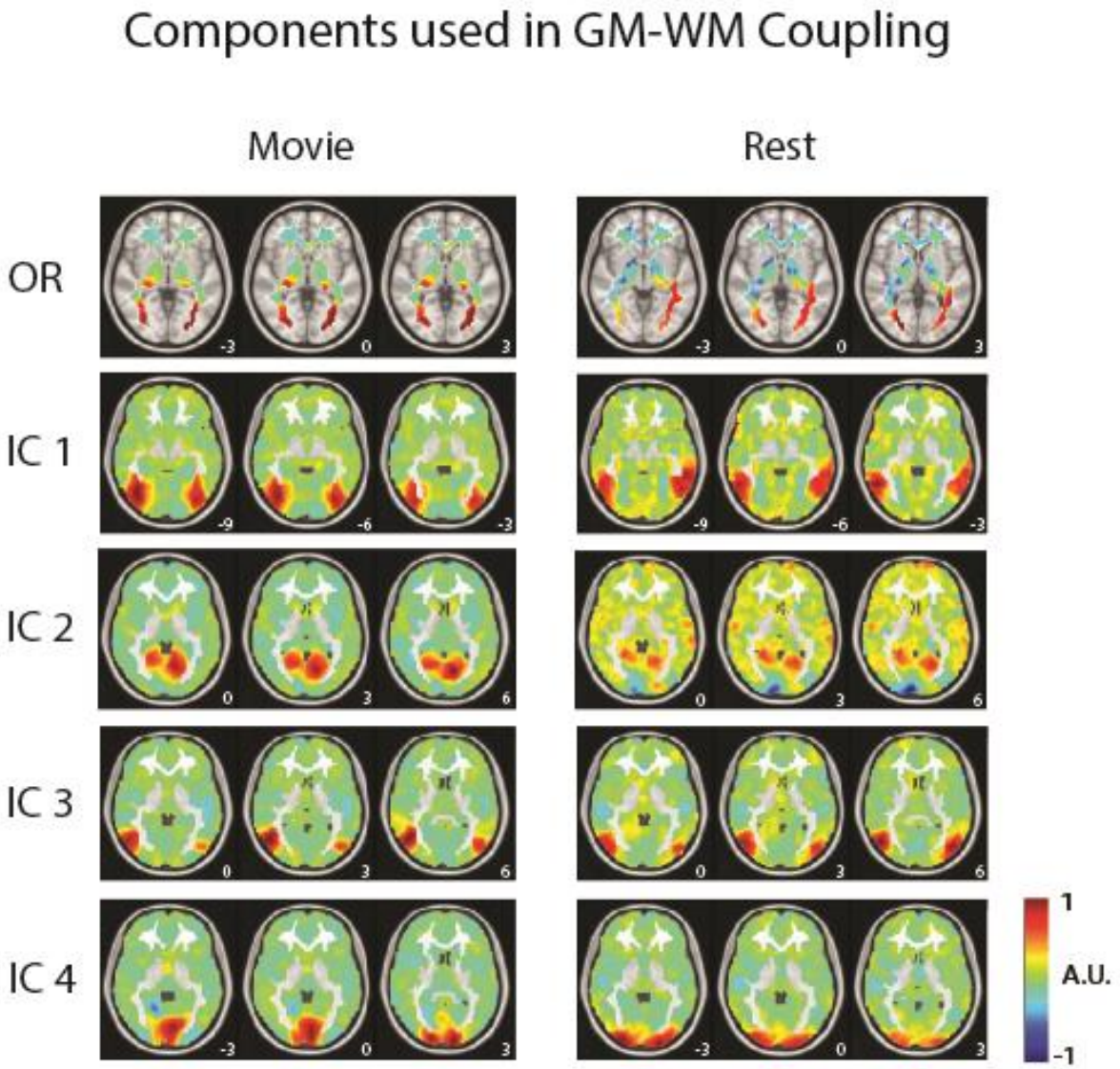

Figure 3.9. White-matter (the first row) and gray-matter (the second through forth row) components derived from the fMRI data in the natural-vision state (left) and the resting state (right).

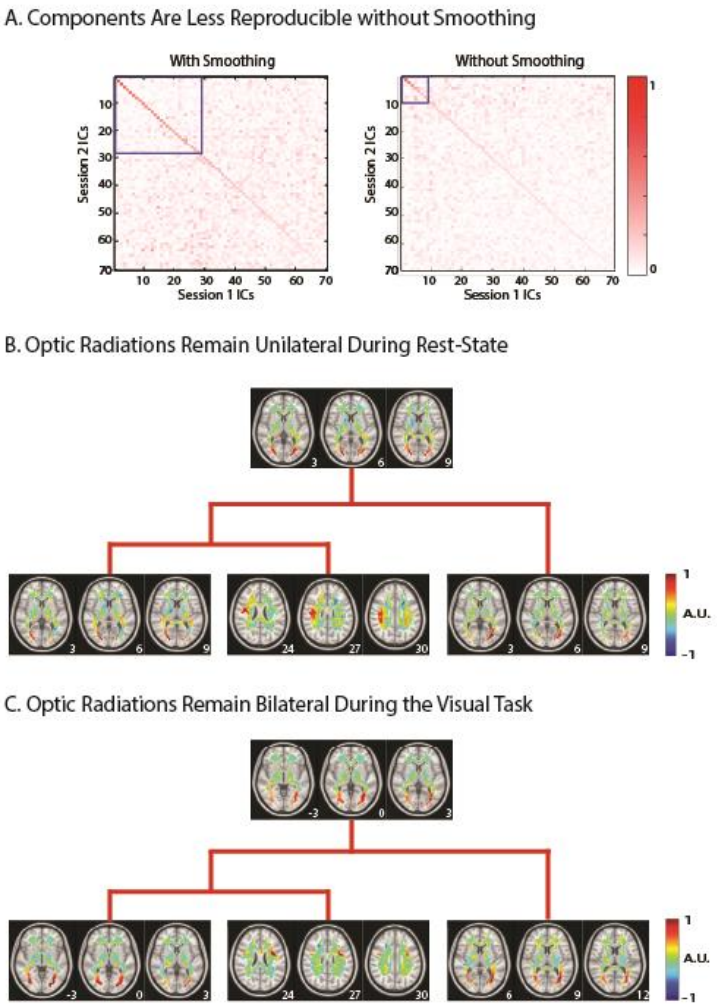

Figure 3.10. WM ICA without smoothing. A. Components are less reproducible without smoothing. The spatial maps between session 1 and session 2 were optimally matched into pairs sorted in descending order of their spatial cross correlations. The matrices show the spatial correlations of one session's 70 components to the other session's 70 components for the resting state, with (left) and without smoothing (right). The diagonal elements are the spatial correlations between individually 'paired' components. The blue box represents the extent of the paired components that were reproducible; the 'paired' components generated with spatial smoothing demonstrated stronger spatial correlations with one another than without smoothing (right). B. Using the best matched 29 'paired' components for consistency, the un-smoothed optic radiations components obtained during resting-state remained unilateral and were clustered together to form a bilateral tract. The components that formed part of this branch on the dendrogram are shown. The z-value (mm) of the position of each axial image is shown in the lower right corner. C. Using the best matched 28 'paired' components for consistency, the un-smoothed optic radiations components obtained during the task remained bilateral. Interestingly, the components were split into superior and inferior components, and those were clustered together. The components that formed part of this branch on the dendrogram are shown. The z-value (mm) of the position of each axial image is shown in the lower right corner.

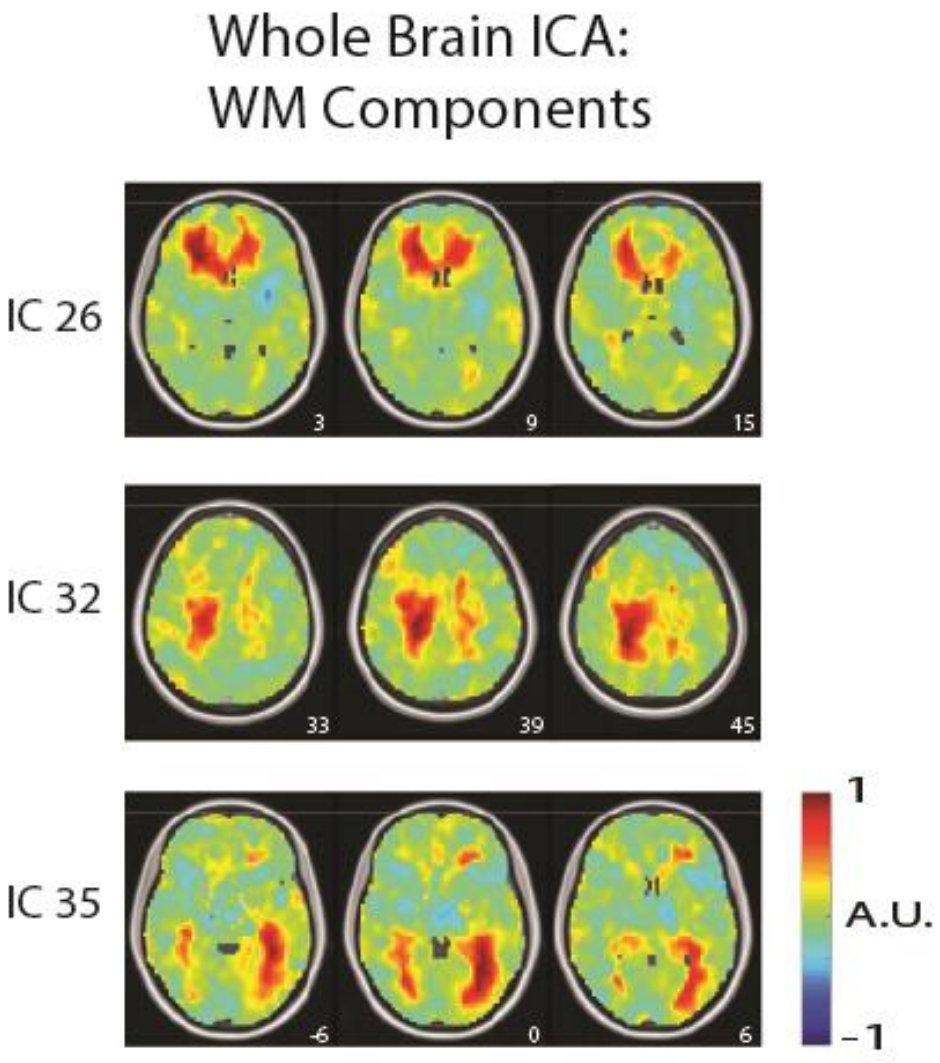

Figure 3.11. Three ICA maps with activity in white matter regions that were obtained with the whole brain (i.e. without masking out white matter) are shown. The z-value (mm) of the position of each axial image is shown in the lower right corner.

4. ALTERATIONS IN THE BRAIN'S FUNCTIONAL ORGANIZATION IN PRECLINICAL ALZHEIMER'S DISEASE

4.1 Rationale

Memory complaints are a key feature of mild cognitive impairment (MCI) (Petersen, 2016; Petersen et al., 2001), which has increasingly been considered a prodromal state for Alzheimer's Disease (AD) (Albert et al., 2011; Apostolova et al., 2006; Hodges, 2006; Small, 2007; Villemagne et al., 2013). In addition, there is growing evidence that older individuals with cognitive complaints, despite normal performance on cognitive tests, also have an increased risk for future cognitive decline and AD dementia (see Jessen et al. (2014); Reisberg et al. (2008) for review). Thus, cognitive complaints, or subjective cognitive decline (SCD), may in fact indicate the very first effects of AD pathology on cognitive function, between completely intact functioning and first detectable decline (Chao et al., 2010; Glodzik-Sobanska et al., 2007). This model would thereby suggest a continuum of Alzheimer's disease pathologies rather than a simple dichotomy of health and disease.

Consistent with this theory, several studies have demonstrated intermediate morphometric (Jessen et al., 2006; Saykin et al., 2006; Tepest et al., 2008; Van Norden et al., 2008; Wang et al., 2012), serological (Mosconi et al., 2008; Rami et al., 2011; Visser et al., 2009), and functional (Mosconi et al., 2008; Risacher et al., 2013; Wang et al., 2013) profiles of this patient group compared to MCI and cognitively normal control (CN) cohorts. This continuity makes intuitive sense; the pathologic features (e.g. neurofibrillary tangles (NFTs)) of the disease only insidiously build up in the hippocampus after amassing in neighboring regions (e.g. transentorhinal cortex) (Braak and Braak, 1995; Morrison and Hof, 1997). Using appropriately sensitive instrumentation and analysis methods, changes in neuronal wiring should be therefore perceptible before clinically detectable memory impairments and have been demonstrated in susceptible populations (Filbey et al., 2006; Filippini et al., 2009).

Despite the evidence and rationale, there is a paucity of functional neuroimaging (specifically fMRI) findings on SCD patients in the literature. Wang et al. (2013) demonstrated

that among MCI, SCD, and CN patient groups, significantly different functional connectivity (FC) of the DMN was localized to the hippocampus in MCI and SCD groups; further, the number of significantly different voxels appeared to have a direct relationship with disease progression. Contreras et al. (2016) included SCD patients in a conn-ICA analysis to identify three FC-related components related to cognitive change. Moreover, Lopez-Sanz et al. (2017) showed that a common pattern of FC alterations occurs between CN and SCD and CN and MCI patients, with the MCI group showing slightly more FC differences than the MCI group. To the best of our knowledge, these are the only three studies using fMRI to characterize changes in this potentially important patient population.

In the present study, we used complex scene encoding task and resting-state fMRI data to characterize activations and connectivity in CN, SCD, and MCI patients. In doing so, we sought to compare the similarity and extent of activation and FC changes in SCD and MCI patients. We hypothesized that MCI patients would show reduced activations and connectivity in the hippocampus and areas of the ventral visual pathway, and that SCD findings would be intermediate to that of CN and MCI groups.

4.2 Methods and Materials

4.2.1 Subjects

Participants were older adults selected from a larger cohort recruited for a longitudinal study of brain aging and memory (Indiana Memory and Aging Study). The participants completed this study in accordance with a protocol approved by the Institutional Review Board at Indiana University in which written informed consent was obtained. The present sample included 12 subjects with mild cognitive impairment (MCI), 12 subjects with significant cognitive complains despite cognitive test performance within the normal range (SCD group), and 12 cognitively normal, healthy controls (CN) with minimal cognitive complaints. Two subjects in the MCI group were excluded because their MRI images showed extensive neurodegeneration or an alternate pathology (temporal lobe infarct).

4.2.2 Experimental Design

Each subject underwent one fMRI session in each of two conditions. One session was obtained in the eyes-closed resting state, and the other session occurred during a block-design

scene-encoding task (Detre et al., 1998). Resting-state sessions were 10 minutes in length, and subjects were instructed to lay still with their eyes closed and keep their minds clear. In the task paradigm, following an initial 12-second period in which no stimuli were presented (i.e. a blank screen), complex visual scene encoding was compared with a control condition using alternating 36-second epochs. In the scene-encoding blocks, subjects were presented with a new scene every 4 seconds. Each scene was shown for 3.5 seconds, followed by 0.5 seconds of a blank screen. In total, eight 36-second epochs were used (288 seconds) were used, with 8.4 seconds of blank screen following the end of the alternating epochs. Pictures from a commercial library of digitized images (Photodisc, Seattle, WA) were used. Scenes containing diverse elements were selected to eliminate simple verbal encoding of the content. In the control condition, subjects viewed a single image containing the same luminosity and color content of one of the photographs but degraded using a scrambling algorithm. The repeated presentation of a single control image was repeated every 4 seconds, with presentations lasting 3.5 seconds, in order to match the frequency and duration of scene presentations. Prior to the scan, subjects were instructed to attempt memorization of the photographs but not of the control image and were informed that their performance would be later tested.

4.2.3 Data Acquisition

Whole-brain structural and functional MRI images were acquired using a 3-Tesla Prisma MRI system (Siemens, Erlangen, Germany). The fMRI data were acquired using a multi-band (MB) echo- planar imaging (EPI) sequence (gradient echo, 54 interleaved axial slices with 2.5mm thickness and 2.5×2.5 mm^2 in-plane resolution, TR=1200 ms, TE=29 ms, flip angle=65°, field of view=22×22 cm^2, MB factor = 3). T1-weighted anatomical images covering the whole head were acquired with a high-resolution magnetization-prepared rapid gradient echo (MPRAGE) sequence ($1.05 \times 1.05 \times 1.2$mm^3 voxel size). A 64-channel receive-only head and neck coil was used for all image acquisitions.

4.2.4 Pre-processing

Pre-processing of the fMRI images was carried out with a combination of AFNI (Cox, 1996), FSL (Smith et al., 2004), and MATLAB (Mathworks, Natick, MA). T_1-weighted anatomical images were non-linearly registered to the Montreal Neurological Institute (MNI) brain

template using a combination of *flirt* and *fnirt* in FSL (Smith et al., 2004). T_2*-weighted functional image time series were corrected for slice time variations using *slicetimer* in FSL, co-registered to the first volume within each series to account for head motion using *mcflirt* in FSL, restricted to within-brain tissues using *3dcalc* in AFNI (Cox, 1996), aligned to the T_1-weighted structural MRI using FSL's Boundary Based-Registration (BBR) function (Greve and Fischl, 2009), and registered to the MNI space with 3-mm isotropic voxels using *applywarp* in FSL. The first six volumes in the fMRI data were discarded to avoid any pre-steady-state longitudinal magnetization. Spatial smoothing was applied by using a Gaussian kernel (FWHM=6 mm). For each session and each voxel, the voxel time series was detrended by regressing out a third-order polynomial function that modeled the slow trend; the detrended signal was bandpass filtered (0.0001 - 0.1 Hz). Finally, the voxel time series were demeaned and normalized to unit variance.

4.2.5 Assessing Group-Level Task Activations

We first explored group-level task-activation differences using the task data. The stimulus effects at each voxel were estimated by fitting the amplitude of a boxcar function corresponding to the scene encoding epochs convolved with an estimate of the hemodynamic response function based on two gamma functions (http://www.fil.ion.ucl.ac.uk/spm/). This covariate was also filtered, de-meaned, and variance normalized in an identical manner to the data, and a global signal covariate was also included in the model. For each session and each voxel, a map of standardized estimated activation parameters was then obtained. For each patient group (CN, SCD, MCI), one sample t-tests (df = 11 for CN and SCD, 9 for MCI) were applied to these activation parameters to obtain group-level activation maps, and the number of significant voxels for each group was quantified. Activation maps were corrected for multiple comparisons using the false discovery rate (FDR) $q<0.05$.

4.2.6 Evaluating Group-Level Functional Connectivity

We then explored seed-based functional connectivity differences in relevant areas in the resting-state data. Seed voxels were selected by taking the intersection of voxels that were significantly activated in the CN group with voxels contained within three small, but aggregate, regions, "Perirhinal", "Posterior Parahippocampal Gyrus" ("PPhG"), and "Hippocampus", defined using the Brainnetome Atlas (Fan et al., 2016). Specifically, the perirhinal region consisted of

rostral area 35/36 bilaterally and caudal area 35/36 bilaterally (labels 109-112), the PPhG included area TL bilaterally (lateral PPhG) and area TH bilaterally (medial PPhG) (labels 113-114, 119-120), and the hippocampus was composed of the rostral hippocampus and caudal hippocampus areas bilaterally (labels 215-218). These seed locations were chosen because they are known to have early involvement in AD pathology (Braak and Braak, 1995); the "transentorhinal" region first implicated in NFT formation is actually located within the medial portion of the perirhinal cortex (Taylor and Probst, 2008). Included voxels were significant at the $q<0.05$ level for Perirhinal and PPhG regions and at the $p<0.001$ level for the Hippocampus.

Within each resting-state session, the correlation between the mean time series of the voxels contained within the seed and every other voxel's time series was calculated (after global signal regression), and the correlation coefficient was converted to a z-score using the Fisher's transform. The significance of the mean z-score (against zero) was evaluated by using one-sample t-tests ($df = 11$ for CN and SCD groups, $df = 9$ for MCI) with the threshold for significance at $p < 0.001$ (uncorrected).

4.2.7 Relating Connectivity and Activation Data

Finally, we sought to relate the activation and connectivity data at the individual subject level to uncover trends in the data that may not be immediately obvious by categorical groupings. Therefore, each subject's mean task data activation parameters in selected voxels were compared against each subject's mean resting-state connectivity values in a separate set of voxels. The voxels used for the task activation data were selected by conducting a two-sample t-test comparing the activation parameters in the MCI group to those of the CN group ($q<0.05$, FDR corrected). Similarly, the voxels used for the resting-state connectivity data were selected by conducting a two-sample t-test comparing the activation parameters in the MCI group to those of the CN group ($q<0.05$, FDR corrected) for each of the three seeds.

In doing so, there were some voxels that were more de-activated during the scene-encoding task than the control condition in the CN group compared to the MCI group, giving rise to more positive t-scores, whereas other voxels were more activated in the CN group than the MCI group. Because we were interested in mean values, we wanted to avoid artificially reducing the magnitude of these effects because of sign differences; therefore, we opted to segregate voxels based on the sign of the effect. Likewise, the same issue arose in the connectivity data in that some voxels were

more positively connected in the MCI condition than the control condition, and vice-versa. Therefore, the analysis for this section was four-fold for each of the three seeds: 1) each subject's mean activation parameter among voxels giving a positive t-score in the task data plotted against each subject's mean connectivity value in voxels giving a positive t-score; 2) each subject's mean activation parameter among voxels giving a positive t-score in the task data plotted against each subject's mean connectivity value in voxels giving a negative t-score; 3) each subject's mean activation parameter among voxels giving a negative t-score in the task data plotted against each subject's mean connectivity value in voxels giving a positive t-score; and 4) each subject's mean activation parameter among voxels giving a negative t-score in the task data plotted against each subject's mean connectivity value in voxels giving a negative t-score. Then, a linear regression model was fit to the data in each plot.

4.3 Results

4.3.1 Differences in Group-Level Task Activations

The scene-encoding task elicited clear activations along the ventral visual pathway toward mesial temporal regions in all patient groups (Fig. 4.1). A clear, progressive reduction in scene-encoding-related activations by phenotypic severity was made evident (Fig. 4.1). Quantitatively, In the CN group, 6454 voxels were significant, 3666 voxels were significant in the SCD group, and 201 voxels were significant in the MCI group (Fig. 4.1B). Small numbers of voxels within the hippocampus, as defined by the Brainnetome Atlas (Fan et al., 2016) (labels 215-218), were activated at the FDR-corrected threshold ($q < 0.05$) in some groups (CN – 1 voxel, SCD – 8 voxels, MCI – 0 voxels); after relaxing this multiple-comparisons corrected threshold somewhat to $p<0.001$, more activations were revealed (CN – 22 voxels, SCD – 52 voxels, MCI – 25 voxels voxels). Similar findings were obtained in other mesial temporal regions, including the perirhinal cortex (labels 109-112) (CN – 14 voxels, SCD – 83 voxels, MCI – 18 voxels, $p<0.001$, uncorrected) and the PPhG (CN – 4 voxels, SCD – 24 voxels, MCI – 0 voxels, $p<0.001$ uncorrected).

Elements of the default mode network (Raichle et al., 2001), including the precuneus, lateral parietal cortices, and medial prefrontal cortex, also appeared to be de-activated, in contrast with the voxels in the ventral visual pathway (Fig. 4.1A). This de-activation also appeared to

include the most DMN voxels in the CN group, contained less voxels in the SCD group, and encompassed the fewest voxels in the MCI group, much like the activation findings.

4.3.2 Altered FC Across Groups

As in the activation data, a progressive reduction in the connectivity was again apparent using all three seeds (Fig. 4.2). Using the perirhinal seed, 845 voxels were significantly correlated in the CN group, 182 voxels were significantly correlated in the SCD group, and 24 voxels were significantly correlated in the MCI group. Using the PPhG seed, 3687 voxels were significantly correlated in the CN group, 755 voxels were significantly correlated in the SCD group, and 126 voxels were significantly correlated in the MCI group (Fig. 4.1B). Finally, using the hippocampus seed, 102 voxels were significantly correlated in the CN group, 241 voxels were significantly correlated in the SCD group, and 31 voxels were significantly correlated in the MCI group (Fig. 4.1B). In this case, there was a relatively uniform, if not increased, FC of the hippocampus between SCD and CN groups, with a reduction in FC in the MCI group.

Each seed elicited connected in broader inferotemporal regions; the perirhinal cortex, PPhG, and hippocampus seeds exhibited FC across one another, as well as with the entorhinal cortex (defined using Brainnetome Atlas labels 115-116). Again, smaller scale connectivity revealed a similar reduction in FC across disease severity. The perirhinal cortex seed was most correlated with the PPhG, hippocampus, and entorhinal cortex in CN (PPhG – 109 voxels, hippocampus – 84 voxels, entorhinal cortex – 2 voxels) and least correlated with these regions in MCI (PPhG – 8 voxels, hippocampus – 0 voxels, entorhinal cortex – 0 voxels). The SCD group had an intermediate effect (PPhG – 23 voxels, hippocampus – 21 voxels, entorhinal cortex – 0 voxels). The PPhG seed was also most correlated with the perirhinal cortex, hippocampus, and entorhinal cortex in CN (perirhinal cortex – 35 voxels, hippocampus – 171 voxels, entorhinal cortex – 15 voxels) and least correlated with these regions in MCI (perirhinal cortex – 11 voxels, hippocampus – 3 voxels, entorhinal cortex – 0 voxels). Here too the SCD group had an intermediate effect (perirhinal cortex– 27 voxels, hippocampus – 126 voxels, entorhinal cortex – 4 voxels). Finally, the hippocampus seed was also better correlated with the other inferior temporal regions (PPhG, perirhinal cortex, and entorhinal cortex) in CN (PPhG – 2 voxels, perirhinal cortex – 0 voxels, entorhinal cortex – 8 voxels) than in MCI (PPhG – 0 voxels, perirhinal cortex – 0 voxels, entorhinal cortex – 0 voxels). In this case, however, the SCD group actually had slightly

enhanced FC between these regions (PPhG – 25 voxels, perirhinal cortex – 1 voxel, entorhinal cortex – 3 voxels).

4.3.3 Relationship Between Task-Activations and Resting-State Functional Connectivity

Using two-sample t-tests, voxels that exhibited significantly stronger activation in MCI relative to CN were considered to be "positive activation contrasts" (Fig. 4.3, left column, "Activation, MCI>CN"), and voxels that exhibited significantly weaker and/or more negative activation values in MCI relative controls were considered "negative activation contrasts (Fig. 4.3, right column, "Activation, CN<MCI"). Positive activation contrast areas included small regions of voxels in the middle frontal gyrus (inferior frontal junction (IFJ)), superior frontal gyrus (Brodmann area 8), and lateral temporal cortex (Brodmann area 21). Negative activation contrast areas included parts of the ventral visual pathway in the inferior occipital gyrus, the middle temporal visual area (V5/MT+), the cuneal gyrus (medially), the fusiform gyrus, the hippocampus, and the precuneus. Likewise, for each FC seed, we also used two-sample t-tests to determine positive and negative FC contrasts. These were defined as voxels with significantly stronger FC in MCI compared to CN (Fig. 4.3, bottom rows for each seed, "MCI>CN") and voxels with significantly weaker and/or more negative FC in MCI compared to CN (Fig. 4.3, top rows for each seed, "MCI<CN"), respectively. Using the perirhinal cortex seed, areas with a positive FC contrast included the thalamus, the cingulate cortex, and the middle temporal gyrus. Areas with a negative FC contrast included medial visual regions (cuneal and lingual regions near the parieto-occipital sulcus), inferior temporal regions (i.e. ventral visual pathway), and a very small area in the inferor frontal gyrus (Brodmann 45, likely Broca's area). Using the PPhG seed, areas with a positive FC contrast included the thalamus, the cingulate cortex, and very sparsely in lateral visual areas. Areas with a negative FC contrast with this seed included the inferior occipital gyrus, V5/MT+, several medial visual regions (cuneal and lingual regions near the parieto-occipital sulcus), and near the occipital poles. Finally, using the hippocampus seed, positive FC contrast regions were concentrated in the cingulate cortex. Negative FC contrast regions included the middle occipital gyrus, V5/MT+, and the inferior frontal gyrus.

For all seeds used, there was a clear relationship between task activation data and connectivity data based on disease severity. The results of the linear regression parameters for each of the plots is shown in Table 1. Overall, there was a fairly linear trend between the FC and

activation data, showing the relatedness of these two measures. The relationship between voxels in which MCI patients had reduced task activations and resting-state FC were relatively clear cut. Interestingly, voxels in which the mean activation parameters were more negative in CN were actually negative in terms of their sign; MCI patients tended to have values closer to zero (in many cases, slightly positive). We observed a similar effect with connectivity. Voxels in which the mean connectivity values were more negative in CN were also negative in terms of their sign, with MCI patients having values closer to zero (also in many cases slightly positive).

The distances of the data points for each subject demonstrated that the subjects were fairly well clustered around their group centroids (Fig 4.4), with few instances for which a subject's data point was actually closer to another group's centroid. The results of each plot's analysis are summarized in Table 2 and presented in Fig. 4.5. For the CN group, the perirhinal cortex seed had the most tightly clustered data (mean distance to centroid = 1.9779±0.8909), and the greatest accuracy in that the fewest number of subjects were actually closer to centroid from SCD or MCI groups. Conversely, the Hippocampus seed had the broadest spread of data (mean distance to centroid = 2.4068±1.0142) and the poorest accuracy in that the most number of subjects were actually closer to centroid from SCD or MCI groups. For the SCD group, the perirhinal cortex seed again gave the most tightly clustered data (mean distance to centroid = 1.7996±0.9048) and had the greatest accuracy. Here, the broadest spread of data was actually found using the PPhG seed (mean distance to centroid = 2.6483±1.2988), which had the worst discrimination between SCD and MCI or CN, with the SCD-MCI separability being the poorer of the two. Finally, for the MCI patients, the hippocampus in fact gave rise to the most tightly clustered data (mean distance to centroid = 1.5625±0.7949) that also had the greatest accuracy in terms of the spread of the MCI subjects being closest to the correct centroid. Here again, the broadest spread of data occurred using the PPhG seed (mean distance to centroid = 2.0811±1.0892), which had the worst discrimination between SCD and MCI or CN, with the SCD-MCI separability being the poorer of the two.

Table 1. Linear regression parameters for FC versus activation plots.

Connectivity Seed Location	Sign of Activation Contrast (Relative to CN)	Sign of Connectivity Contrast (Relative to CN)	Slope (±SD)	Intercept (±SD)	R^2
Perirhinal Cortex	Pos.	Pos.	1.0994(±0.1774)	-0.9312(±0.3178)	0.5454
	Pos.	Neg.	-1.3327(±0.2247)	1.5580(±0.4024)	0.5237
	Neg.	Pos.	-0.5854(±0.1028)	2.1591(±0.7060)	0.5034
	Neg.	Neg.	0.6506(±0.1390)	-1.8277(±0.9550)	0.4063
PPhG	Pos.	Pos.	1.2335(±0.1795)	-1.0736(±0.3216)	0.5961
	Pos.	Neg.	-1.6396(±0.3262)	2.5943(±0.5844)	0.4412
	Neg.	Pos.	-0.6782(±0.1007)	2.5248(±0.6914)	0.5866
	Neg.	Neg.	0.8234(±0.1931)	-1.7119(±1.3267)	0.3622
Hippocampus	Pos.	Pos.	1.2303(±0.2124)	-0.8678(±0.3804)	0.5119
	Pos.	Neg.	-1.2148(±0.2360)	0.3561(±0.4228)	0.4529
	Neg.	Pos.	-0.6838(±0.1174)	2.7667(±0.8061)	0.5148
	Neg.	Neg.	0.7421(±0.1186)	-3.6416(±0.8148)	0.5502

Table 2. Discriminability Measures Among CN, SCD, and MCI groups.

FC Seed Location	Sign of Activation Contrast (Relative to CN)	Sign of FC Contrast (Relative to CN)	Mean Distance to Centroid, CN(±SD)	No. CN Subj. Closer to Other Centroids (SCD, MCI)	Mean Distance to Centroid, SCD(±SD)	No. SCD Subj. Closer to Other Centroids (CN, MCI)	Mean Distance to Centroid, MCI(±SD)	No. MCI Subj. Closer to Other Centroids (CN, SCD)
Perirhinal Cortex	Pos.	Pos.	1.5078(±0.7566)	0, 0	1.3926(±0.6047)	0, 2	1.0883(±0.7495)	0, 1
	Pos.	Neg.	2.0177(±0.8707)	2, 0	1.4077(±0.5834)	1, 1	1.8212(±0.8871)	0, 3
	Neg.	Pos.	1.9928(±0.9083)	0, 0	2.2344(±1.1413)	0, 2	2.0296(±0.7569)	0, 2
	Neg.	Neg.	2.3931(±1.0278)	1, 0	2.1636(±1.2896)	0, 2	2.5331(±0.7841)	0, 2
	Mean		1.9779(±0.8909)	0.75, 0	1.7996(±0.9048)	0.25, 1.75	1.8681(±0.7944)	0, 2
PPhG	Pos.	Pos.	1.2980(±0.8383)	1, 0	1.5656(±0.7069)	1, 1	1.2436(±0.6993)	0, 2
	Pos.	Neg.	2.3734(±1.7639)	1, 1	3.0637(±1.6103)	1, 4	2.1294(±1.5685)	1, 2
	Neg.	Pos.	1.9873(±0.5808)	0, 0	2.3455(±1.1999)	1, 3	2.0796(±0.8208)	0, 2
	Neg.	Neg.	2.9033(±1.4716)	2, 1	3.6185(±1.6782)	2, 4	2.8716(±1.2681)	0, 3
	Mean		2.1405(±1.1637)	1, 0.5	2.6483(±1.2988)	1.25, 3	2.0811(±1.0892)	0.25, 2.25
Hippo-campus	Pos.	Pos.	2.1219(±0.9278)	1, 1	1.7024(±1.0787)	1, 1	1.0617(±0.7107)	0, 0
	Pos.	Neg.	2.3070(±1.063)	2, 0	1.5862(±0.7056)	1, 0	1.2243(±0.6494)	0, 0
	Neg.	Pos.	2.5479(±0.8918)	0, 0	2.5107(±1.3102)	1, 2	1.9581(±0.8771)	0, 1
	Neg.	Neg.	2.6502(±1.1740)	2, 0	2.4070(±1.091)	1, 3	2.0059(±0.9425)	0, 1
	Mean		2.4068(±1.0142)	1.25, 0.25	2.0516(±1.0464)	1, 1.5	1.5625(±0.7949)	0, 0.5

4.4 Discussion

We have shown that fMRI-based measurements relate to severity of patient diagnoses – from relative neurocognitive health, to initial subjective cognitive decline below clinically-detectable thresholds, to mild cognitive impairment. The results lead to the following findings: 1) a progressive reduction in the extent of significantly activated voxels occurred using a scene encoding task among CN, SCD, and MCI patient groups; 2) a progressive reduction in connectivity using seeds in the inferior temporal cortex (perirhinal cortex, PPhG, and hippocampus) was observed during the resting-state among CN, SCD, and MCI patient groups; 3) a linear relationship existed between the connectivity and activation data, enabling a two-dimensional representation each subject's (and group's) fMRI-based measurements. Therefore, the results further support that SCD is an intermediate stage between relative a cognitively normal status and mild cognitive impairment, a precursor stage of Alzheimer's disease.

4.4.1 Explaining Heterogeneity of Findings via Alzheimer's Disease Pathogenesis

It is difficult to pinpoint the underlying pathophysiology of Alzheimer's Disease at the earliest stages because many of the histologic hallmarks of Alzheimer's Disease, such as NFT aggregation in the medial temporal lobe and amyloid deposition, also occur in normal aging (Dubois et al., 2016; Morrison and Hof, 1997). However, we do know that that there is a progression of regional involvement. Even in the earliest stages, some parts of the inferior temporal cortex are affected earlier than others; namely, the transentorhinal cortex (actually located within the medial perirhinal cortex (Taylor and Probst, 2008)) precedes the entorhinal cortex in involvement, which in turn is affected before the hippocampus.

This pattern of development may explain some of our findings. Seed-based connectivity differences were marked among all three groups using the Perirhinal and PPhG seeds. However, using the Hippocampus seed, a reduction in connectivity between CN and SCD conditions was not observed (Fig. 4.2). Additionally, we found the fact that different seed locations elicited better clustering of data points and greater diagnostic accuracy (as measured by determining whether Euclidean distances from each subject's data point to the centroid of the assigned group or other groups were closer) using the 2-dimensional plots very interesting and also likely related to disease pathogenesis. For the CN and SCD groups, this was the case with the perirhinal cortex seed, but for the MCI group, the hippocampus, the worst seed location for the CN group for these measures,

was optimal. The greater degree of overlap between the CN and SCD groups using the hippocampus seed was noticeable on the plots (Fig. 4.3). This similarity may result from AD-like pathology not yet significantly affecting the hippocampus in SCD patients. Early, subclinical memory deficits may instead be observed from the loss of projection cells in the transentorhinal and entorhinal cortices to parts of the hippocampus (Braak and Braak, 1995; Morrison and Hof, 1997), which could explain why the perirhinal cortex seed provided the best separation between groups in MCI and SCD groups. The fact that this process may have already occurred in both SCD and MCI groups may explain why this seed did not elicit the same degree of diagnostic separability.

4.4.2 Task Activation and FC Data are Related and Informative

It is difficult to pinpoint the underlying pathophysiology of Alzheimer's Disease at the earliest stages because many of the histologic hallmarks of Alzheimer's Disease, such as NFT aggregation in the medial temporal lobe and amyloid deposition, also occur in normal aging (Dubois et al., 2016; Morrison and Hof, 1997). However, we do know that that there is a progression of regional involvement. Even in the earliest stages, some parts of the inferior temporal cortex are affected earlier than others; namely, the transentorhinal cortex (actually located within the medial perirhinal cortex (Taylor and Probst, 2008)) precedes the entorhinal cortex in involvement, which in turn is affected before the hippocampus.

This pattern of development may explain some of our findings. Seed-based connectivity differences were marked among all three groups using the Perirhinal and PPhG seeds. However, using the Hippocampus seed, a reduction in connectivity between CN and SCD conditions was not observed (Fig. 4.2). Additionally, we found the fact that different seed locations elicited better clustering of data points and greater diagnostic accuracy (as measured by determining whether Euclidean distances from each subject's data point to the centroid of the assigned group or other groups were closer) using the 2-dimensional plots very interesting and also likely related to disease pathogenesis. For the CN and SCD groups, this was the case with the perirhinal cortex seed, but for the MCI group, the hippocampus, the worst seed location for the CN group for these measures, was optimal. The greater degree of overlap between the CN and SCD groups using the hippocampus seed was noticeable on the plots (Fig. 4.3). This similarity may result from AD-like pathology not yet significantly affecting the hippocampus in SCD patients. Early, subclinical memory deficits may instead be observed from the loss of projection cells in the transentorhinal

and entorhinal cortices to parts of the hippocampus (Braak and Braak, 1995; Morrison and Hof, 1997), which could explain why the perirhinal cortex seed provided the best separation between groups in MCI and SCD populations. The fact that this process may have already occurred in both SCD and MCI groups may explain why this seed did not elicit the same degree of diagnostic separability.

4.4.3 Relationship to MCI and AD findings

AD patients have demonstrated alterations in both task activations and resting-state connectivity. Many task activation studies have revealed reduced activations in medial temporal lobe structures in AD patients compared to controls (Golby et al., 2005; Kato et al., 2001; Machulda et al., 2003; Rombouts et al., 2000; Sperling et al., 2003), with some reports of compensatory hyperactivations in the prefrontal cortex (Grady et al., 2003). FC studies have shown decreased DMN connectivity (Damoiseaux et al., 2012; Greicius et al., 2004; Jones et al., 2011), increased prefrontal connectivity (Agosta et al., 2012), and increased salience network connectivity (Zhou et al., 2010) in AD patients.

However, research in MCI patients has generated conflicting results. Some groups have shown that MCI patients mostly mirror the medial temporal lobe hypo-activations and reduced connectivity found in AD populations (Machulda et al., 2003; Petrella et al., 2007; Rombouts et al., 2005; Sorg et al., 2007), whereas others have encountered paradoxical hyper-activations and hyper-connectivity of these same regions (Bai et al., 2011; Dickerson et al., 2005; Kircher et al., 2007). To disentangle this difference, Celone et al. (2006) posited that there may be a nonlinear trajectory of changes.

Here, we that the dominant effect, particularly in the ventral visual pathway, appeared to be reduced activations in MCI and SCD patients, with the MCI patients showing a greater reduction. However, within the structures of the inferior temporal lobe, we found a mixture of more positive and more negative activations in MCI patients versus controls. In terms of FC, we found that MCI patients and SCD patients exhibited reduced FC to inferior temporal seeds, with the MCI patients again showing a greater reduction. However, there were also some voxels that were more strongly connected to the seeds in MCI than in CN conditions. Perhaps instead of a spatially-uniform, purely temporal heterogeneity in affected areas (Celone et al., 2006), a spatial

heterogeneity of differences may occur as the brain attempts to compensate for the impaired signaling in these early stages.

SCD patients exhibiting similar differences to CN patients as MCI patients, though slightly reduced in magnitude, provides strong imaging-based evidence that clinically, SCD likely precedes MCI in AD pathology. Further, we were able to delineate differences among the three different groups, giving promise to the notion that non-invasive, imaging-based measures can be used in early-stage diagnosis of this extremely pervasive disease.

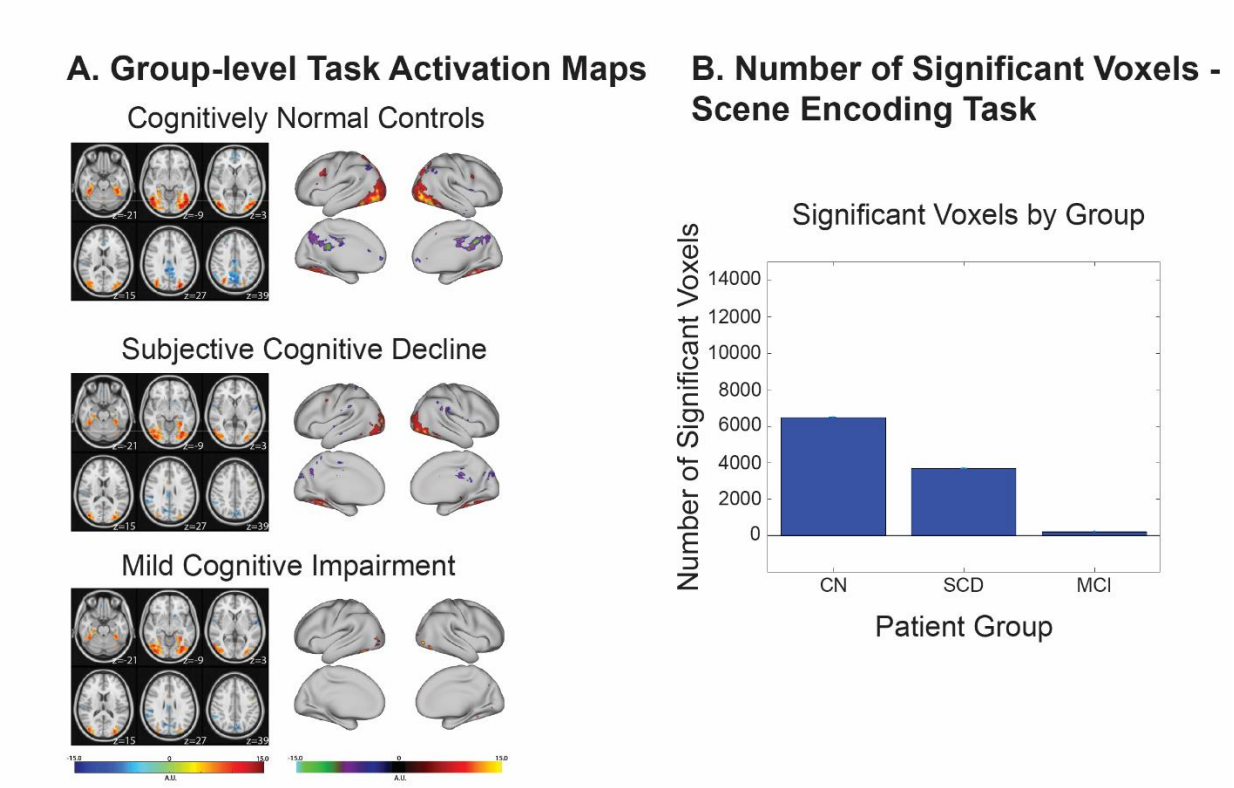

Figure 4.1. Group-level Activations. Group level activation maps by patient group and number of significant voxels. Activation data was evaluated for significance using one-sample t-tests (df = 11 for CN and SCD groups, 9 for MCI). Z-values of MNI coordinates for slices are shown in the lower right corner of each image.

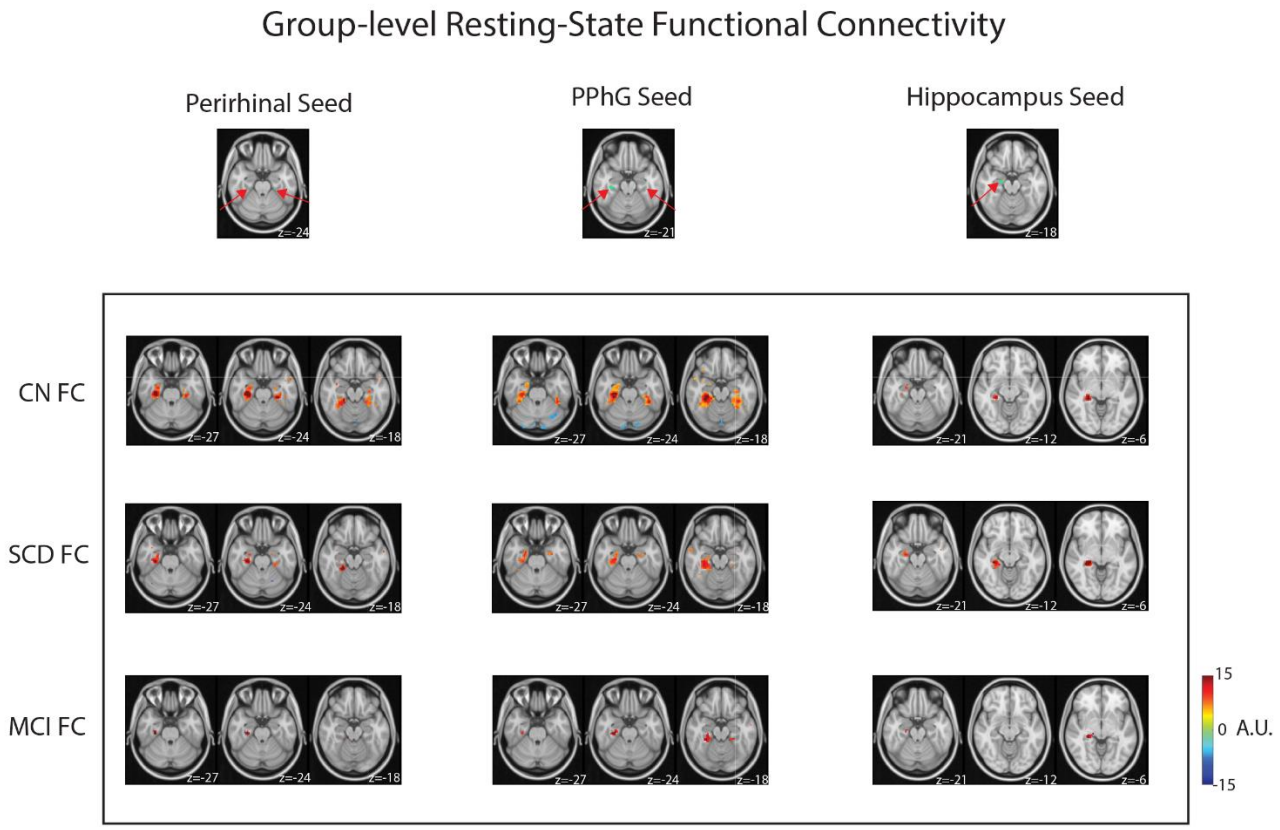

Figure 4.2. Group level connectivity maps using seeds in the Perirhinal Cortex, Posterior Parahippocampal Gyrus, and Hippocampus. FC data were evaluated for significance using one-sample t-tests (df = 11 for CN and SCD groups, 9 for MCI group). Z-values of MNI coordinates are displayed in the lower right corner of each image.

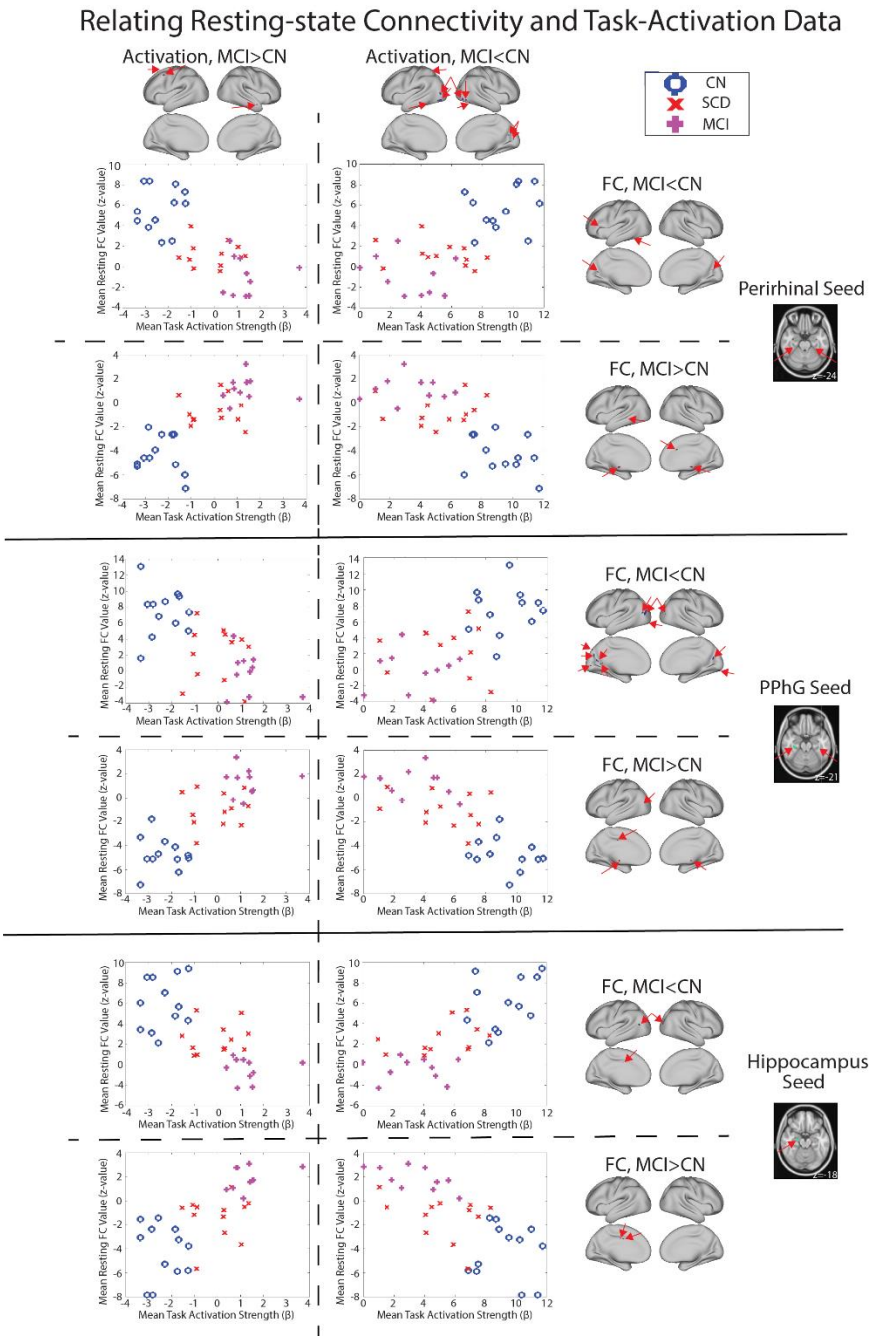

Figure 4.3. Relationship Between Task Activation and Resting-State Connectivity Data. Voxels with significantly different activation parameters across CN and MCI groups were determined using a two-sample t-test; likewise, voxels with significantly different correlations to the seed across CN and MCI groups were also determined using a two-sample t-test. Voxels with activation parameters that were more negative in MCI were then separated from voxels that were more positive in MCI, and voxels that were strongly correlated with the seed in MCI were separated from voxels that were more weakly correlated with the seed in MCI, creating 4 subplots. Then, each subject's mean activation and correlation values over these voxels were plotted. Z-values of MNI coordinates for slices of seeds are shown in the lower right corner of images, and the FC contrasts were shown projected onto the cortical surface.

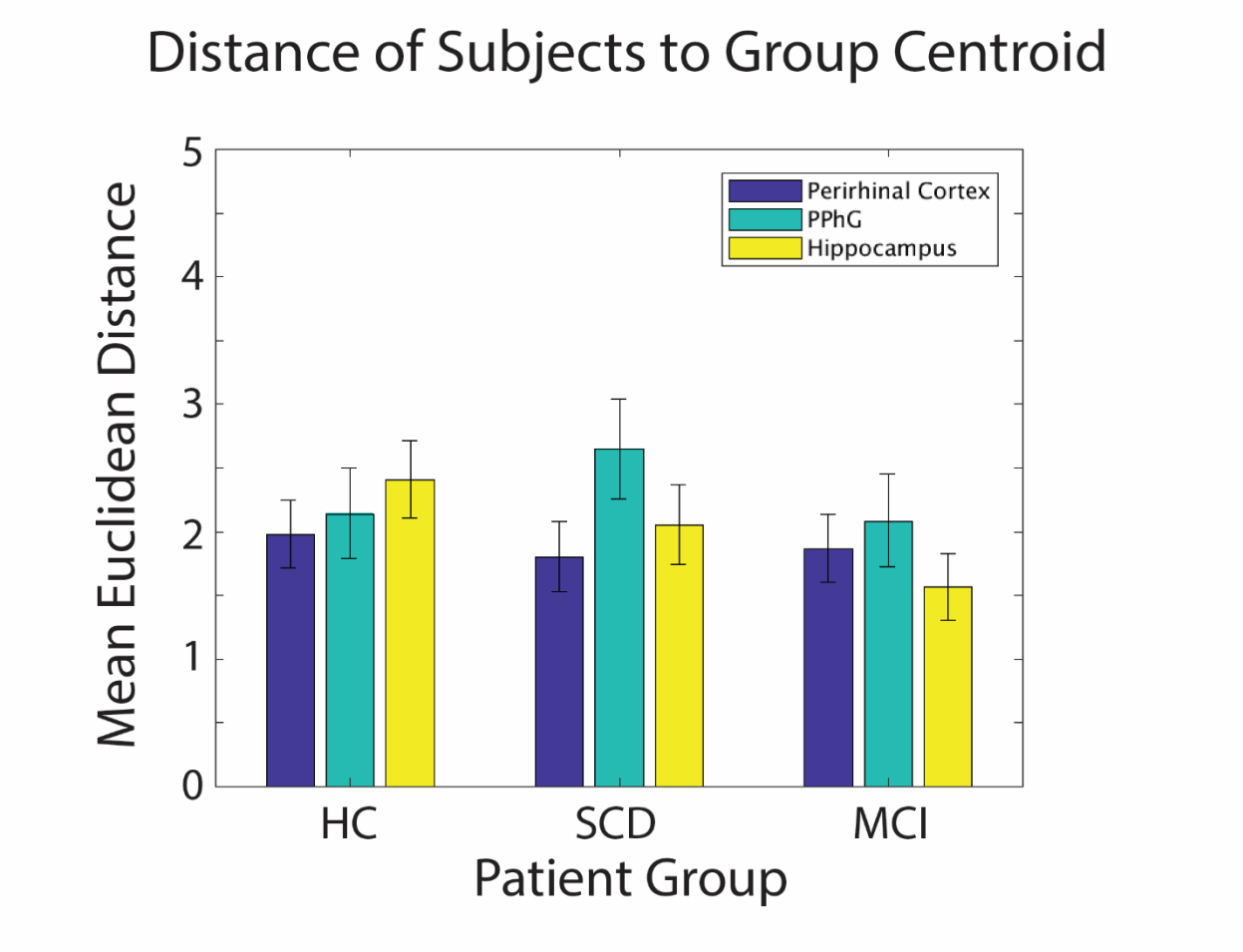

Figure 4.4. Mean Distance to Centroid by Patient Group and FC Seed Location. The distance of each subject to its diagnostic group's centroid was calculated for each of the four plots in Fig. 4.3. Then, the mean distance values for each seed and each diagnostic group were calculated and included in the bar graph. Different patient groups were better clustered by different seeds. The perirhinal cortex seed had optimal clustering (as measured by distance to centroid) of HC and SCD groups, whereas the hippocampus seed had the shortest distance to centroid in MCI.

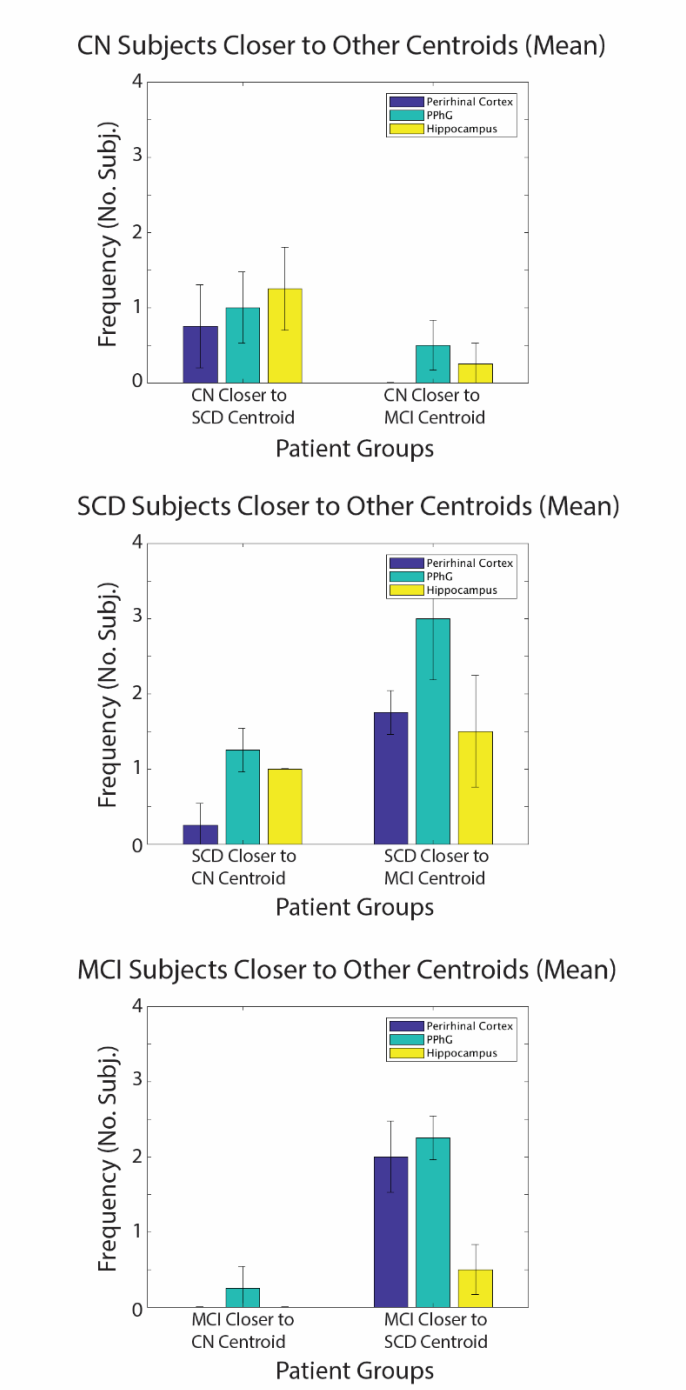

Figure 4.5. Mean Distance to Other Diagnostic Groups' Centroids by Patient Group and FC Seed Location. The distance of each subject to each diagnostic group's centroid was calculated for each of the four plots in Fig. 4.3. Then, the number of subjects closer to other diagnostic groups' centroids was calculated for each seed and included in the bar graph as an indirect measure of diagnostic discrimination. Different patient groups had better discriminability using different seeds. The perirhinal cortex seed had the best separation HC and SCD groups, whereas the hippocampus had the best separation of SCD and MCI.

5. CONCLUSIONS AND RECOMMENDATIONS

5.1 Conclusions

The work presented in this dissertation has shed light on how and why FC may change in brain states, including tasks and disease. It is my hope that the work conducted during my doctoral training may enable others to think about the applications of FC in fMRI somewhat differently, toward uncovering novel information about how the brain functions in everyday life. Notwithstanding, neuroimaging-based tools will likely continue to elucidate the underpinnings of the interaction between physical form and cognitive function (i.e. the "mind-body" problem, presented early in Chapter 1), with the goal of improving our fundamental understanding of the brain and of health and disease.

In Chapter 2, we showed that the difference between FC at rest and during a naturalistic visual task, which contains an unknown mixture of task-evoked and spontaneous signals, cannot be explained by separating the task-evoked FC from the connectivity profile. Further, we observed that FC between resting-state and task states is mostly conserved. Moreover, during the resting-state, non-visual sensory-related functional networks (e.g. somatomotor, auditory) were more coupled to visual networks than during the natural movie; the task-evoked FC was predominantly characterized by positive and restricted correlations among regions within the visual system. Finally, the task-evoked FC accounted for only 3-15% of the FC difference between task and rest conditions. Ultimately, our results suggested that task-evoked FC and spontaneous FC are neither linear nor additive, which we found somewhat surprising.

In Chapter 3, we were able to show subtle task-related differences in the white matter using fMRI, which has only rarely been used to study functions in this tissue type. Using data-driven analysis methods, we investigated the spatiotemporal characteristics of white-matter fMRI time series in the cerebral white matter in the resting state and during naturalistic visual perception. We found that spatially independent components (ICs) of resting-state fMRI signals in the white-matter revealed reproducible fiber-like structures. Further, the ICs were temporally correlated in an intrinsically hierarchical manner. The intrinsic WM structures and their hierarchical organization were mostly preserved during naturalistic visual stimulation. However, a subset of these structures (e.g. the optic radiations) involved with visual processing showed stronger within-

component synchronization and even exhibited significant interactions with cortical visual networks. Considering this evidence, we conclude that fMRI signals in WM may be used to elucidate the intrinsic functional organization of WM; further, they may even be used to map axonal pathways that support neural signaling between cortical networks during complex tasks.

In Chapter 4, we examined the utility of combining resting-state FC with task-activation studies in uncovering changes in brain activity during preclinical Alzheimer's Disease (mild cognitive impairment (MCI) and subjective cognitive decline (SCD) populations), based on data collected at the Indiana University School of Medicine. We showed a progressive reduction in the extent of significantly activated voxels occurred using a scene encoding task among CN, SCD, and MCI patient groups, as well as a progressive reduction in connectivity using seeds in the inferior temporal cortex (perirhinal cortex, PPhG, and hippocampus) in these patient groups. We also observed a linear relationship between the connectivity and activation data, enabling a two-dimensional representation each subject's (and group's) fMRI-based measurements. Overall, the results further support that SCD is an intermediate stage between a cognitively normal status and mild cognitive impairment, a precursor stage of Alzheimer's disease.

5.2 Future Work

The methods, analyses, and findings of this dissertation present several opportunities for future investigations. Recommended future areas of inquiry for each chapter are presented below.

With respect to the rest-task interaction and the contributions of task-evoked FC, it may be beneficial to include different types of tasks (active vs. passive) and/or anesthesia states to determine if the negative interaction exhibits a task-dependence or state-dependence. We also observed regional heterogeneity in the suppression of spontaneous FC (occipital/visual regions exhibited stronger suppression) during the task, so using a task targeted toward a different sensory system (e.g. auditory) would be beneficial in revealing this interplay. Further, if we attempted to classify the brain's task state, would the task-evoked FC lead to better classification performance than the apparent task FC? Finally, although many studies have used electrophysiological recordings or fMRI to reveal this phenomenon (Churchland et al., 2010; He, 2013; Ponce-Alvarez et al., 2013), to the best of my knowledge, there are no existing studies that combine the two. Integrating neural recordings with fMRI may provide complementary mechanistic information and

insights about which signal types (action potentials, LFPs, fMRI) exhibit these effects most strongly.

Concerning white-matter fMRI, investigations that combine neural recordings with fMRI measurements, such as Logothetis et al. (2001), in the WM may elucidate the neurophysiological origins of the T_2^* signal. The relationships between action potentials or LFPs and fMRI signal may be different in white matter versus gray matter. Further, multi-echo fMRI protocols (Kundu et al., 2012) can also clarify whether the signal is in fact BOLD due to TE dependence (see also Ding et al. (2016)). Moreover, the usefulness of the WM fMRI signal can be explored by investigating whether the WM signal can be used to classify brain states (either different tasks or health/disease status); some studies of this nature have recently been published (Chen et al., 2017; Zhang et al., 2017). Additional analysis methods to further improve the SNR in white matter may be necessary for this work, and may include additional ICA-based de-noising or usage of task-evoked signals (Simony et al., 2016; see also Chapter 2).

Finally, the Alzheimer's Disease data, though promising, was somewhat under-powered and would benefit from increased sample sizes. Using a naturalistic task or beta-series correlations (Rissman et al., 2004) would enable us to better understand how changes in FC during tasks translate to diagnostic group. In addition, such analysis methods would allow us to determine whether the suppression of spontaneous correlations we found in Chapter 2 has a relationship to disease status. Importantly, we also would be interested in the utility of neuroimaging measures in explicitly classifying diagnostic groups. By establishing an imaging biomarker for earliest detectable changes, it may be possible to uncover an optimal time at which future therapeutic interventions may halt the progression of disease.

REFERENCES

Agosta, F., Pievani, M., Geroldi, C., Copetti, M., Frisoni, G.B., Filippi, M., 2012. Resting state fMRI in Alzheimer's disease: Beyond the default mode network. Neurobiology of Aging 33, 1564-1578.

Albert, M.S., DeKosky, S.T., Dickson, D., Dubois, B., Feldman, H.H., Fox, N.C., Gamst, A., Holtzman, D.M., Jagust, W.J., Petersen, R.C., Snyder, P.J., Carrillo, M.C., Thies, B., Phelps, C.H., 2011. The diagnosis of mild cognitive impairment due to Alzheimer's disease: Recommendations from the National Institute on Aging-Alzheimer's Association workgroups on diagnostic guidelines for Alzheimer's disease. Alzheimer's and Dementia 7, 270-279.

Andrews-Hanna, J.R., Smallwood, J., Spreng, R.N., 2014. The default network and self-generated thought: component processes, dynamic control, and clinical relevance. Ann N Y Acad Sci 1316, 29-52.

Apostolova, L.G., Dutton, R.A., Dinov, I.D., Hayashi, K.M., Toga, A.W., Cummings, J.L., Thompson, P.M., 2006. Conversion of mild cognitive impairment to Alzheimer disease predicted by hippocampal atrophy maps. Archives of Neurology 63, 693-699.

Aramaki, Y., Honda, M., Okada, T., Sadato, N., 2006. Neural correlates of the spontaneous phase transition during bimanual coordination. Cerebral Cortex 16, 1338-1348.

Arfanakis, K., Cordes, D., Haughton, V.M., Moritz, C.H., Quigley, M.A., Meyerand, M.E., 2000. Combining independent component analysis and correlation analysis to probe interregional connectivity in fMRI task activation datasets. Magnetic Resonance Imaging 18, 921-930.

Arieli, A., Sterkin, A., Grinvald, A., Aertsen, A., 1996. Dynamics of ongoing activity: explanation of the large variability in evoked cortical responses. Science 273, 1868-1871.

Association, A.s., 2017. 2017 Alzheimer's Disease Facts and Figures.

Astafiev, S.V., Shulman, G.L., Metcalf, N.V., Rengachary, J., MacDonald, C.L., Harrington, D.L., Maruta, J., Shimony, J.S., Ghajar, J., Diwakar, M., Huang, M.-X., Lee, R.R., Corbetta, M., 2015. Abnormal White Matter Blood-Oxygen-Level-Dependent Signals in Chronic Mild Traumatic Brain Injury. Journal of Neurotrauma 32, 1254-1271.

Astafiev, S.V., Zinn, K.L., Shulman, G.L., Corbetta, M., 2016. Exploring the physiological correlates of chronic mild traumatic brain injury symptoms. NeuroImage: Clinical 11, 10-19.

Attwell, D., Laughlin, S.B., 2001. An Energy Budget for Signaling in the Grey Matter of the Brain. Journal of Cerebral Blood Flow & Metabolism 21, 1133-1145.

Azouz, R., Gray, C.M., 1999. Cellular mechanisms contributing to response variability of cortical neurons in vivo. The Journal of Neuroscience 19, 2209-2223.

Bai, F., Watson, D.R., Shi, Y., Wang, Y., Yue, C., YuhuanTeng, Wu, D., Yuan, Y., Zhang, Z., 2011. Specifically progressive deficits of brain functional marker in amnestic type mild cognitive impairment. PLoS One 6.

Baldauf, D., Desimone, R., 2014. Neural Mechanisms of Object-Based Attention. Science 344, 424-427.

Bandettini, P.a., Wong, E.C., Hinks, R.S., Tikofsky, R.S., Hyde, J.S., 1992. Time course EPI of human brain function during task activation. Magnetic resonance in medicine : official journal of the Society of Magnetic Resonance in Medicine / Society of Magnetic Resonance in Medicine 25, 390-397.

Becker, R., Reinacher, M., Freyer, F., Villringer, A., Ritter, P., 2011. How Ongoing Neuronal Oscillations Account for Evoked fMRI Variability. Journal of Neuroscience 31, 11016-11027.

Beckmann, C.F., DeLuca, M., Devlin, J.T., Smith, S.M., 2005. Investigations into resting-state connectivity using independent component analysis. Philosophical transactions of the Royal Society of London. Series B, Biological sciences 360, 1001-1013.

Beckmann, C.F., Smith, S.M., 2004. Probabilistic Independent Component Analysis for Functional Magnetic Resonance Imaging. IEEE Transactions on Medical Imaging 23, 137-152.

Belitski, a., Gretton, a., Magri, C., Murayama, Y., Montemurro, M., Logothetis, N., Panzeri, S., 2008. Local Field Potentials and Spiking Activity in Primary Visual Cortex Convey Independent Information about Natural Stimuli. Journal of Neuroscience 28, 5696-5709.

Bell, a.J., Sejnowski, T.J., 1995. An information-maximization approach to blind separation and blind deconvolution. Neural computation 7, 1129-1159.

Benjamin, C., Lieberman, D.A., Chang, M., Ofen, N., Whitfield-Gabrieli, S., Gabrieli, J.D., Gaab, N., 2010. The influence of rest period instructions on the default mode network. Front Hum Neurosci 4, 218.

Bianciardi, M., Fukunaga, M., Gelderen, P.V., Horovitz, S.G., De, J.A., Duyn, J.H., 2009a. Modulation of spontaneous fMRI activity in human visual cortex by behavioral state. Neuroimage 45, 160-168.

Bianciardi, M., Fukunaga, M., van Gelderen, P., Horovitz, S.G., de Zwart, J.A., Shmueli, K., Duyn, J.H., 2009b. Sources of functional magnetic resonance imaging signal fluctuations in the human brain at rest: a 7 T study. Magnetic Resonance Imaging 27, 1019-1029.

Biswal, B., Yetkin, F.Z., Haughton, V.M., Hyde, J.S., 1995. Functional connectivity in the motor cortex of resting human brain using echo-planar MRI. Magnetic Resonance in Medicine 34, 537-541.

Boly, M., Balteau, E., Schnakers, C., Degueldre, C., Moonen, G., Luxen, A., Phillips, C., Peigneux, P., 2007. Baseline brain activity fluctuations predict somatosensory perception in humans. Proceedings of the National Academy of Sciences of the United States of America 104, 12187–12192.

Borg-Graham, L.J., Monier, C., Fregnac, Y., 1998. Visual input evokes transient and strong shunting inhibition in visual cortical neurons. Nature 393, 369-373.

Braak, H., Braak, E., 1995. Staging of alzheimer's disease-related neurofibrillary changes. Neurobiology of Aging 16, 271-278.

Brainard, D.H., 1997. The Psychophysics Toolbox. Spatial Vision 10, 433-436.

Bray, S., Arnold, A.E., Levy, R.M., Iaria, G., 2015. Spatial and temporal functional connectivity changes between resting and attentive states. Hum Brain Mapp 36, 549-565.

Broca, P.P., 1861. Perte de la Parole, Ramollissement Chronique et Destruction Partielle du Lobe Antérieur Gauche du Cerveau. Bulletin de la Société Anthropologique 2, 235-238.

Buckner, R.L., Andrews-Hanna, J.R., Schacter, D.L., 2008. The brain's default network: Anatomy, function, and relevance to disease. Annals of the New York Academy of Sciences 1124, 1-38.

Buckner, R.L., Krienen, F.M., Yeo, T.B.T., 2013. Opportunities and limitations of intrinsic functional connectivity MRI. Nature Reviews Neuroscience 16, 832-837.

Buxton, R.B., Wong, E.C., Frank, L.R., 1998. Dynamics of blood flow and oxygenation changes during brain activation: the ballon model. Magn Reson Med 39, 855-864.

Calhoun, V.D., Kiehl, K.A., Pearlson, G.D., 2008. Modulation of temporally coherent brain networks estimated using ICA at rest and during cognitive tasks. Human Brain Mapping 29, 828-838.

Catani, M., Jones, D.K., Donato, R., Ffytche, D.H., 2003. Occipito-temporal connections in the human brain. Brain 126, 2093-2107.

Celone, K.A., Calhoun, V.D., Dickerson, B.C., Atri, A., Chua, E.F., Miller, S.L., DePeau, K., Rentz, D.M., Selkoe, D.J., Blacker, D., Albert, M.S., Sperling, R.A., 2006. Alterations in memory networks in mild cognitive impairment and Alzheimer's disease: an independent component analysis. J Neurosci 26, 10222-10231.

Chao, L.L., Mueller, S.G., Buckley, S.T., Peek, K., Raptentsetseng, S., Elman, J., Yaffe, K., Miller, B.L., Kramer, J.H., Madison, C., Mungas, D., Schuff, N., Weiner, M.W., 2010. Evidence of neurodegeneration in brains of older adults who do not yet fulfill MCI criteria. Neurobiol Aging 31, 368-377.

Chen, X., Zhang, H., Zhang, L., Shen, C., Lee, S.W., Shen, D., 2017. Extraction of dynamic functional connectivity from brain grey matter and white matter for MCI classification. Hum Brain Mapp 38, 5019-5034.

Chou, Y.H., Sundman, M., Whitson, H.E., Gaur, P., Chu, M.L., Weingarten, C.P., Madden, D.J., Wang, L., Kirste, I., Joliot, M., Diaz, M.T., Li, Y.J., Song, A.W., Chen, N.K., 2017. Maintenance and Representation of Mind Wandering during Resting-State fMRI. Sci Rep 7, 40722.

Churchland, M.M., Yu, B.M., Cunningham, J.P., Sugrue, L.P., Cohen, M.R., Corrado, G.S., Newsome, W.T., Clark, A.M., Hosseini, P., Scott, B.B., Bradley, D.C., Smith, M.A., Kohn, A., Movshon, J.A., Armstrong, K.M., Moore, T., Chang, S.W., Snyder, L.H., Lisberger, S.G., Priebe, N.J., Finn, I.M., Ferster, D., Ryu, S.I., Santhanam, G., Sahani, M., Shenoy, K.V., 2010. Stimulus onset quenches neural variability: a widespread cortical phenomenon. Nature Neuroscience 13, 369-378.

Cole, M.W., Bassett, D.S., Power, J.D., Braver, T.S., Petersen, S.E., 2014. Intrinsic and task-evoked network architectures of the human brain. Neuron 83, 238-251.

Cole, M.W., Reynolds, J.R., Power, J.D., Repovs, G., Anticevic, A., Braver, T.S., 2013. Multi-task connectivity reveals flexible hubs for adaptive task control. Nature Neuroscience 16, 1348-1355.

Contreras, J.A., Goñi, J., Risacher, S.L., Amico, E., Yoder, K., Dzemidzic, M., West, J.D., McDonald, B.C., Farlow, M.R., Sporns, O., Saykin, A.J., 2016. Cognitive complaints in older adults at risk for Alzheimer's disease are associated with altered resting-state networks. Alzheimer's & Dementia: Diagnosis, Assessment & Disease Monitoring 6, 40-49.

Cordes, D., Haughton, V., Carew, J.D., Arfanakis, K., Maravilla, K., 2002. Hierarchical clustering to measure connectivity in fMRI resting-state data. Magnetic Resonance Imaging 20, 305-317.

Cordes, D., Haughton, V.M., Arfanakis, K., Wendt, G.J., Turski, P.A., Moritz, C.H., Quigley, M.A., Meyerand, M.E., 2000. Mapping functionally related regions of brain with functional connectivity MR imaging. American Journal of Neuroradiology 21, 1636-1644.

Cox, R.W., 1996. AFNI: Software for Analysis and Visualization of Functional Magnetic Resonance Neuroimages. Computers and Biomedical Research 29, 162-173.

Crochet, S., Petersen, C.C., 2006. Correlating whisker behavior with membrane potential in barrel cortex of awake mice. Nat Neurosci 9, 608-610.

Cronin-Golomb, A., Hof, P.R., 2004. Vision in Alzheimer ' s Disease. The Gerontologist 35, 370-376.

D'Arcy, R.C.N., Hamilton, A., Jarmasz, M., Sullivan, S., Stroink, G., 2006. Exploratory data analysis reveals visuovisual interhemispheric transfer in functional magnetic resonance imaging. Magnetic Resonance in Medicine 55, 952-958.

Damoiseaux, J.S., Prater, K.E., Miller, B.L., Greicius, M.D., 2012. Functional connectivity tracks clinical deterioration in Alzheimer's disease. Neurobiology of Aging 33, 828.e819-828.e830.

Dasgupta, S., Long, P.M., 2005. Performance guarantees for hierarchical clustering. Journal of Computer and System Sciences 70, 555-569.

De Luca, M., Beckmann, C.F., De Stefano, N., Matthews, P.M., Smith, S.M., 2006. fMRI resting state networks define distinct modes of long-distance interactions in the human brain. Neuroimage 29, 1359-1367.

De Souza, L.C., Sarazin, M., Goetz, C., Dubois, B., 2009. Clinical Investigations in Primary Care. Dementia in Clinical Practice, pp. 1-11.

Delamillieure, P., Doucet, G., Mazoyer, B., Turbelin, M.R., Delcroix, N., Mellet, E., Zago, L., Crivello, F., Petit, L., Tzourio-Mazoyer, N., Joliot, M., 2010. The resting state questionnaire: An introspective questionnaire for evaluation of inner experience during the conscious resting state. Brain Research Bulletin 81, 565-573.

Deneux, T., Grinvald, A., 2017. Milliseconds of Sensory Input Abruptly Modulate the Dynamics of Cortical States for Seconds. Cereb Cortex 27, 4549-4563.

Detre, J.A., Maccotta, L., King, D., Alsop, D.C., Glosser, G., D'Esposito, M., Zarahn, E., Aguirre, G.K., French, J.A., 1998. Functional MRI lateralization of memory in temporal lobe epilepsy. Neurology 50, 926-932.

Dickerson, B.C., Salat, D.H., Greve, D.N., Chua, E.F., Rand-Giovannetti, E., Rentz, D.M., Bertram, L., Mullin, K., Tanzi, R.E., Blacker, D., Albert, M.S., Sperling, R.A., 2005. Increased hippocampal activation in mild cognitive impairment compared to normal aging and AD. Neurology 65, 404-411.

Ding, Z., Newton, A.T., Xu, R., Anderson, A.W., Morgan, V.L., Gore, J.C., 2013. Spatio-temporal correlation tensors reveal functional structure in human brain. PLoS One 8.

Ding, Z., Xu, R., Bailey, S.K., Wu, T.-L., Morgan, V.L., Cutting, L.E., Anderson, A.W., Gore, J.C., 2016. Visualizing functional pathways in the human brain using correlation tensors and magnetic resonance imaging. Magnetic Resonance Imaging 34, 8-17.

Dixon, M.L., Andrews-Hanna, J.R., Spreng, R.N., Irving, Z.C., Mills, C., Girn, M., Christoff, K., 2017. Interactions between the default network and dorsal attention network vary across default subsystems, time, and cognitive states. Neuroimage 147, 632-649.

Doucet, G., Naveau, M., Petit, L., Zago, L., Crivello, F., Jobard, G.l., Delcroix, N., Mellet, E., Tzourio-Mazoyer, N., Mazoyer, B., Joliot, M., 2012. Patterns of hemodynamic low-frequency oscillations in the brain are modulated by the nature of free thought during rest. Neuroimage 59, 3194-3200.

Dubois, B., Hampel, H., Feldman, H.H., Scheltens, P., Aisen, P., Andrieu, S., Bakardjian, H., Benali, H., Bertram, L., Blennow, K., Broich, K., Cavedo, E., Crutch, S., Dartigues, J.F., Duyckaerts, C., Epelbaum, S., Frisoni, G.B., Gauthier, S., Genthon, R., Gouw, A.A., Habert, M.O., Holtzman, D.M., Kivipelto, M., Lista, S., Molinuevo, J.L., O'Bryant, S.E., Rabinovici, G.D., Rowe, C., Salloway, S., Schneider, L.S., Sperling, R., Teichmann, M., Carrillo, M.C., Cummings, J., Jack, C.R., 2016. Preclinical Alzheimer's disease: Definition, natural history, and diagnostic criteria. Alzheimer's and Dementia 12, 292-323.

Duncan, N.W., Northoff, G., 2013. Overview of potential procedural and participant-related confounds for neuroimaging of the resting state. J Psychiatry Neurosci 38, 84-96.

Duyn, J., 2013. MR susceptibility imaging. Journal of Magnetic Resonance 229, 198-207.

Fabri, M., Polonara, G., Mascioli, G., Salvolini, U., Manzoni, T., 2011. Topographical organization of human corpus callosum: An fMRI mapping study. Brain Research 1370, 99-111.

Fair, D.A., Schlaggar, B.L., Cohen, A.L., Miezin, F.M., Dosenbach, N.U.F., Wenger, K.K., Fox, M.D., Snyder, A.Z., Raichle, M.E., Petersen, S.E., 2007. A method for using blocked and event-related fMRI data to study "resting state" functional connectivity. Neuroimage 35, 396-405.

Fan, L., Li, H., Zhuo, J., Zhang, Y., Wang, J., Chen, L., Yang, Z., Chu, C., Xie, S., Laird, A.R., Fox, P.T., Eickhoff, S.B., Yu, C., Jiang, T., 2016. The Human Brainnetome Atlas: A New Brain Atlas Based on Connectional Architecture. Cereb Cortex 26, 3508-3526.

Fedorov, A., Beichel, R., Kalpathy-Cramer, J., Finet, J., Fillion-Robin, J.C., Pujol, S., Bauer, C., Jennings, D., Fennessy, F., Sonka, M., Buatti, J., Aylward, S., Miller, J.V., Pieper, S., Kikinis, R., 2012. 3D Slicer as an image computing platform for the Quantitative Imaging Network. Magnetic Resonance Imaging 30, 1323-1341.

Ferezou, I., Bolea, S., Petersen, C.C., 2006. Visualizing the cortical representation of whisker touch: voltage-sensitive dye imaging in freely moving mice. Neuron 50, 617-629.

Ferezou, I., Deneux, T., 2017. Review: How do spontaneous and sensory-evoked activities interact? Neurophotonics 4, 031221.

Ffytche, D.H., Catani, M., 2005. Beyond localization: from hodology to function. Philosophical transactions of the Royal Society of London. Series B, Biological sciences 360, 767-779.

Filbey, F.M., Slack, K.J., Sunderland, T.P., Cohen, R.M., 2006. Functional magnetic resonance imaging and magnetoencephalography differences associated with APOE4 in young healthy adults. NeuroReport 17, 1585-1590.

Filippini, N., MacIntosh, B.J., Hough, M.G., Goodwin, G.M., Frisoni, G.B., Smith, S.M., Matthews, P.M., Beckmann, C.F., Mackay, C.E., 2009. Distinct patterns of brain activity in young carriers of the APOE-epsilon4 allele. Proceedings of the National Academy of Sciences of the United States of America 106, 7209-7214.

Finn, I.M., Priebe, N.J., Ferster, D., 2007. The emergence of contrast-invariant orientation tuning in simple cells of cat visual cortex. Neuron 54, 137-152.

Fox, M.D., Corbetta, M., Snyder, A.Z., Vincent, J.L., Raichle, M.E., 2006a. Spontaneous neuronal activity distinguishes human dorsal and ventral attention systems. Proc. Natl. Acad. Sci. U. S. A. 103, 10046-10051.

Fox, M.D., Raichle, M.E., 2007. Spontaneous fluctuations in brain activity observed with functional magnetic resonance imaging. Nat Rev Neurosci 8, 700-711.

Fox, M.D., Snyder, A.Z., Zacks, J.M., Raichle, M.E., 2006b. Coherent spontaneous activity accounts for trial-to-trial variability in human evoked brain responses. Nature Neuroscience 9, 23-25.

Fox, M.D., Zhang, D., Snyder, A.Z., Raichle, M.E., 2009. The global signal and observed anticorrelated resting state brain networks. Journal of neurophysiology 101, 3270-3283.

Friston, K.J., Holmes, A.P., Worsley, K.J., Poline, J.-B., Frith, C.D., Frackowiak, R.S., 1995. Statistical parametric maps in functional imaging: a general linear model approach. Human Brain Mapping 2, 189-210.

Galvin, J.E., Sadowsky, C.H., NINCDS-ADRDA, 2012. Practical guidelines for the recognition and diagnosis of dementia. Journal of the American Board of Family Medicine : JABFM 25, 367-382.

Garrett, D.D., McIntosh, A.R., Grady, C.L., 2014. Brain signal variability is parametrically modifiable. Cerebral Cortex 24, 2931-2940.

Gawryluk, J.R., D'Arcy, R.C.N., Mazerolle, E.L., Brewer, K.D., Beyea, S.D., 2011a. Functional mapping in the corpus callosum: a 4T fMRI study of white matter. Neuroimage 54, 10-15.

Gawryluk, J.R., Mazerolle, E.L., Brewer, K.D., Beyea, S.D., D'Arcy, R.C.N., 2011b. Investigation of fMRI activation in the internal capsule. BMC Neuroscience 12, 56.

Gawryluk, J.R., Mazerolle, E.L., D'Arcy, R.C.N., 2014. Does functional MRI detect activation in white matter? A review of emerging evidence, issues, and future directions. Frontiers in Neuroscience 8, 1-12.

Gilson, M., Deco, G., Friston, K.J., Hagmann, P., Mantini, D., Betti, V., Romani, G.L., Corbetta, M., 2017. Effective connectivity inferred from fMRI transition dynamics during movie viewing points to a balanced reconfiguration of cortical interactions. Neuroimage.

Glodzik-Sobanska, L., Reisberg, B., De Santi, S., Babb, J.S., Pirraglia, E., Rich, K.E., Brys, M., De Leon, M.J., 2007. Subjective memory complaints: Presence, severity and future outcome in normal older subjects. Dementia and Geriatric Cognitive Disorders 24, 177-184.

Golby, A., Silverberg, G., Race, E., Gabrieli, S., O'Shea, J., Knierim, K., Stebbins, G., Gabrieli, J., 2005. Memory encoding in Alzheimer's disease: an fMRI study of explicit and implicit memory. Brain 128, 773-787.

Gonzalez-Castillo, J., Hoy, C.W., Handwerker, D.a., Robinson, M.E., Buchanan, L.C., Saad, Z.S., Bandettini, P.A., 2015. Tracking ongoing cognition in individuals using brief, whole-brain functional connectivity patterns. Proceedings of the National Academy of Sciences 112, 8762-8767.

Grady, C.L., McIntosh, A.R., Beig, S., Keightley, M.L., Burian, H., Black, S.E., 2003. Evidence from functional neuroimaging of a compensatory prefrontal network in Alzheimer's disease. The Journal of neuroscience : the official journal of the Society for Neuroscience 23, 986-993.

Gratton, C., Laumann, T.O., Gordan, E.M., Adeyemo, B., Petersen, S.E., 2016. Evidence for two independent factors that modify brain networks to meet task goals. Cell Report 16, 338-348.

Greicius, M.D., Srivastava, G., Reiss, A.L., Menon, V., 2004. Default-mode network activity distinguishes Alzheimer's disease from healthy aging: evidence from functional MRI. Proc. Natl. Acad. Sci. U. S. A. 101, 4637-4642.

Greicius, M.D., Supekar, K., Menon, V., Dougherty, R.F., 2009. Resting-state functional connectivity reflects structural connectivity in the default mode network. Cerebral Cortex 19, 72-78.

Greve, D.N., Fischl, B., 2009. Accurate and robust brain image alignment using boundary-based registration. Neuroimage 48, 63-72.

Harlow, J.M., 1848. Passage of an iron rod through the head. Boston Medical and Surgical Journal 39, 281-283.

Harris, J.J., Attwell, D., 2012. The energetics of central nervous system white matter. The Journal of Neuroscience 32, 356-371.

Harrison, B.J., Pujol, J., López-Solà, M., Hernández-Ribas, R., Deus, J., Ortiz, H., Soriano-Mas, C., Yücel, M., Pantelis, C., Cardoner, N., 2008. Consistency and functional specialization in the default mode brain network. Proceedings of the National Academy of Sciences of the United States of America 105, 9781-9786.

Hasson, U., Malach, R., Heeger, D.J., 2010. Reliability of cortical activity during natural stimulation. Trends in Cognitive Sciences 14, 40-48.

Hasson, U., Nir, Y., Levy, I., Fuhrmann, G., Malach, R., 2004. Intersubject synchronization of cortical activity during natural vision. Science 303, 1634-1640.

He, B.J., 2013. Spontaneous and task-evoked brain activity negatively interact. Journal of Neuroscience 33, 4672-4682.

Helenius, J., Perkio, J., Soinne, L., Ostergaard, L., Carano, R.a.D., Salonen, O., Savolainen, S., Kaste, M., Aronen, H.J., Tatlisumak, T., 2003. Cerebral Hemodynamics in a Healthy Population Measured by Dynamic Susceptibility Contrast MR Imaging. Acta Radiologica 44, 538-546.

Henriksson, L., Khaligh-Razavi, S.M., Kay, K., Kriegeskorte, N., 2015. Visual representations are dominated by intrinsic fluctuations correlated between areas. Neuroimage 114, 275-286.

Henry, M.S., Craig, D., Johnston, J.A., Passmore, A.P., McGuiness, B., 2011. Mild Cognitive Impairment: An Overview. In: Corso, J.A. (Ed.), Perspectives on Alzheimer's Disease. Nova Science Publishers, Inc., New York, pp. 103-113.

Hesselmann, G., Kell, C.A., Eger, E., Kleinschmidt, A., 2008. Spontaneous local variations in ongoing neural activity bias perceptual decisions. Proceedings of the National Academy of Sciences of the United States of America 105, 10984-10989.

Hodges, J.R., 2006. Alzheimer's centennial legacy: Origins, landmarks and the current status of knowledge concerning cognitive aspects. Brain 129, 2811-2822.

Horovitz, S.G., Fukunaga, M., De Zwart, J.A., Van Gelderen, P., Fulton, S.C., Balkin, T.J., Duyn, J.H., 2008. Low frequency BOLD fluctuations during resting wakefulness and light sleep: A simultaneous EEG-fMRI study. Human Brain Mapping 29, 671-682.

Hubel, D.H., Wiesel, T.N., 1959. Receptive fields of single neurones in the cat's striate cortex. The Journal of Physiology 148, 574-591.

Hutchison, R.M., Womelsdorf, T., Allen, E.A., Bandettini, P.A., Calhoun, V.D., Corbetta, M., Penna, S.D., Duyn, J.H., Glover, G.H., Gonzalez-Castillo, J., Handwerker, D.A., Keilholz, S., Kiviniemi, V., Leopold, D.A., de Pasquale, F., Sporns, O., Walter, M., Chang, C., 2013. Dynamic functional connectivity: Promise, issues, and interpretations. Neuroimage 80, 1-43.

Jääskeläinen, I.P., Koskentalo, K., Balk, M.H., Autti, T., Kauramäki, J., Pomren, C., Sams, M., 2008. Inter-subject synchronization of prefrontal cortex hemodynamic activity during natural viewing. The Open Neuroimaging Journal 2, 14-19.

Jensen, J.H., Lu, H., Inglese, M., 2006. Microvessel density estimation in the human brain by means of dynamic contrast-enhanced echo-planar imaging. Magnetic Resonance in Medicine 56, 1145-1150.

Jessen, F., Amariglio, R.E., van Boxtel, M., Breteler, M., Ceccaldi, M., Chetelat, G., Dubois, B., Dufouil, C., Ellis, K.A., van der Flier, W.M., Glodzik, L., van Harten, A.C., de Leon, M.J., McHugh, P., Mielke, M.M., Molinuevo, J.L., Mosconi, L., Osorio, R.S., Perrotin, A., Petersen, R.C., Rabin, L.A., Rami, L., Reisberg, B., Rentz, D.M., Sachdev, P.S., de la Sayette, V., Saykin, A.J., Scheltens, P., Shulman, M.B., Slavin, M.J., Sperling, R.A., Stewart, R., Uspenskaya, O., Vellas, B., Visser, P.J., Wagner, M., Subjective Cognitive Decline Initiative Working, G., 2014. A conceptual framework for research on subjective cognitive decline in preclinical Alzheimer's disease. Alzheimers Dement 10, 844-852.

Jessen, F., Feyen, L., Freymann, K., Tepest, R., Maier, W., Heun, R., Schild, H.H., Scheef, L., 2006. Volume reduction of the entorhinal cortex in subjective memory impairment. Neurobiology of Aging 27, 1751-1756.

Jo, H.J., Saad, Z.S., Simmons, W.K., Milbury, L.a., Cox, R.W., 2010. Mapping sources of correlation in resting state FMRI, with artifact detection and removal. Neuroimage 52, 571-582.

Johnstone, T., Ores Walsh, K.S., Greischar, L.L., Alexander, A.L., Fox, A.S., Davidson, R.J., Oakes, T.R., 2006. Motion correction and the use of motion covariates in multiple-subject fMRI analysis. Human Brain Mapping 27, 779-788.

Jones, D.T., MacHulda, M.M., Vemuri, P., McDade, E.M., Zeng, G., Senjem, M.L., Gunter, J.L., Przybelski, S.A., Avula, R.T., Knopman, D.S., Boeve, B.F., Petersen, R.C., Jack, C.R., 2011. Age-related changes in the default mode network are more advanced in Alzheimer disease. Neurology 77, 1524-1531.

Kato, T., Knopman, D., Liu, H., 2001. Dissociation of regional activation in mild AD during visual encoding: a functional MRI study. Neurology 57, 812-816.

Kenet, T., Bibitchkov, D., Tsodyks, M., Grinvald, A., Arieli, A., 2003. Spontaneously emerging cortical representations of visual attributes. Nature 425, 954-956.

Kim, D., Kay, K., Shulman, G.L., Corbetta, M., 2017. A New Modular Brain Organization of the BOLD Signal during Natural Vision. Cerebral Cortex, 1-17.

Kircher, T.T., Weis, S., Freymann, K., Erb, M., Jessen, F., Grodd, W., Heun, R., Leube, D.T., 2007. Hippocampal activation in patients with mild cognitive impairment is necessary for successful memory encoding. J Neurol Neurosurg Psychiatry 78, 812-818.

Klimesch, W., Sauseng, P., Hanslmayr, S., 2007. EEG alpha oscillations: the inhibition-timing hypothesis. Brain Res Rev 53, 63-88.

Krienen, F.M., Yeo, B.T.T., Buckner, R.L., Buckner, R.L., 2014. Reconfigurable task-dependent functional coupling modes cluster around a core functional architecture. Philosophical transactions of the Royal Society B.

Kundu, P., Inati, S.J., Evans, J.W., Luh, W.-M., Bandettini, P.A., 2012. Differentiating BOLD and non-BOLD signals in fMRI time series using multi-echo EPI. Neuroimage 60, 1759-1770.

Kwong, K.K., Belliveau, J.W., Chesler, D.A., Goldberg, I.E., Robert, M., Poncelet, B.P., Kennedy, D.N., Hoppel, B.E., Cohen, M.S., Cheng, H.-m., Brady, T.J., Rosen, B.R., 1992. Dynamic Magnetic Resonance Imaging of Human Brain Activity During Primary Sensory Stimulation Source : Proceedings of the National Academy of Sciences of the United States of America , Vol . Published by : National Academy of Sciences Stable URL : http://. Proceedings of the National Academy of Sciences of the United States of America 89, 5675-5679.

Lauritzen, M., 2001. Relationship of Spikes, Synaptic Activity, and Local Changes of Cerebral Blood Flow. Journal of Cerebral Blood Flow & Metabolism 21, 1367-1383.

Lee, J., van Gelderen, P., Kuo, L.W., Merkle, H., Silva, A.C., Duyn, J.H., 2011. T2*-based fiber orientation mapping. Neuroimage 57, 225-234.

Leopold, D.A., Maier, A., 2012. Ongoing physiological processes in the cerebral cortex. Neuroimage 62, 2190-2200.

Leyton, C.E., Hodges, J.R., Piguet, O., Ballard, K.J., 2017. Common and divergent neural correlates of anomia in amnestic and logopenic presentations of Alzheimer's disease. Cortex 86, 45-54.

Lierse, W., Horstmann, E., 1965. Anatomy of the Cerebral Vascular Bed with Special Emphasis on Homogeneity and Inhomogeneity in Small Parts of the Gray and White Matter. Acta Neurologica Scandinavica S14, 15-19.

Logothetis, N.K., Pauls, J., Augath, M., Trinath, T., Oeltermann, A., 2001. Neurophysiological investigation of the basis of the fMRI signal. Nature 412, 150-157.

Logothetis, N.K., Wandell, B.A., 2004. Interpreting the BOLD signal. Annual review of physiology 66, 735-769.

Lopez-Sanz, D., Bruna, R., Garces, P., Martin-Buro, M.C., Walter, S., Delgado, M.L., Montenegro, M., Lopez Higes, R., Marcos, A., Maestu, F., 2017. Functional Connectivity Disruption in Subjective Cognitive Decline and Mild Cognitive Impairment: A Common Pattern of Alterations. Front Aging Neurosci 9, 109.

Lowe, M.J., Mock, B.J., Sorenson, J.A., 1998. Functional Connectivity in Single and Multislice Echoplanar Imaging Using Resting-State Fluctuations. Neuroimage 7, 119-132.

Lu, K.H., Hung, S.C., Wen, H., Marussich, L., Liu, Z., 2016. Influences of high-level features, gaze, and scene transitions on the reliability of BOLD responses to natural movie stimuli. PLoS One 11, 1-19.

Maandag, N.J.G., Coman, D., Sanganahalli, B.G., Herman, P., Smith, A.J., Blumenfeld, H., Shulman, R.G., Hyder, F., 2007. Energetics of neuronal signaling and fMRI activity. Proceedings of the National Academy of Sciences of the United States of America 104, 20546–20551.

Machulda, M.M., Ward, H.a., Borowski, B., Gunter, J.L., Cha, R.H., O'Brien, P.C., Petersen, R.C., Boeve, B.F., Knopman, D., Tang-Wai, D.F., Ivnik, R.J., Smith, G.E., Tangalos, E.G., Jack, C.R.J., 2003. Comparison of memory fMRI response among normal, MCI, and Alzheimer's patients. Neurology 61, 500-506.

Makedonov, I., Chen, J.J., Masellis, M., MacIntosh, B.J., 2015. Physiological fluctuations in white matter are increased in Alzheimer's disease and correlate with neuroimaging and cognitive biomarkers. Neurobiology of Aging 37, 12-18.

Mäkinen, V., Tiitinen, H., May, P., 2005. Auditory event-related responses are generated independently of ongoing brain activity. Neuroimage 24, 961-968.

Mandl, R.C.W., Schnack, H.G., Zwiers, M.P., van der Schaaf, A., Kahn, R.S., Hulshoff Pol, H.E., 2008. Functional diffusion tensor imaging: Measuring task-related fractional anisotropy changes in the human brain along white matter tracts. PLoS One 3.

Martinez, L.M., Wang, Q., Reid, R.C., Pillai, C., Alonso, J.-M., Sommer, F.T., Hirsch, J.A., 2005. Receptive field structure varies with layer in the primary visual cortex. Nature Neuroscience 8, 372-379.

Marussich, L., Lu, K.-H., Jeong, J.Y., Hung, S.-C., Liu, Z., 2015. Natural Vision Task Partially Reorganizes Resting State Networks. The Organization of Human Brain Mapping Annual Meeting, p. Poster #3843.

Marussich, L., Lu, K.-H., Wen, H., Liu, Z., 2017. Mapping White-Matter Functional Organization at Rest and during Naturalistic Visual Perception. Neuroimage 146, 1128-1141.

Mazerolle, E.L., Beyea, S.D., Gawryluk, J.R., Brewer, K.D., Bowen, C.V., D'Arcy, R.C.N., 2010. Confirming white matter fMRI activation in the corpus callosum: Co-localization with DTI tractography. Neuroimage 50, 616-621.

Mazerolle, E.L., Gawryluk, J.R., Dillen, K.N.H., Patterson, S.a., Feindel, K.W., Beyea, S.D., Stevens, M., Tynan, R., Newman, A.J., Schmidt, M.H., D'Arcy, R.C.N., 2013. Sensitivity to White Matter fMRI Activation Increases with Field Strength. PLoS One 8, 1-12.

McMahon, D.B.T., Russ, B.E., Elnaiem, H.D., Kurnikova, a.I., Leopold, D.a., 2015. Single-Unit Activity during Natural Vision: Diversity, Consistency, and Spatial Sensitivity among AF Face Patch Neurons. Journal of Neuroscience 35, 5537-5548.

Mennes, M., Kelly, C., Colcombe, S., Xavier Castellanos, F., Milham, M.P., 2013. The extrinsic and intrinsic functional architectures of the human brain are not equivalent. Cerebral Cortex 23, 223-229.

Monier, C., Chavane, F., Baudot, P., Graham, L.J., Frégnac, Y., 2003. Orientation and direction selectivity of synaptic inputs in visual cortical neurons: A diversity of combinations produces spike tuning. Neuron 37, 663-680.

Mori, S., Oishi, K., Jiang, H., Jiang, L., Li, X., Akhter, K., Hua, K., Faria, A.V., Mahmood, A., Woods, R., Toga, A.W., Pike, G.B., Neto, P.R., Evans, A., Zhang, J., Huang, H., Miller, M.I., van Zijl, P., Mazziotta, J., 2008. Stereotaxic white matter atlas based on diffusion tensor imaging in an ICBM template. Neuroimage 40, 570-582.

Morrison, J.H., Hof, P.R., 1997. Life and Death of Neurons in the Aging Brain. Science 278, 412-419.

Mosconi, L., Santi, S.D., Brys, M., Tsui, W.H., Pirraglia, E., Glodzik-, L., Rich, K.E., Switalski, R., Mehta, P.D., Pratico, D., Blennow, K., Leon, M.J.D., 2008. Hypometabolism and altered cerebrospinal fluid markers in normal apolipoprotein E E4 carriers with subjective memory complaints. Biological Psychiatry 63, 609-618.

Mosier, K.M., Liu, W.-c., Maldjian, J.a., Shah, R., Modi, B., 1999. Lateralization of Cortical Function in Swallowing : A Functional MR Imaging Study. American Journal of Neuroradiology 20, 1520-1526.

Mukamel, R., Gelbard, H., Arieli, A., Hasson, U., Fried, I., Malach, R., 2005. Coupling Between Neuronal Firing, Field Potentials, and fMRI in Human Auditory Cortex. Science 309, 951-954.

Murphy, K., Birn, R.M., Handwerker, D.A., Jones, T.B., Bandettini, P.A., 2009. The impact of global signal regression on resting state correlations: Are anti-correlated networks introduced? Neuroimage 44, 893-905.

Muthukumaraswamy, S.D., Edden, R.A.E., Jones, D.K., Swettenham, J.B., Singh, K.D., 2009. Resting GABA concentration predicts peak gamma frequency and fMRI amplitude in response to visual stimulation in humans. Proceedings of the National Academy of Sciences of the United States of America 106, 8356-8361.

Nir, Y., Hasson, U., Levy, I., Yeshurun, Y., Malach, R., 2006. Widespread functional connectivity and fMRI fluctuations in human visual cortex in the absence of visual stimulation. Neuroimage 30, 1313-1324.

Northoff, G., Qin, P., Nakao, T., 2010. Rest-stimulus interaction in the brain: a review. Trends Neurosci 33, 277-284.

Northoff, G., Walter, M., Schulte, R.F., Beck, J., Dydak, U., Henning, A., Boeker, H., Grimm, S., Boesiger, P., 2007. GABA concentrations in the human anterior cingulate cortex predict negative BOLD responses in fMRI. Nat Neurosci 10, 1515-1517.

Ogawa, S., Lee, T.M., Kay, A.R., Tank, D.W., 1990. Brain magnetic resonance imaging with contrast dependent on blood oxygenation. Proceedings of the National Academy of Sciences of the United States of America 87, 9868-9872.

Ogawa, S., Tank, D.W., Menon, R., Ellermann, J.M., Kim, S.G., Merkle, H., Ugurbil, K., 1992. Intrinsic signal changes accompanying sensory stimulation: functional brain mapping with magnetic resonance imaging. Proceedings of the National Academy of Sciences of the United States of America 89, 5951-5955.

Oishi, K., Zilles, K., Amunts, K., Faria, A., Jiang, H., Li, X., Akhter, K., Hua, K., Woods, R., Toga, A.W., Pike, G.B., Rosa-Neto, P., Evans, A., Zhang, J., Huang, H., Miller, M.I., van Zijl, P.C.M., Mazziotta, J., Mori, S., 2008. Human brain white matter atlas: Identification and assignment of common anatomical structures in superficial white matter. Neuroimage 43, 447-457.

Oram, M.W., 2011. Visual Stimulation Decorrelates Neuronal Activity. Journal of Neurophysiology 105, 942-957.

Otazu, G.H., Tai, L.H., Yang, Y., Zador, A.M., 2009. Engaging in an auditory task suppresses responses in auditory cortex. Nat Neurosci 12, 646-654.

Patriat, R., Molloy, E.K., Meier, T.B., Kirk, G.R., Nair, V.a., Meyerand, M.E., Prabhakaran, V., Birn, R.M., 2013. The effect of resting condition on resting-state fMRI reliability and consistency: A comparison between resting with eyes open, closed, and fixated. Neuroimage 78, 463-473.

Pelled, G., Bergstrom, D.a., Tierney, P.L., Conroy, R.S., Chuang, K.-H., Yu, D., Leopold, D.a., Walters, J.R., Koretsky, A.P., 2009. Ipsilateral cortical fMRI responses after peripheral nerve damage in rats reflect increased interneuron activity. Proceedings of the National Academy of Sciences of the United States of America 106, 14114-14119.

Pelli, D.G., 1997. The VideoToolbox software for visual psychophysics: Transforming numbers into movies. Spatial Vision 10, 437-442.

Perry, R.J., Hodges, J.R., 1999. Attention and executive deficits in Alzheimer's disease. A critical review. Brain 122 (Pt 3, 383-404.

Petersen, R.C., 2016. Mild cognitive impairment. Continuum 22, 404-418.

Petersen, R.C., Doody, R., Kurz, A., Mohs, R.C., Morris, J.C., Rabins, P.V., Ritchie, K., Rossor, M., Thal, L., Winblad, B., 2001. Current Concepts in Mild Cognitive Impairment. Arch Neurol 58, 1985-1992.

Petrella, J.R., Wang, L., Krishnan, S., Slavin, M.J., Prince, S.E., Tran, T.-T.T., Doraiswamy, P.M., 2007. Cortical Deactivation in Mild Cognitive Impairment: High-Field-Strength Functional MR Imaging. Radiology 245, 224-235.

Petzold, G.C., Murthy, V.N., 2011. Role of astrocytes in neurovascular coupling. Neuron 71, 782-796.

Ponce-Alvarez, A., He, B.J., Hagmann, P., Deco, G., 2015. Task-Driven Activity Reduces the Cortical Activity Space of the Brain: Experiment and Whole-Brain Modeling. PLoS Computational Biology 11, 1-26.

Ponce-Alvarez, A., Thiele, A., Albright, T.D., Stoner, G.R., Deco, G., 2013. Stimulus-dependent variability and noise correlations in cortical MT neurons. Proceedings of the National Academy of Sciences 110, 13162-13167.

Power, J.D., Barnes, K.A., Snyder, A.Z., Schlaggar, B.L., Petersen, S.E., 2012. Spurious but systematic correlations in functional connectivity MRI networks arise from subject motion. Neuroimage 59, 2142-2154.

Power, J.D., Cohen, A.L., Nelson, S.M., Wig, G.S., Barnes, K.A., Church, J.A., Vogel, A.C., Laumann, T.O., Miezin, F.M., Schlaggar, B.L., Petersen, S.E., 2011. Functional Network Organization of the Human Brain. Neuron 72, 665-678.

Preibisch, C., Haase, A., 2001. Perfusion Imaging Using Spin-Labeling Methods : Contrast- to-Noise Comparison in Functional MRI Applications. Magn Reson Mater Phy 46, 172-182.

Raichle, M.E., 2010. Two views of brain function. Trends Cogn Sci 14, 180-190.

Raichle, M.E., 2015. The restless brain: how intrinsic activity organizes brain function. Philosophical Transactions of the Royal Society of London B: Biological Sciences 370, 20140172.

Raichle, M.E., MacLeod, A.M., Snyder, A.Z., Powers, W.J., Gusnard, D.a., Shulman, G.L., 2001. A default mode of brain function. Proceedings of the National Academy of Sciences 98, 676-682.

Raichle, M.E., Mintun, M.a., 2006. Brain Work and Brain Imaging. Annual Review of Neuroscience 29, 449-476.

Rami, L., Fortea, J., Bosch, B., Sole-Padulles, C., Llado, A., Iranzo, A., Sanchez-Valle, R., Molinuevo, J.L., 2011. Cerebrospinal fluid biomarkers and memory present distinct associations along the continuum from healthy subjects to AD patients. J Alzheimers Dis 23, 319-326.

Rash, J.E., 2010. Molecular disruptions of the panglial syncytium block potassium siphoning and axonal saltatory conduction: pertinence to neuromyelitis optica and other demyelinating diseases of the central nervous system. Neuroscience 168, 982-1008.

Rauch, A., Rainer, G., Logothetis, N.K., 2008. The effect of a serotonin-induced dissociation between spiking and perisynaptic activity on BOLD functional MRI. Proceedings of the National Academy of Sciences of the United States of America 105, 6759-6764.

Rehme, A.K., Eickhoff, S.B., Grefkes, C., 2013. State-dependent differences between functional and effective connectivity of the human cortical motor system. Neuroimage 67, 237-246.

Reisberg, B., Prichep, L., Mosconi, L., John, E.R., Glodzik-Sobanska, L., Boksay, I., Monteiro, I., Torossian, C., Vedvyas, A., Ashraf, N., Jamil, I.A., de Leon, M.J., 2008. The pre-mild cognitive impairment, subjective cognitive impairment stage of Alzheimer's disease. Alzheimers Dement 4, S98-S108.

Risacher, S.L., Saykin, A.J., 2013. Neuroimaging biomarkers of neurodegenerative diseases and dementia. Seminars in Neurology 33, 386:416.

Risacher, S.L., WuDunn, D., Pepin, S.M., MaGee, T.R., McDonald, B.C., Flashman, L.A., Wishart, H.A., Pixley, H.S., Rabin, L.A., Pare, N., Englert, J.J., Schwartz, E., Curtain, J.R., West, J.D., O'Neill, D.P., Santulli, R.B., Newman, R.W., Saykin, A.J., 2013. Visual contrast sensitivity in Alzheimer's disease, mild cognitive impairment, and older adults with cognitive complaints. Neurobiology of Aging 34, 1133-1144.

Rissman, J., Gazzaley, A., D'Esposito, M., 2004. Measuring functional connectivity during distinct stages of a cognitive task. Neuroimage 23, 752-763.

Roland, P.E., Eriksson, L., Stone-Elander, S., Widen, L., 1987. Does mental activity change the oxidative metabolism of the brain? The Journal of Neuroscience 7, 2373-2389.

Rombouts, S.A., Barkhof, F., Goekoop, R., Stam, C.J., Scheltens, P., 2005. Altered resting state networks in mild cognitive impairment and mild Alzheimer's disease: an fMRI study. Hum Brain Mapp 26, 231-239.

Rombouts, S.A., Barkhof, F., Veltman, D.J., Machielsen, W.C., Witter, M.P., Bierlaagh, M.A., Lazeron, R.H., Valk, J., Scheltens, P., 2000. Functional MR imaging in Alzheimer's disease during memory encoding. American Journal of Neuroradiology 21, 1869-1875.

Rosen, B.R., Savoy, R.L., 2012. FMRI at 20: Has it changed the world? Neuroimage 62, 1316-1324.

Rostrup, E., Law, I., Blinkenberg, M., Larsson, H.B., Born, a.P., Holm, S., Paulson, O.B., 2000. Regional differences in the CBF and BOLD responses to hypercapnia: a combined PET and fMRI study. Neuroimage 11, 87-97.

Saka, M., Berwick, J., Jones, M., 2010. Linear superposition of sensory-evoked and ongoing cortical hemodynamics. Frontiers in neuroenergetics 2, 1-13.

Saykin, A.J., Wishart, H.A., Rabin, L.A., Santulli, R.B., Flashman, L.A., West, J.D., McHugh, T.L., Mamourian, A.C., 2006. Older adults with cognitive complaints show brain atrophy similar to that of amnestic MCI. Neurology 67, 834-842.

Sepulcre, J., Liu, H., Talukdar, T., Martincorena, I.i., Thomas Yeo, B.T., Buckner, R.L., 2010. The organization of local and distant functional connectivity in the human brain. PLoS Computational Biology 6, 1-15.

Shattuck, D.W., Mirza, M., Adisetiyo, V., Hojatkashani, C., Salamon, G., Narr, K.L., Poldrack, R.A., Bilder, R.M., Toga, A.W., 2008. Construction of a 3D probabilistic atlas of human cortical structures. Neuroimage 39, 1064-1080.

Shirer, W.R., Ryali, S., Rykhlevskaia, E., Menon, V., Greicius, M.D., 2012. Decoding Subject-Driven Cognitive States with Whole-Brain Connectivity Patterns. Cerebral Cortex 22, 158-165.

Shulman, R.G., Rothman, D.L., Behar, K.L., Hyder, F., 2004. Energetic basis of brain activity: implications for neuroimaging. Trends Neurosci 27, 489-495.

Simony, E., Honey, C.J., Chen, J., Lositsky, O., Yeshurun, Y., Wiesel, A., Hasson, U., 2016. Dynamical reconfiguration of the default mode network during narrative comprehension. Nature Communications 7, 1-13.

Small, B.J., Gagnon, E., Robinson, B.A.B., 2007. Early identification of cognitive deficits. Geriatrics 62, 19-23.

Small, B.J., Gagnon, E., & Robinson, B. A. B., 2007. Early identification of cognitive deficits. Geriatrics 62, 19-23.

Smith, A.J., Blumenfeld, H., Behar, K.L., Rothman, D.L., Shulman, R.G., Hyder, F., 2002. Cerebral energetics and spiking frequency: The neurophysiological basis of fMRI. Proceedings of the National Academy of Sciences 99, 10765-10770.

Smith, S.M., Fox, P.T., Miller, K.L., Glahn, D.C., Fox, P.M., Mackay, C.E., Filippini, N., Watkins, K.E., Toro, R., Laird, A.R., Beckmann, C.F., 2009. Correspondence of the brain's functional architecture during activation and rest. Proceedings of the National Academy of Sciences 106, 13040-13045.

Smith, S.M., Jenkinson, M., Woolrich, M.W., Beckmann, C.F., Behrens, T.E.J., Johansen-Berg, H., Bannister, P.R., De Luca, M., Drobnjak, I., Flitney, D.E., Niazy, R.K., Saunders, J., Vickers, J., Zhang, Y., De Stefano, N., Brady, J.M., Matthews, P.M., 2004. Advances in functional and structural MR image analysis and implementation as FSL. Neuroimage 23, 208-219.

Sokoloff, L., Mangold, R., Wechsler, R.L., Kenney, C., Kety, S.S., 1955. The effect of mental arithmetic on cerebral circulation and metabolism. The Journal of Clinical Investigation 34, 1101-1108.

Sorg, C., Riedl, V., Mühlau, M., Calhoun, V.D., Eichele, T., Läer, L., Drzezga, A., Förstl, H., Kurz, A., Zimmer, C., Wohlschläger, A.M., 2007. Selective changes of resting-state networks in individuals at risk for Alzheimer's disease. Proceedings of the National Academy of Sciences of the United States of America 104, 18760-18765.

Spees, W.M., Lin, T.-H., Song, S.-K., 2013. White-Matter Diffusion fMRI of Mouse Optic Nerve. Neuroimage 65, 209-215.

Sperling, R.A., Bates, J.F., Chua, E.F., 2003. fMRI studies of associative encoding in young and elderly controls and mild Alzheimer's disease. Journal of Neurology, Neurosurgery, and Psychiatry 74, 44-50.

Sporns, O., Tononi, G., Kötter, R., 2005. The human connectome: A structural description of the human brain. PLoS Computational Biology 1, 0245-0251.

Spreng, R.N., Mar, N.A., Kim, A.S.N., 2008. The common neural basis of autobiographical memory, prospection, navigation, theory of mind and the default mode: a quantitative meta-analysis. Journal of Cognitive Neuroscience 21, 489-510.

Sundermann, B., Pfleidferer, B., 2012. Functional connectivity profile of the human inferior frontal junction: involvement in a cognitive control network. BMC Neuroscience 3.

Szostakiwskyj, J.M.H., Willatt, S.E., Cortese, F., Protzner, A.B., 2017. The modulation of EEG variability between internally- and externally-driven cognitive states varies with maturation and task performance. PLoS One 12, e0181894.

Tavor, I., Parker Jones, O., Mars, R.B., Smith, S.M., Behrens, T.E., Jbabdi, S., 2016. Task-free MRI predicts individual differences in brain activity during task performance. Science (New York, N.Y.) 352, 216-220.

Taylor, K.I., Probst, A., 2008. Anatomic localization of the transentorhinal region of the perirhinal cortex. Neurobiol Aging 29, 1591-1596.

Tepest, R., Wang, L., Csernansky, J.G., Neubert, P., Heun, R., Scheef, L., Jessen, F., 2008. Hippocampal surface analysis in subjective memory impairment, mild cognitive impairment and Alzheimer's dementia. Dementia and Geriatric Cognitive Disorders 26, 323-329.

Tettamanti, M., Paulesu, E., Scifo, P., Maravita, a., Fazio, F., Perani, D., Marzi, C.a., 2002. Interhemispheric transmission of visuomotor information in humans: fMRI evidence. Journal of neurophysiology 88, 1051-1058.

Thomas, B.P., Liu, P., Park, D.C., van Osch, M.J.P., Lu, H., 2014. Cerebrovascular reactivity in the brain white matter: magnitude, temporal characteristics, and age effects. J Cereb Blood Flow Metab.

Tsodyks, M., Kenet, T., Grinvald, A., Arieli, A., 1999. Linking spontaneous activity of single cortical neurons and the underlying functional architecture. Science (New York, N.Y.) 286, 1943-1946.

van den Heuvel, M.P., Sporns, O., 2013. An Anatomical Substrate for Integration among Functional Networks in Human Cortex. Journal of Neuroscience 33, 14489-14500.

Van Dijk, K.R.a., Hedden, T., Venkataraman, A., Evans, K.C., Lazar, S.W., Buckner, R.L., 2010. Intrinsic Functional Connectivity As a Tool For Human Connectomics: Theory, Properties, and Optimization. Journal of Neurophysiology 103, 297-321.

Van Dijk, K.R.A., Sabuncu, M.R., Buckner, R.L., 2012. The Influence of Head Motion on Intrinsic Functional Connectivity MRI. Neuroimage 59, 431-438.

Van Norden, A.G.W., Fick, W.F., De Laat, K.F., Van Uden, I.W.M., Van Oudheusden, L.J.B., Tendolkar, I., Zwiers, M.P., De Leeuw, F.E., 2008. Subjective cognitive failures and hippocampal volume in elderly with white matter lesions. Neurology 71, 1152-1159.

Van Osch, M.J.P., Teeuwisse, W.M., Van Walderveen, M.a.a., Hendrikse, J., Kies, D.a., Van Buchem, M.a., 2009. Can arterial spin labeling detect white matter perfusion signal? Magnetic Resonance in Medicine 62, 165-173.

Vanderwal, T., Eilbott, J., Finn, E.S., Craddock, R.C., Turnbull, A., Castellanos, F.X., 2017. Individual differences in functional connectivity during naturalistic viewing conditions. Neuroimage 157, 521-530.

Villemagne, V.L., Burnham, S., Bourgeat, P., Brown, B., Ellis, K.A., Salvado, O., Szoeke, C., Macaulay, S.L., Martins, R., Maruff, P., Ames, D., Rowe, C.C., Masters, C.L., 2013. Amyloid β deposition, neurodegeneration, and cognitive decline in sporadic Alzheimer's disease: a prospective cohort study. The Lancet Neurology 12, 357-367.

Villringer, A., Rosen, B.R., Belliveau, J.W., Ackerman, J.L., Lauffer, R.B., Buxton, R.B., Chao, Y.S.S., Wedeenand, V.J., Brady, T.J., 1988. Dynamic imaging with lanthanide chelates in normal brain: Contrast due to magnetic susceptibility effects. Magnetic Resonance in Medicine 6, 164-174.

Vincent, J.L., Patel, G.H., Fox, M.D., Snyder, a.Z., Baker, J.T., Van Essen, D.C., Zempel, J.M., Snyder, L.H., Corbetta, M., Raichle, M.E., 2007. Intrinsic functional architecture in the anaesthetized monkey brain. Nature 447, 83-86.

Visser, P.J., Verhey, F., Knol, D.L., Scheltens, P., Wahlund, L.O., Freund-Levi, Y., Tsolaki, M., Minthon, L., Wallin, Å.K., Hampel, H., Bürger, K., Pirttila, T., Soininen, H., Rikkert, M.O., Verbeek, M.M., Spiru, L., Blennow, K., 2009. Prevalence and prognostic value of CSF markers of Alzheimer's disease pathology in patients with subjective cognitive impairment or mild cognitive impairment in the DESCRIPA study: a prospective cohort study. The Lancet Neurology 8, 619-627.

Viswanathan, A., Freeman, R.D., 2007. Neurometabolic coupling in cerebral cortex reflects synaptic more than spiking activity. Nature Neuroscience 10, 1308-1312.

Wang, Y., Li, T.-Q., 2013. Analysis of Whole-Brain Resting-State fMRI Data Using Hierarchical Clustering Approach. PLoS One 8, e76315.

Wang, Y., Risacher, S.L., West, J.D., McDonald, B.C., Magee, T.R., Farlow, M.R., Gao, S., O'Neill, D.P., Saykin, A.J., 2013. Altered default mode network connectivity in older adults with cognitive complaints and amnestic mild cognitive impairment. J Alzheimers Dis 35, 751-760.

Wang, Y., West, J.D., Flashman, L.A., Wishart, H.A., Santulli, R.B., Rabin, L.A., Pare, N., Arfanakis, K., Saykin, A.J., 2012. Selective changes in white matter integrity in MCI and older adults with cognitive complaints. Biochim Biophys Acta 1822, 423-430.

Waxman, S.G., Ritchie, J.M., 1993. Molecular dissection of the myelinated axon. Annals of Neurology 33, 121-136.

Weber, B., Fouad, K., Burger, C., Buck, a., 2002. White Matter Glucose Metabolism during Intracortical Electrostimulation : A Quantitative [18 F] Fluorodeoxyglucose Autoradiography Study in the Rat. Neuroimage 998, 993-998.

Weissenbacher, A., Kasess, C., Gerstl, F., Lanzenberger, R., Moser, E., Windischberger, C., 2009. Correlations and anticorrelations in resting-state functional connectivity MRI: a quantitative comparison of preprocessing strategies. Neuroimage 47, 1408-1416.

Wen, H., Liu, Z., 2016. Broadband Electrophysiological Dynamics Contribute to Global Resting-State fMRI Signal. J Neurosci 36, 6030-6040.

Wilf, M., Strappini, F., Golan, T., Hahamy, A., Harel, M., Malach, R., 2017. Spontaneously emerging patterns in human visual cortex reflect responses to naturalistic sensory stimuli. Cerebral Cortex 27, 750-763.

Wong, C.W., Olafsson, V., Tal, O., Liu, T.T., 2013. The amplitude of the resting-state fMRI global signal is related to EEG vigilance measures. Neuroimage 83, 983-990.

Wong, S., Flanagan, E., Savage, G., Hodges, J.R., Hornberger, M., 2014. Contrasting prefrontal cortex contributions to episodic memory dysfunction in behavioural variant frontotemporal dementia and alzheimer's disease. PLoS One 9.

Yeo, B.T.T., Krienen, F.M., Sepulcre, J., Sabuncu, M.R., Lashkari, D., Hollinshead, M., Roffman, J.L., Smoller, J.W., Zollei, L., Polimeni, J.R., Fischl, B., Liu, H., Buckner, R.L., 2011. The organization of the human cerebral cortex estimated by intrinsic functional connectivity. Journal of Neurophysiology 106, 1125-1165.

Yuan, B.K., Zang, Y.F., Liu, D.Q., 2016. Influences of Head Motion Regression on High-Frequency Oscillation Amplitudes of Resting-State fMRI Signals. Front Hum Neurosci 10, 243.

Zhang, L., Zhang, H., Chen, X., Wang, Q., Yap, P.T., Shen, D., 2017. Learning-based structurally-guided construction of resting-state functional correlation tensors. Magn Reson Imaging 43, 110-121.

Zhou, J., Greicius, M.D., Gennatas, E.D., Growdon, M.E., Jang, J.Y., Rabinovici, G.D., Kramer, J.H., Weiner, M., Miller, B.L., Seeley, W.W., 2010. Divergent network connectivity changes in behavioural variant frontotemporal dementia and Alzheimer's disease. Brain 133, 1352-1367.

VITA

Lauren Kelly Lynch, née Marussich, was born in Jacksonville, Florida and grew up in Palm Beach Gardens, Florida. She graduated from Suncoast High School in 2008 as a National Merit Finalist and matriculated in the Biomedical Engineering program at the University of Miami as a Foote Fellow later that year. During her undergraduate years, Lauren was a part of the Florida-Georgia Louis Stokes Alliance for minority participation (FGLSAMP) under the leadership of Dr. Michael S. Gaines, Kappa Kappa Gamma Women's Fraternity, the Engineering Advisory Board, and Tau Beta Pi. In 2009, she had a summer undergraduate research experience in Nanochemistry at the University of Miami under Dr. Roger Leblanc in which she explored factors contributing to robust quantum dot synthesis. In 2010, she began working in the Ophthalmic Biophysics Center (OBC) at the Bascom Palmer Eye Institute under Drs. Fabrice Manns and Jean-Marie Parel; there she participated in an international, multi-institutional project to develop improved methods and instruments for cataract surgery designed to restore ocular accommodation. While at the OBC, Lauren's project was to determine whether the lens volume changes during accommodation. Lauren remained at the OBC for the duration of her time as an undergraduate.

In 2012, Lauren graduated from the University of Miami and matriculated into the Indiana University-Purdue University joint Medical Scientist Training Program (MSTP). From 2012-2014, Lauren completed the first two year of medical school. While there, she participated in the Global Health ENLACE Project in La Mora, El Salvador, focusing on global health infrastructure development and was also a student in the advanced Spanish-language section of Introduction to Clinical Medicine I and II. In addition, she became deeply interested in the brain as a result of the Neuroanatomy course taught by Dr. Donald Wong.

Prior to starting work in the Laboratory for Integrated Imaging, Lauren conducted research rotations with Dr. Kevin Otto (cortical microstimulation), Dr. Pedro Irazoqui and Simon John (glaucoma device development), and Dr. Edward Bartlett (neuronal ion channel modelling). Under the direction of Dr. Zhongming Liu and Dr. Andrew Saykin, Lauren has worked on fMRI analytical tools to uncover task-related changes in brain signaling in the whole brain, white matter, and in Alzheimer's Disease. In her time at Purdue, she was awarded an Indiana Clinical and Translational Sciences (CTSI) pre-doctoral fellowship and the Fearnot-Laufman-Greatbatch Award for best BME summer seminar presentation. Lauren has given several poster presentations

at leading international conferences in the field and has published one first-author paper with another two first-author papers in the publication process (submitted for peer review or under revision). After graduation, Lauren plans to complete her medical school studies at the Indiana University School of Medicine and pursue a career as a physician-scientist.

PUBLICATIONS

Lynch LK, Risacher SL, McDonald BC, Apostolova LG, Unverzagt FW, West JD, Tallman EF, Lu KH, Wen H, Liu Z, Saykin AJ. "Scene-Encoding Activation and Resting-state Functional Connectivity in Older Adults with Subjective Cognitive Decline and Mild Cognitive Impairment," (in revision)

Lynch LK, Lu KH, Wen H, Zhang Y, Saykin AJ, Liu Z. Task-Evoked Functional Connectivity During Natural Vision Does Not Explain Functional Connectivity Differences Between Rest and Task Conditions. (submitted)

Lu KH, **Marussich L,** Cao J, Hu TCC, Liu Z. Mapping Abdominal Inflammatory Response Using Manganese-Enhanced Magnetic Resonance Imaging. (submitted)

Marussich L, Lu KH, Wen H, Liu Z. Mapping white matter functional organization at rest and during naturalistic visual perception (2017). *NeuroImage* 146, 1128-1141.

Lu KH, Hung SC, Wen H, **Marussich L**, Liu Z. Influences of High-Level Features, Gaze, and Scene Transitions on the Reliability of BOLD Responses to Natural Movie Stimuli (2016). *PLoS One* 11(8): e0161787.

Marussich L, Manns F, Nankivil D, Maceo B, Yao Y, Arrieta-Quintero E, Ho A, Augusteyn R, Parel JM (2015). Crystalline lens volume measurement during accommodation in a lens stretcher. *IOVS* 56(8): 42394248.

INVITED TALKS AND CONFERENCE PRESENTATIONS

Lynch LK, Risacher SL, McDonald BC, Apostolova LG, Unverzagt FW, West JD, Tallman EF, Lu KH, Wen H, Liu Z, Saykin AJ. Scene-Encoding Activation and Resting-state Functional Connectivity in Older Adults with Subjective Cognitive Decline and Mild Cognitive Impairment. Alzheimer's Association International Conference 2018. Poster #

Lynch LK, Lu KH, Wen H, Zhang Y, Saykin AJ, Liu Z. Non-linear interaction of resting-state and task-evoked networks. Organization for Human Brain Mapping (OHBM) Annual Meeting. Abstract and Poster #1237. Singapore, 2018.

Lynch LK, Lu KH, Wen H, Zhang Y, Saykin, AJ, Liu Z. Task-Evoked Functional Connectivity Does Not Explain Functional Connectivity Differences Between Rest and Task Conditions. 5th Indiana Neuroimaging Symposium, Poster # A.2. West Lafayette, Indiana, 2017.

Lu KH, Cao J, **Marussich L,** Hu TCC, Liu Z. Mapping Abdominal Inflammatory Response Using Manganese-Enhanced MRI. 25th Annual International Society for Magnetic Resonance in Medicine Meeting & Exhibition. Abstract and Oral #1236. Honolulu, HI, 2017.

Marussich L, Lu KH, Wen H, Shi J, Zhang Y, Liu Z. Functional connectivity within white matter supports classification of brain states. *Invited Talk* - Midwest Student Speaker Exchange, BME Seminar Series, Northwestern University, 2017.

Marussich L, Lu KH, Wen H, Liu Z. Hierarchical Clusters of White-Matter fMRI are Coupled with Cortical Visual Networks. Organization for Human Brain Mapping (OHBM) Annual Meeting. Abstract and Poster #2362; Geneva, Switzerland, 2016.

Lu KH, Hung SC, Wen H, **Marussich L**, Liu Z. Sources of Reliable fMRI Responses to Natural Movie Stimuli. Organization for Human Brain Mapping (OHBM) Annual Meeting Abstract and Poster #1611; Geneva, Switzerland, 2016.

Marussich L, Jeong JY, Lu KH, Hung SC, Liu Z. Natural vision task reorganizes related task networks. Organization for Human Brain Mapping (OHBM) Annual Meeting Abstract and Poster #7436; Honolulu, HI, 2015.

Manns F, **Marussich L**, Maceo B, Nankivil D, Arrieta E, Ho A, Parel J-M. Lens volume measurements during accommodation in a lens stretcher. 8th Accommodation Club meeting, www.accommodationclub.org